Solar power water pump studies for small-scale irrigation

By

Erin Williamson
Department of Bioresource Engineering
McGill University, Montreal

August 2006

A thesis submitted to McGill University
in partial fulfillment of the requirements of the degree of
Master of Science

Your file Votre référence
ISBN: 978-0-494-32801-9
Our file Notre référence
ISBN: 978-0-494-32801-9

ABSTRACT

Master of Science Erin Williamson **Bioresource Engineering**

Solar water pump studies for small-scale irrigation

Irrigation is a well established procedure on many farms in western Canada and is practiced on various levels around the world. It allows diversification of crops, while increasing crop yields. However, typical irrigation systems consume a great amount of conventional energy through the use of electric motors and generators powered by fuel.

The overall objective of this research was to determine the feasibility of using photovoltaic (PV) modules to power a water pump for a small-scale drip irrigation system in Montréal (Québec, Canada). The study involved field observations, as well as computer simulations of global solar radiation and PV electrical output.

Field observations involved a summer and winter installation of two amorphous silicon 42 W PV modules, directly connected to a 12 V surface water pump. The parameters monitored were voltage, current, back-of-panel temperature, pressure, and flow. These observed parameters were used to determine PV electrical output and volume of water pumped. Site latitude, elevation, and panel tilt were applied to the solar radiation and PV electrical output models, along with the following meteorological data: daily average, maximum, and minimum temperatures, and global solar radiation.

Daily solar radiation prediction showed a linear correlation of 0.69 with the observed daily values, over the years 2000 to 2005. The correlation coefficient was improved to 0.91, when 7 day moving averages of both the observed and predicted solar radiation data were used. PV electrical output and volume of water pumped were monitored between August 2005 and May 2006. Both the power and water output observations were less than expected. However, the predicted daily PV electrical output ranged from 1.0 MJ d^{-1} in the summer to approximately 0.6 MJ d^{-1} in the winter. As expected, an increase in power caused an increase in the volume of water pumped.

RÉSUMÉ

Maîtrise ès Science Erin Williamson **Génie des bioressources**

Étude d'un système de pompage à énergie solaire pour l'irrigation à petite échelle

L'irrigation est une pratique nécessaire pour plusieurs fermes, tant au Canada qu'ailleurs dans le monde. Elle permet une diversification des cultures et améliore les rendements. Cependant, les technologies d'irrigation disponibles sont souvent caractérisées par une utilisation peu efficace de l'eau et par une forte consommation d'énergie provenant de sources conventionnelles.

L'objectif général de cette recherche était d'évaluer la faisabilité d'utiliser des modules photovoltaïques (PV) pour alimenter la pompe de surface d'un petit système d'irrigation goutte-à-goutte dans la région de Montréal (Québec, Canada). Pour ce faire, le projet était constitué d'une expérience de terrain et de l'évaluation de deux modèles prédictifs, soit le modèle modifié de Hargreaves-Samani pour le taux de radiation solaire globale en régions continentales et le modèle HDKR-Evans pour le courant électrique généré par les modules PV. De plus, le volume d'eau pouvant être pompé sur une base quotidienne était calculé à partir des estimations de courant produit.

L'expérience de terrain a été menée avec deux installations distinctes pour l'été et l'hiver. Les composantes des installations étaient les mêmes dans les deux cas, seuls l'emplacement et la disposition des composantes ayant varié entre la première et la deuxième installation. Le système était composé de deux modules PV de silicone amorphe directement connectés à une pompe de surface de 12 volts. Les paramètres enregistrés étaient le voltage, l'intensité du courant, la température à l'arrière des modules PV, ainsi que la pression et le débit d'eau. Les données météorologiques suivantes ont aussi été colligées tout au long de l'étude : température quotidienne (moyenne, minimale et maximale), radiation solaire globale et précipitations. Ces mesures ont servi à calculer le courant électrique généré par les modules PV et le volume d'eau pompé. La latitude et l'élévation des sites expérimentaux, de même que l'inclinaison des modules et les

données météorologiques, ont servi d'entrées pour les modèles de radiation solaire et de courant généré par les modules PV.

Entre 2000 et 2005, les prédictions de radiation solaire quotidienne ont démontré une bonne corrélation linéaire avec les données quotidiennes observées, avec un coefficient de corrélation de 0,69. Ce coefficient est passé à 0,91 avec l'emploi d'une moyenne mobile de sept jours. Le courant électrique produit a été enregistré d'août 2005 à mai 2006. L'efficacité du modèle de courant PV généré a été très faible pour cette période (coefficient de corrélation de 0,13). L'utilisation de moyennes mensuelles a mené, selon les cas, à des hausses ou à des baisses du coefficient de corrélation. Celui-ci a varié de 0,65 pour octobre 2005 à 0,01 pour février 2006. À cause d'un mauvais fonctionnement de la pompe, il s'est avéré impossible de comparer directement les débits d'eau prédits aux valeurs quotidiennes observées. Toutefois, il a été possible d'observer un lien direct entre le courant et le volume d'eau pompé.

ACKNOWLEDGEMENTS

I would like to thank all the people whose help and support made this thesis possible. First of all, I would like to thank my supervisor, Professor Chandra A. Madramootoo, who encouraged me to start anew after an unfortunate and abrupt change of the initial project. I am also very grateful for the financial support and guidance he has provided. A special thanks to Mr. Peter Enright, who from start to finish, has shown great patience and provided invaluable assistance, for which I am very grateful. I would also like to thank my committee members, Dr. Ning Wang and Dr. Robert Bonnell for thesis guidance and for taking time to inspect my experimental setup. I extend thanks also to Mr. Richard Smith and Mr. Sam Sotocinal who helped me to find my way around the greenhouse and electrical work.

Many thanks to the staff at Brace – Bano Mehdi, Nicolas Stampfli, and Wendy Ouellette – whose support and advice smoothed the progress of this endeavour. Credit goes to Nicolas for his help with the French version of the abstract.

Thanks also to my fellow graduate students– Apurva Gollamudi, Joumana Abou Nohra, Caroline Hebraud, Heidi Webber, and Rufa Doria – whose help and friendship made this process enjoyable. I would like to thank the summer students – Meghan Bichsel, Ghislaine Johnson, Kenton Ollivierre, and Phil Sawoszczuk – whose work in the field was most appreciated. I extend thanks to Jeannie Shaddy for her editorial help in the final stages.

Last but not least, I express my deep thanks to my family and to Gavin, for their never ending support, understanding, and patience.

TABLE OF CONTENTS

LIST OF TABLES

LIST OF FIGURES

LIST OF ABBREVIATIONS

A:	ampere
AC:	alternating current
a-Si:	amorphous silicon
AWG:	American wire gauge
BOS:	balance of system
d:	day
DC:	direct current
DOY:	day of year
E_{PV}:	photovoltaic electrical output (power)
FAO:	Food and Agriculture Organisation
H:	global horizontal solar radiation
H_o:	extraterrestrial solar radiation
H_t:	solar radiation in the plane of the photovoltaic array
HDKR:	Hay, Davies, Klucher, Reindl (Duffie and Beckman, 1991)
kPa:	kilopascals
L:	litres
m:	metre
MAE:	mean absolute error
min:	minute
MJ:	megajoules
NOCT:	nominal operating cell temperature
PE:	polyethylene
psi:	pounds per square inch
PV:	photovoltaic
Q:	flow
RMSE:	root mean square error
rpm:	revolutions per minute
s:	second
SI:	Système International d'Unités
STC:	standard test conditions
T_t:	atmospheric transmissivity
V:	volt
W:	watt

1.0 INTRODUCTION

The agricultural sector accounts for 2% of Canada's energy consumption and 12% of the country's water use. Installation, maintenance, and operation of various conventional irrigation systems contribute to this energy and water consumption. Solar powered irrigation offers the potential to reduce the energy and water consumption of such irrigation systems, including the two common practices of spray and flood irrigation. This is accomplished through the use of renewable energy resources and increased efficiency in water application. A solar powered pumping system enables automated control of irrigation timing and water levels. The drip component of the irrigation system would provide precision application of water, thus ensuring a decrease in water loss from wind and evaporation. The long-term advantages would be lower energy operating costs and savings in water use.

The importance of this research, involving a complete photovoltaic water pumping system, falls within the potential application for sustainable agriculture. Given that Canada has signed the Kyoto Protocol, it is important for Canadian industries, including the agri-food sector, to reduce fossil fuel consumption and greenhouse gas emissions. Through a reduction in energy and water consumption, a solar powered drip irrigation system would allow farmers in rural and developing areas to contribute toward reaching the objectives of the Kyoto Protocol, while decreasing their long-term energy costs, thus balancing economic development and environmental sustainability. Off-grid solar powered irrigation systems would be ideal for those in rural areas where electrical power is not well developed and the cost is prohibitive. It may also be implemented in areas with a limited water supply. Consequently, this technology could be important for Canadian farmers and could also be promoted and transferred to other countries.

Photovoltaic (PV) panel electrical outputs are rated according to industry Standard Test Conditions (STC) of 1000 W m^{-2} incident solar radiation at an operating cell temperature of 25 °C and under an absolute air mass of 1.5. Environmental conditions met outside the laboratory will cause a decrease in PV performance from the STC rating, the magnitude of which depends on the module technology. Many additional losses are incurred due to the inefficiencies in transferring energy from the PV panels to a load, such as a pump or battery bank, thus resulting in a secondary decline of performance. Though

there have been studies measuring outdoor performance of PV modules, there is a great need for further field studies of complete PV systems. Another important aspect would be the ability to model the potential solar radiation, PV power output, and subsequent water output for the purpose of irrigation scheduling. The results attained from this field research can be used to determine the viability of PV powered drip irrigation systems for a range of crop areas, and a variety of crop types in regions of similar latitude and climate.

1.1 Objectives

The overall objective of this research was to determine the feasibility of using photovoltaic (PV) modules to power a water pump for a small drip irrigation system in Ste. Anne de Bellevue (Québec, Canada). Specific objectives were to:

i. Predict the available solar radiation, using current and historical climate data from Ste. Anne de Bellevue and Montréal Pierre Elliott Trudeau International Airport weather stations, using the modified Hargreaves-Samani inland model.

ii. Predict the associated photovoltaic electrical output using a combination of module and installation specifications, meteorological input, and solar geometry.

iii. Predict the consequent water flow output using pump and installation specifications along with the PV input power.

iv. Determine the accuracy of the aforementioned models for this region of Québec through comparison with observed data from the field sites.

1.2 Scope

The duration of this project was just over one year from May 2005 to August 2006. The summer of 2005 was dedicated to the design and installation of the equipment and instrumentation. Data were collected late summer, to late fall 2005, after which, the winter experimentation was installed, and data collected from November 2005 to May 2006. It would have been ideal to collect further data in the summer of 2006, however, due to time and financial constraints this was not possible.

2.0 LITERATURE REVIEW

2.1 Energy and Water Use in Agriculture

Agriculture accounts for 2% of Canada's energy consumption by sector. Industry and transportation are the main consumers at 37% and 29%, respectively (International Energy Agency, 2003). Within the agricultural sector, the energy uses vary from the operation of irrigation systems and agricultural machinery, to that required for animal husbandry and maintenance. In the agri-food industry, there is great potential for a reduction of conventional energy consumption.

Complementary to the reduction of energy consumption is an increase in water use efficiency. In 2000, agriculture accounted for 12% of Canada's water use, as compared with industrial and domestic water use at 68% and 20%, respectively (FAO Statistics Division, 2004). According to Statistics Canada (Census of Agriculture, 2001), 784,451 hectares of land were under irrigation in 2001, which accounted for approximately 2% of the total cultivated land. The use of irrigation varies widely across the provinces, from 17% of total cultivated land in British Columbia to 0.4% in PEI. Table 2.1 shows this provincial distribution of dependence on irrigation, as presented in Madramootoo *et al.* (2006).

Table 2.1: Irrigated area in Canada

Table 1: Irrigated area in Canada, and proportion of total cultivated area, by province, 2001.

Province	Irrigated Area in ha	Percent of Total Irrigated Area	Irrigated Area % of Total Cultivated Area
British Columbia	111,181	14.2%	17.0%
Alberta	499,241	63.6%	4.6%
Saskatchewan	68,470	8.7%	0.4%
Manitoba	28,146	3.6%	0.6%
Ontario	49,271	6.3%	1.3%
Quebec	22,579	2.9%	1.2%
New Brunswick	1,145	0.2%	0.8%
Nova Scotia	3,491	0.4%	2.9%
Prince Edward Island	740	0.1%	0.4%
Newfoundland	187	--	2.2%
Canada	784,451	100%	1.9%

-- Less than 0.1 percent

Source: Statistics Canada (2001)

(Source: Madramootoo *et al.*, 2006)

The need for irrigation depends on location and crop type. In Western Canada for instance, the cereals in Alberta require irrigation due to the soil type and climate. However, those same cereals may or may not require irrigation in Manitoba, depending only on the soil type, as Manitoba is a wetter province over all (Madramootoo *et al.*, 2006). In Eastern Canada, on the other hand, irrigation is generally not a necessity. However, it is commonly used for specialty crops, such as fruits and vegetables. This is demonstrated by the percentages seen in the last column of Table 2.1. Irrigation can be very beneficial to the farmer as it allows them to diversify their land use, often including the addition of value-added crops and animal husbandry.

Irrigation systems in Canada vary from large, public infrastructures, where the system and water is governed by the municipality, to small, privately owned irrigation systems, where the water is drawn from a local source, such as a pond or well. The associated costs of these systems vary markedly. Publicly owned irrigation infrastructures involve large capital investment and high maintenance fees due to the diversion structures, storages, and canals required. Smaller, on-farm systems also have high capital costs, as well as increasing operation costs, as many small-scale irrigation systems are run using a motor or a generator, requiring fuel for operation. The cost of fuel is continually on the rise, as well as being a contributor to greenhouse gas emissions.

There are many different types of irrigation systems in use today, including flood, spray, and drip irrigation, each with their own advantages and disadvantages. Flood irrigation uses the gradient of the land so that water may flow through furrows by gravity. Once the land is appropriately graded, flood irrigation requires a limited amount of equipment, and is therefore inexpensive (Burt *et al.*, 2000). However, water use efficiency is quite low due to water loss from runoff and evaporation, and there is a greater occurrence of nutrient leaching, as water is able to percolate deeply. Spray irrigation, on the other hand, can be applied to any topography and is the most common type of irrigation used in Canada (Madramootoo *et al.*, 2006). It requires specialised equipment varying from centre pivots to hand-moved sprinklers. Though water use efficiency is greatly increased over flood irrigation, much water is still lost to wind and evaporation from the spray. Drip irrigation is mostly used for horticultural crops (Madramootoo *et al.*, 2006). The water use efficiency is high as it continually trickles a

small amount of water right to the base of the plant. The simplest of drip systems, which consists of drip tape and a pressure regulator, are inexpensive.

The use of drip irrigation powered by solar energy could contribute to the necessary long-term reduction of energy and water consumption in the agricultural sector.

2.2 Solar Energy Basics

Renewable energy sources are beginning to play more of a role in urban areas such as building integrated photovoltaics, as well as in rural areas where wind, solar, biomass, and geothermal are gaining in popularity. When it comes to replacing the mass energy production of fossil fuels, renewable energy has not yet proven to be practical. However, renewable energy sources do excel in local applications where there is limited or no access to an electricity grid, or where access to conventional energy is prohibitively expensive. They are most efficient in local applications because the energy production is at the same location as the end-use, thus minimising the need for energy storage and transport. Of the energy consumers within agriculture, the timing of irrigation requirements conveniently coincides with an increase in insolation or intensity of solar radiation, creating great potential for the union of irrigation and solar energy, specifically photovoltaics.

2.2.1 Photovoltaic cells and modules

Much like other active solar energy technologies, photovoltaics use the sun's energy to complete a task that would otherwise require the use of conventional electricity. Photovoltaic (PV) technology directly converts sunlight into electricity using semi conducting PV cells. Photovoltaic or solar cells are composed of semiconductor materials, such as silicon, single-crystalline thin films, and polycrystalline thin films. A key feature of solar cells is the built-in electric field. This is formed due to the differing semiconductor materials placed in contact with each other within the cell. One semiconductor is n-type that has an abundance of electrons, which have a negative charge, while the other semiconductor is p-type that has an abundance of "holes" with a positive electrical charge. Both semiconductors are neutral overall, but when placed in contact with each other a p-n junction is formed creating an electric field. It is this

electric field that facilitates the flow of current. PV technology is based on the photoelectric effect as discovered by physicist Edmond Becquerel in 1839 (Galdabini, 1992). The photoelectric or PV effect is the process through which a solar cell is able to convert sunlight, which is made up of photons, into electricity. Photons contain varying amounts of energy corresponding to the different wavelengths of light. The photons strike the solar cell and are either reflected, absorbed, or pass through. Those with a certain amount of energy are absorbed, enabling an electron to jump from the tightly bound valence band to the conduction band, where it is able to move around within the semiconductor. The electron will move from the n-type semiconductor toward the p-type side, thus forming part of the current in an electrical circuit. The built-in electric field provides the voltage required to drive this current through the external load (Michael and Khepar, 1989).

Individual PV cells are assembled into PV modules of varying capacity. PV modules are often combined to form PV arrays. They are combined in series to increase supply voltage, and combined in parallel when the application requires an increased current.

2.2.2 Balance of system (BOS) components

The electrical power from PV modules must be controlled and sometimes modified. PV modules are commercially available unregulated. This means that a rated 12 V panel will more typically give an output of 20 V on a sunny day, as indicated by the manufacturers. Included in this group of controllers, but not limited to, are battery charge controllers, which regulate the charge and discharge cycles of batteries; maximum power point trackers, which maintain the operating voltage of the array to a specific value that maximises the array output; inverters, which convert the direct current output of the array to alternating current that is required by many loads, such as AC motors and utility grids; and linear current boosters, which convert any excess voltage, over the rated value, into increased current at an efficiency of approximately 95%, as indicated by the manufacturers.

Another important BOS component of the PV system is energy storage capacity. Often, the application will require electrical energy on demand so that the solar panels are

used to charge batteries (during sunlight hours), in turn, the batteries then provide electricity when required. Deep-cycle batteries are most appropriate for PV application as they can withstand cycles of up to 80% discharge. Another method of storing energy is to use the solar power to pump water to a higher elevation, thus transferring the electrical energy to potential energy. Water pumps vary markedly, thus the selection of pump depends greatly on the application. Positive displacement pumps offer low volume with high lift capabilities, whereas rotating pumps are best for large water requirements over any lift. Floating and surface suction pumps offer a range of volumes at low lift only (RETScreen, 2004). Submersible pumps are the most efficient for use in a PV pumping system, as they eliminate the suction line (Michael and Khepar, 1989). Another aspect of the pump to consider is the type of motor. The motor can be DC or AC and the decision should be based on price, reliability, and the technical support that is available. Permanent magnet DC motors can connect directly to the PV array and are reliable, efficient, and operate over a wide range of voltages (Pulfrey *et al.*, 1987; Hsiao and Blevins, 1984). AC motors require the use of an inverter, but are less expensive and more readily available.

2.2.3 Current-voltage characteristics

Photovoltaic (PV) panel electrical outputs are rated according to industry Standard Test Conditions (STC) of 1000 W m^{-2} incident solar radiation at an operating cell temperature of 25 °C and under an absolute air mass of 1.5. Environmental conditions met outside the laboratory will cause a decrease in PV performance from the STC rating, depending on the module technology (Gxasheka *et al.*, 2005; van Dyk *et al.*, 2002). Important environmental conditions to consider are the insolation, ambient temperature, and wind speed (van Dyk *et al.*, 2005).

The insolation incident on the solar panels is maximised by the orientation of the module relative to the sun. This is because the reflection of the direct beam component of solar radiation, off of the panel surface, greatly increases when the angle of incidence, the angle between the beam incident on the surface and a line perpendicular to the surface, is greater than 60° (King *et al.*, 2002). Tracking panels that follow the movement of the sun decrease the angle of incidence, and therefore increase the amount of available solar

radiation (Duffie and Beckman, 1991). Two-dimensional tracking systems allow the panels to be directed toward the sun, maintaining an angle of incidence of 0° through all hours of the day and in any season. If tracking is not available, a good year round compromise is to mount the panels at an angle from the horizontal that is equal to the site latitude, facing solar South (when panels are located in the Northern Hemisphere). Otherwise, the optimal tilt angle varies with the seasons depending on the declination or the angular position of the sun at solar noon (Lewis, 1987). The tilt angle for each season should be the site latitude, minus the average declination for that season as further discussed in section 3.3.

The effect of irradiance levels on the performance of the solar array is governed by the module technology. Each module is defined by its rated parameters. One such parameter is the maximum power voltage, V_{mp}, which indicates the modules' behaviour or performance in low light conditions. This is an important variable to consider when the solar array will be situated in a typically cloudy location, where the levels of irradiance will be consistently less than the STC. Amorphous-silicon (a-Si) modules excel in this area when compared to other technologies. The V_{mp}, or voltage at the maximum power point, increases as the irradiance level decreases, allowing the a-Si modules to maintain a similar or higher voltage output at lower levels of irradiance, as compared to the operating voltage at STC (King *et al.*, 2002; Meike, 1998).

The operating cell temperature, which is governed by the panel mount, insolation, ambient temperature, as well as wind speed and direction, also plays an important role in module performance. It is well documented that as the temperature increases, voltage will decrease while current typically increases at a rate defined by the temperature coefficient of the module (King *et al.*, 2002; Meneses-Rodriguez, 2005). Voltage however, is more greatly affected, and thus there is an overall decrease on the power output and on the panels' actual efficiency (King *et al.*, 2002). This has been shown for various module technologies including crystalline silicon, polycrystalline silicon, and copper indium diselenide module types, which have strong, negative temperature dependence (del Cueto, 2002; King *et al.*; 2002; van Dyk and Meyer, 2000). However, the temperature dependence of the power output is not as straightforward for a-Si panels (Hishikawa and Okamoto, 1994). del Cueto (2002) found that a-Si modules show less

temperature dependence and that it is in fact positive. This means that as the temperature increases, the module efficiency increases within the operating cell temperature range of approximately 15 °C to 35 °C. This is explained by the hypothesis of Ruther *et al.* (2003) that the long-term power output of a-Si modules depends on both the environmental conditions, and the temperature history of light exposure. Ruther *et al.* (2003) go further in saying that if an a-Si module is operating at a higher temperature site, thus at higher operating cell temperatures, the module will stabilise at higher performance levels. In other words, a warmer climate could suggest a greater long-term performance from a-Si solar arrays. Further studies have been carried out (Gottschalg *et al.*, 2005) to suggest that long-term behaviour of a-Si modules may not be as straight forward as this. Moreover, to determine the unique drivers behind seasonal variations, each and every case would require long-term study and comparison to other sites, and that one sweeping generalisation would not be possible.

2.2.4 Photovoltaic application

The use of PV technology varies considerably, from PV cells in calculators and watches, to solar modules in telecommunications equipment and highway signs, to PV arrays for water pumping and generation of electricity in agricultural and rural areas.

Water pumping using photovoltaics may be the most common use of complete PV systems in both developed and developing areas. Water pumping applications include, but are not limited to domestic water, irrigation, livestock watering, and village water supplies. In combining irrigation and solar energy, a small PV system can be used to power a water pump for small-scale irrigation. PV water pumping for agriculture and irrigation is especially prevalent due to the correspondence of plant water requirements and solar availability. There are many advantages of using a PV system to generate power for water pumping.

The location of the system is very flexible in that it can be completely off-grid or grid-tied. Off-grid applications are where PV systems are most competitive against the alternatives: extension of a utility grid, disposable batteries, and generators of all types (diesel, gasoline or thermoelectric) (Hamza and Taha, 1995). The most common use of off-grid PV systems is the charging of batteries to provide electrical energy on demand

(RETScreen, 2004). Grid-tied refers to a system that is tied into the utility grid and therefore do not require the use of an energy storage device.

The setup of a PV system is also very flexible. The most efficient use of solar energy is when the panels are directly connected to the load. In fact, the success of water pumping lies partly with the elimination of the intermediate phase, namely the battery bank, for energy storage. With a direct connection between the PV array and the pump, water can be pumped during sunlight hours. The most efficient form of direct-connect systems is when the water is being pumped to an elevated storage tank, thus the electrical energy from the panels is converted to potential energy of the elevated water, to be used on demand, often by gravity (Hamidat *et al.*, 2003). The overall efficiency, from sunlight to water flow, has been recorded to exceed 3% (Daud and Mahmoud, 2005; Pulfrey *et al.*, 1987).

A less efficient, but more convenient setup is when there is intermediate energy storage in the form of a battery bank. This is less efficient as there are more points at which energy can be lost. However, it is more practical in terms of the requirement for electrical energy on demand. With the addition of a controller, both timing and power delivered can be automated. The overall efficiency of this setup varies and depends on such factors as type of battery selected, size of the battery bank, and any additional components. The typical life span of a solar panel is 25 years and though the initial investment can be quite large, the payback is usually within five to ten years, depending on the size of the system (RETScreen, 2004). PV systems are also easy to install and maintain.

2.3 Solar Radiation Modelling

Solar radiation is an important variable to consider when estimating the potential photovoltaic electrical output along with temperature, wind, and precipitation. The successful application of photovoltaics calls for the availability of long-term daily global horizontal solar radiation data, H (MJ m^{-2} d^{-1}). This is the total radiation incident on a horizontal plane at the earth's surface. Both historic and current climate data rarely include such solar radiation data, as there are a limited number of weather stations that have long-term solar radiation measurements. In fact, world wide the ratio of weather

stations collecting solar radiation data relative to those collecting temperature data, is estimated to be 1:500 (NCDC, 1995 as cited by Thornton and Running, 1999). On the rare occasion that the data is available it is often unreliable due to the meticulous maintenance required of the sensors, namely pyranometers, which need to be kept dust, dirt, bird, and snow free year round (Ouranos, personal communications 2006; Myers, 2005; Duffie and Beckman, 1991). Further sources of error include, but are not limited to shade-ring misalignment, incorrect sensor levelling, cosine response error, mechanical loading of cables, electric fields in the vicinity of the cables, spectral selectivity, and dark offset long-wave radiation error (Younes *et al.*, 2005; Li and Lam, 2004). It is for these reasons that many solar radiation prediction models have been developed around the world, which use only commonly measured climate data.

2.3.1 Extraterrestrial solar radiation

The prediction models can be empirical in nature in that they are site-specific and depend on the relationships between local solar radiation and climate data. The development of these models initially requires a large solar radiation data set to determine the appropriate site-specific coefficients. Mechanistic models on the other hand, once designed, are more robust geographically, but are much more complex to initially develop. Typical mechanistic models use extraterrestrial solar radiation, H_o (MJ m^{-2} d^{-1}), and atmospheric transmissivity, T_t, to determine the solar radiation at the Earth's surface, H (Ball *et al.*, 2004).

The site specific inputs for the calculation of extraterrestrial solar radiation are latitude and sunset hour angle. The extraterrestrial daily solar radiation (in MJ m^{-2} d^{-1}) is determined by Equations 2.1 to 2.4 (Allen *et al.*, 1998).

$$H_o = \frac{24(60)}{\pi} G_{sc} d_r \left[\omega_s \sin\varphi \sin\delta + \cos\varphi \cos\delta \sin\omega_s\right] \tag{2.1}$$

$$d_r = 1 + 0.033 \cos\left(\frac{2\pi}{365} n\right) \tag{2.2}$$

$$\delta = 0.409 \sin\left(\frac{2\pi}{365} n - 1.39\right) \tag{2.3}$$

$$\omega_s = \cos^{-1}(-\tan\varphi \tan\delta) \tag{2.4}$$

where G_{sc} = 0.082 MJ m^{-2} min^{-1}, solar constant

d_r = inverse relative distance Earth-Sun

δ = solar declination (rad)

ω_s = sunset hour angle (rad)

φ = latitude (rad)

n = number day of year (DOY).

A few models commonly employed will be discussed in the following sub-sections. They are: (1) Bristow-Campbell model (Bristow and Campbell, 1984), (2) Thornton-Running model (Thornton and Running, 1999; Thornton *et al.*, 2000) and (3) Hargreaves-Samani model (Hargreaves and Samani, 1982; Annandale *et al.*, 2002). Of these models, the modified Hargreaves-Samani inland model was identified to have the best performance for the Montréal region.

2.3.2 Bristow – Campbell model

The Bristow-Campbell model is based solely on an exponential relationship between solar irradiance and the daily temperature extremes. To reduce the effect of hot or cold air masses on the predicted solar radiation, it was important to include the mean of the two minimum temperatures on either side of the maximum daily temperature in the calculation of the daily range, ΔT. Also, the total transmittance for the day was used to relate ΔT and radiation, rather than using only the measured solar radiation. The transmittance takes into account both the direct and diffuse components of the incident radiation, thus incorporating the effect of atmospheric attenuation. The presence of rain is also addressed in this model. On a rainy day, the observed ΔT is adjusted to be $0.75\Delta T$. If ΔT on the day before rain occurs is more than 2 °C less than ΔT two days before the rain occurred, then ΔT for the day before the rain must also be adjusted to $0.75\Delta T$. By making these modifications, it is assumed that cloudy conditions begin the day before rain occurs and thus the incoming solar radiation is reduced. For long periods of rain, the adjustments are applied only to the first couple of days. This model was

developed for areas receiving most of their precipitation in the winter, and recognised that areas receiving most of the precipitation in the summer may experience different patterns.

The direct inputs for this model are DOY and daily maximum and minimum temperatures. These are used in conjunction with 3 site specific coefficients to determine the total transmission coefficient, T_t. In turn, T_t is used along with the extraterrestrial solar radiation (Equation 2.1) to determine the predicted horizontal solar radiation at the earth's surface.

The limiting factor of this model is the incorporation of 3 empirical coefficients A, B, and C. Coefficient A (or $T_{t,max}$) represents the maximum clear sky T_t characteristics dependent on the site area, which varies with location, elevation, and levels of pollution. The other two coefficients represent the division of energy particular to the site area, which partially depends on humidity. Though coefficient B can be determined using monthly mean ΔT, accurate solar radiation data is required at the site to determine the other two coefficients. This model requires calibration on a site-by-site basis, which is not conducive to on-farm general application purposes (Ball *et al.*, 2004; Thornton and Running, 1999).

2.3.3 Thornton - Running model

The Thornton-Running model is based on the Bristow-Campbell model. Thornton and Running reformulated the model to include the direct inputs of humidity, daily dew point temperature, and precipitation, along with the original DOY and daily maximum and minimum temperatures. Similar to the Bristow-Campbell model, these are used to determine the total transmission coefficient T_t, which can then be used along with the extraterrestrial solar radiation (Equation 2.1) to determine the horizontal solar radiation at the earth's surface. However, recognising the spatial and temporal variability of the maximum clear sky T_t characteristics ($T_{t,max}$ or coefficient A), they developed a more robust equation to determine this coefficient that does not require site specific solar radiation observations. This makes the model adequate over a much wider range of climates, as it is for the most part, independent of geographical location.

Thornton and Running (1999) acknowledged the limitations of a model based on the Bristow-Campbell model. The structure of this model is best for stable sky

conditions, including both clear and completely overcast skies, and leaves room for error during partially cloudy conditions. This is due to the fact that the model relies on two instantaneous measurements, namely the daily maximum and minimum temperatures, with the assumption that there is a smooth curve between the two. However, partly cloudy days cause a high variation in air temperature through out the day, nullifying the assumption of a smooth curve between the maximum and minimum temperatures. It is because of this that the model is most accurate on clear and entirely overcast days.

Another drawback is the necessity of the daily dew point temperature, which is not a commonly measured parameter. Kimball *et al.* (1997) devised a method for estimating the dew point temperature based on solar radiation, temperature, and precipitation. However, when solar radiation data is not available, the best estimate of the daily dew point temperature is to assume that it is equal to the daily minimum temperature (Allen *et al.*, 1998); this is especially true for areas that receive a lot of water. Finally, although the prediction of coefficient B is greatly improved in the Thornton-Running model, as compared to the original Bristow-Campbell model, there still exists great bias between varying climates as a result of this climatologically susceptible coefficient.

2.3.4 Hargreaves – Samani model

Hargreaves and Samani developed a model for predicting solar radiation, at the earth's surface, as a tool for estimating evapotranspiration in order to better understand crop water requirements (Hargreaves and Samani, 1982). An important aspect in the development of their predictive model, to ensure the widest potential efficacy, was to use only readily available observed climate data. Along with daily extraterrestrial solar radiation, the initial method to determine global horizontal solar radiation required only maximum and minimum daily temperatures in °C (T_{max} and T_{min}, respectively), as seen in Equation (2.5):

$$H = \kappa_H \times H_o \times \sqrt{T_{\max} - T_{\min}} \tag{2.5}$$

where κ_H = empirical coefficient based on climatic data.

To simplify calculations and to ensure geographical robustness, the region in question is determined to be either inland or coastal. An inland region, as defined by Annandale *et al.* (2002), is one whose weather patterns are dominated by a large landmass. Coastal refers to a region whose weather patterns are governed by a large body of water and whose inland width exceeds 20 km. Values for κ_H are then taken to be 0.16 for inland regions and 0.19 for coastal regions (Hargreaves, 1994 as cited by Allen, 1997; Allen *et al.*, 1998; Annandale *et al.*, 2002). The inland value can be applied year round, however, coastal predictions improve when two κ_H values are used for the different seasons (Allen, 1997). Furthermore, Allen (1997) indicated a need for a correction for site elevation, though the initial approach based on atmospheric pressure was not generally accepted. Thus, Annandale *et al.* (2002) modified the Hargreaves-Samani Equation (2.5) to include a factor for altitude as follows in Equation (2.6) for atmospheric transmissivity, T_t:

$$T_t = \kappa_H \times (1 + 2.7 \times 10^{-5} \times Alt) \times \sqrt{T_{\max} - T_{\min}} \qquad (2.6)$$

where Alt = site altitude, and the coefficient 2.7 x 10^{-5} accounts for the effects of reduced atmosphere thickness on solar radiation.

The atmospheric transmissivity along with extraterrestrial solar radiation are then used to determine the global horizontal solar radiation by Equation (2.7) as follows:

$$H = H_o \, x \, T_t \qquad (2.7)$$

This model assumes that the difference between maximum and minimum daily temperatures is an indication of the amount of cloud cover (Allen, 1997). This is because cloud cover reduces the amount of solar radiation reaching the earth's surface. A decrease in global solar radiation will reduce the maximum daily temperature while at the same time increasing the minimum daily temperature, because of the reflection of radiation by clouds throughout the night. Unlike the Thornton-Running model, this model assumes that the daily temperature range implicitly accounts for cloudiness,

including partially cloudy conditions. However, there are many other factors influencing the daily maximum and minimum temperatures such as wind speed, humidity, precipitation, and the movement of weather systems. These climate trends tend to follow long-term averages. This means that the aforementioned assumption would hold true only when employing this model on a monthly basis (Allen, 1997). Nonetheless, this model may be applied on a daily basis with the understanding that there will be less certainty and a larger prediction error (Allen, 1997).

Another drawback to the modified Hargreaves-Samani inland model, which also applies to the Bristow-Campbell and Thornton-Running models, is the lack of a coefficient for ground snow cover. Ground snow cover will greatly increase the activity of solar radiation at the earth's surface due to reflections between the snow and atmosphere, thus increasing the diffuse component of global solar radiation (Ellis and Leathers, 1999; Meek, 1997). This is also true, though to a lesser extent, for bare soil.

2.3.4.1 Selection of modified Hargreaves-Samani inland model

The benefits of using this model far outweigh the limitations. This is a simple, well respected model endorsed by the FAO (Allen *et al.*, 1998), which employs the original Hargreaves-Samani model to fill in missing or suspect solar radiation data for use in crop evapotranspiration predictions. The equations for the modified Hargreaves-Samani model are straight forward and minimal data inputs are required, making this a user friendly model for wide application. These include DOY and site latitude for calculation of the extraterrestrial solar radiation along with DOY, daily maximum and minimum temperatures, and elevation to determine the global solar radiation. This model does not require the user to know the duration of sunshine hours, as many other mechanistic models do (Rivington *et al.*, 2002). It also provides robust coefficients so that site specific calibration is not required. The modified Hargreaves-Samani inland model provides conservative estimates of global solar radiation for continental climates (Ball *et al.*, 2004). For the purposes of PV design this is a much better scenario than over predicting the available solar radiation as it helps to ensure an adequate supply of solar energy.

2.4 Photovoltaic Electrical Output Modelling

The PV array model is dependent on the module characteristics of the specific technology as well as the incoming solar radiation in the plane of the PV array. The module characteristics are used to determine the average array efficiency, η_p (%), whereas, the daily solar radiation in the plane of the PV array, H_t (MJ m^{-2} d^{-1}), is derived from the basic concepts of solar energy. The following Equation (2.8) represents the final step in determining the daily energy output from the PV array, E_{PV} (MJ d^{-1}), as given by RETScreen (2004):

$$E_{PV} = S\eta_p H_t (1-\lambda_p)(1-\lambda_c) \tag{2.8}$$

where S = the area of the array (m^2)

λ_p = miscellaneous PV array losses (%/100)

λ_c = other power conditioning losses (%/100).

2.4.1 Calculation of solar array efficiency

The average array efficiency is determined from the rated module characteristics for each specific solar panel technology. It is a function of the average module temperature, T_c (°C), as seen in Equation (2.9) given by Evans (1981):

$$\eta_p = \eta_r\left(1-\beta_p(T_c - T_r)\right) \tag{2.9}$$

where T_r = reference temperature (°C)

η_r = PV module efficiency at T_r (%)

β_p = temperature coefficient for module efficiency (%/ °C).

The average module temperature, T_c, is related to the mean daily ambient temperature, T_a, through Evans' Equation (2.10) (Evans, 1981):

$$T_c = \left(\frac{NOCT - T_{a,NOCT}}{G_{T,NOCT}}\right)(0.789 + 2.996K_T)\rho C_f + T_a \tag{2.10}$$

where $NOCT$ = nominal operating cell temperature (°C), specific to panel technology

$T_{a,NOCT}$ = ambient dry bulb temperature during NOCT test (°C)

$G_{T,NOCT}$ = instantaneous total solar irradiation on the array during NOCT test (MJ m^{-2}), taken at wind speed of 1 m s^{-1}

ρ = solar reflectance of optical components between the array and the sun

K_T = daily clearness index (Equation 2.11)

C_f = correction factor for panel tilt (Equation 2.12).

$$K_T = H/H_o \tag{2.11}$$

$$C_f = 1 - 0.000117(s_M - s)^2 \tag{2.12}$$

where s = actual panel tilt angle

$s_M = \varphi - \delta$, optimum tilt angle.

2.4.2 HDKR model: solar radiation in the plane of the photovoltaic array

The solar radiation in the plane of the PV array is affected by the beam, diffuse and reflected solar radiation components, which are continually changing. Because of this, there have been recent studies that actually use minutely data to determine the daily solar radiation in the plane of the PV array (Tamura *et al.*, 2003). Minutely observed data of extraterrestrial and global horizontal solar radiation is not readily available, therefore for applicability purposes, it is more suitable to use an hourly model to determine solar radiation in the plane of the PV array. The daily solar radiation in the plane of the PV array is the summation of the hourly solar radiation data in the plane of the PV array, h_t, during daylight hours, for each day of the year, $H_t = \Sigma\, h_t$. The hourly model can be separated into the required daily and hourly parameters.

The daily parameters include the following equations, previously defined in sections 2.3.1 to 2.4.1: daily horizontal solar radiation, H (Equation 2.7); daily extraterrestrial solar radiation, H_o (Equation 2.1); daily clearness index, K_t (Equation

2.11); daily inverse relative distance Earth-Sun, d_r (Equation 2.2); declination, δ (Equation 2.3); and sunset hour angle, ω_s (Equation 2.4).

To determine the hourly solar radiation in the plane of the PV array, the observed total solar radiation must be divided into its total, beam and diffuse components. The first investigations into the relationship between total and diffuse radiation, taking cloudiness into account, were carried out by Liu and Jordan (1960), which laid out the ground work for many correlations to follow. Liu and Jordan (1960) determined a correlation between diffuse and total solar radiation based on calculating the following non-dimensional parameters: the clearness index, K_t; the ratio of daily diffuse insolation on a horizontal surface to the extraterrestrial solar radiation, K_d; and K, the ratio of K_d to K_t. Because of the daily variability in cloud cover, Liu and Jordan (1960) established the correlation using long term averages of a solar radiation data set from Blue Hill, Massachusetts. Though the initial evidence suggested that this correlation was geographically robust, further correlations have been developed that are graphically dissimilar, indicating a latitude dependence (Ruth and Chant, 1976). These correlations include, but are not limited to: Stanhill (1966); Hay (1976); Ruth and Chant (1976); Tuller (1976); Orgill and Hollands (1977); Collares-Pereira and Rabl (1979); Iqbal (1979); and Erbs *et al.* (1982).

Ruth and Chant (1976) determined a graphical correlation for several Canadian sites, including Toronto, Ontario; Montréal, Québec; Goose Bay, Newfoundland; and Resolute Bay, North West Territories. However, for the purpose of application, a mathematical correlation is required for the hourly modeling. Collares-Pereira and Rabl (1979) defined the daily diffuse component, H_d, of solar radiation as a fourth degree polynomial, as seen in Equation (2.13), for $0.17 < K_t < 0.8$:

$$H_d = \left(1.188 - 2.272K_t + 9.473K_t^2 - 21.856K_t^3 + 14.648K_t^4\right) \times H \qquad (2.13)$$

This correlation agrees well graphically with the correlation for Montréal, Québec (Ruth and Chant, 1976), but falls above that of Liu and Jordan (1960).

The other daily parameters required involve solar geometry for a fixed, inclined solar panel. These include the following Equations (2.14 to 2.17) defined by Braun and Mitchell (1983):

$$\omega_{ew} = \cos^{-1}(\cot\varphi \tan\delta) \tag{2.14}$$

$$\sigma_{ns} = \begin{cases} 1\cdots if\varphi(\varphi-\delta) \geq 0 \\ -1\cdots otherwise \end{cases} \tag{2.15}$$

$$\sigma_{ew} = \begin{cases} 1\cdots if|\omega|\langle\omega_{ew} \\ -1\cdots otherwise \end{cases} \tag{2.16}$$

$$\sigma_{\omega} = \begin{cases} 1\cdots if\omega \geq 0 \\ -1\cdots otherwise \end{cases} \tag{2.17}$$

where ω_{ew} = absolute value of hour angle when sun is directly East or West

ω = hour angle, 15°/hr from solar noon (morning negative, afternoon positive)

σ_{ns}, σ_{ew}, and σ_{ω} = coefficients to determine hourly solar azimuth angle, γ_s (Equation 2.20).

Braun and Mitchell (1983) defined the hourly solar geometry parameters as follows, Equations (2.18 to 2.21):

$$\theta_z = \cos^{-1}(\sin\delta\sin\varphi + \cos\delta\cos\varphi\cos\omega) \tag{2.18}$$

$$\gamma_{so} = \sin^{-1}\left(\frac{\sin\omega\cos\delta}{\sin\theta_z}\right) \tag{2.19}$$

$$\gamma_s = \sigma_{ew}\sigma_{ns}\gamma_{so} + \left(\frac{1-\sigma_{ew}\sigma_{ns}}{2}\right)\times\pi\sigma_{\omega} \tag{2.20}$$

$$\theta = \cos^{-1}(\cos\theta_z\cos(s) + \sin\theta_z\sin(s)\cos(\gamma_s - \gamma)) \tag{2.21}$$

where θ_z = zenith angle (in rad)

γ_{so} = coefficient to determine hourly solar azimuth, γ_s (Equation 2.20)

γ_s = solar azimuth angle (in rad)

θ = incidence angle (in rad)

γ = surface azimuth (0° for panel facing South in Northern Hemisphere).

Further hourly parameters are determined using conversion factors from the equivalent daily values. Collares-Pereira and Rabl (1979) defined the factor, r_t, for the conversion from monthly average daily total horizontal solar radiation to monthly average hourly total horizontal solar radiation, as seen in Equation (2.22):

$$r_t = \frac{\pi}{24}(a + b\cos\omega)\left(\frac{\cos\omega - \cos\omega_s}{\sin\omega_s - \omega_s\cos\omega_s}\right) \tag{2.22}$$

where $a = 0.409 + 0.5016\sin(\omega_s - \pi/3)$ (2.23)

$b = 0.6609 - 0.4767\sin(\omega_s - \pi/3)$. (2.24)

Liu and Jordan (1960) defined the conversion factor, r_d, for the diffuse component of solar radiation, Equation (2.25), as:

$$r_d = \frac{\pi}{24}\left(\frac{\cos\omega - \cos\omega_s}{\sin\omega_s - \omega_s\cos\omega_s}\right) \tag{2.25}$$

The hourly components of solar radiation (total h, diffuse h_d, and beam h_b) can then be determined by multiplying the daily components by the conversion factors:

$$h = r_t H \tag{2.26}$$

$$h_d = r_d H_d \tag{2.27}$$

$$h_b = h - h_d \tag{2.28}$$

Hourly extraterrestrial solar radiation, h_o, is also required to determine the final solar radiation in the plane of the PV array. This is defined by Equation 2.29 (Allen *et al.*, 1998).

$$h_o = \frac{12(60)}{\pi} G_{sc} d_r \left[(\omega_2 - \omega_1) \sin\varphi \sin\delta + \cos\varphi \cos\delta \sin(\omega_2 - \omega_1) \right] \quad (2.29)$$

where ω_1 = solar time angle at beginning of hour (in rad) (Equation 2.30)

ω_2 = solar time angle at end of hour (in rad) (Equation 2.31)

and all other parameters remain as defined in section 2.3.1.

$$\omega_1 = \omega - (\pi/24) \quad (2.30)$$

$$\omega_2 = \omega + (\pi/24) \quad (2.31)$$

Equation (2.32) is the final step in determining the hourly solar radiation in the plane of the PV array, h_t, termed the HDKR (Hay, Davies, Klucher, Reindl) model by Duffie and Beckman (1991):

$$h_t = R_b (h_b + h_d A_i) + h_d (1 - A_i) \left(\frac{1 + \cos(s)}{2} \right) \left(1 + f \sin^3 \left(\frac{s}{2} \right) \right) + h \rho_g \left(\frac{1 - \cos(s)}{2} \right) \quad (2.32)$$

where R_b = ratio of beam radiation on the panel to that on the horizontal (Equation 2.33)

A_i = anisotropy index (Equation 2.34)

f = correction factor for cloudiness (Equation 2.35)

ρ_g = ground reflectance, 0.2 if average monthly temperature is greater than 0°C, 0.7 if less than -5°C, and $0.2 < \rho_g < 0.7$ by linear interpolation for temperatures in between these values.

$$R_b = \frac{\cos\theta}{\cos\theta_z} \quad (2.33)$$

$$A_i = \frac{h_b}{h_o} \quad (2.34)$$

$$f = \sqrt{\frac{h_b}{h}} \quad (2.35)$$

The daily solar radiation in the plane of the PV array is determined as the summation of the hourly solar radiation data in the plane of the PV array, h_t, during daylight hours, for each day of the year, $H_t = \Sigma h_t$. Daylight hours are determined as those hours where a positive, real number exists for hourly total solar radiation (h), hourly extraterrestrial solar radiation (h_o), and hourly solar radiation in the plane of the PV array (h_t). For direct comparison of predicted PV electrical output to observed PV power output, the hourly solar radiation data in the plane of the PV array was summed only between the hours of 9h00 and 16h00, and applied to Equation 2.8. This was due to the fact that the observed "daily" PV electrical output was monitored only during pump operation, between 9h00 and 16h00. In the same way, this daily (9h00 to 16h00) predicted PV electrical output could be applied to Equation 3.5 in order to determine the corresponding daily water flow.

2.5 Summary

As the cost of fuel continues to rise and the environmental affects of fossil fuel power become ever more apparent, discovering alternative energy sources as well as practical applications will become increasingly more important. Photovoltaic technology is continually improving, becoming more efficient in a range of environmental conditions, while at the same time decreasing in cost. PV water pumping is a common practice throughout many countries and can only improve in efficiency and effectiveness. Drip irrigation is a highly efficient and proven technology, which is applicable to a variety of crops. With an increasing understanding of solar radiation and the associated PV electrical output, further, more accurate prediction models will be developed. The union of photovoltaics and drip irrigation could be a positive step toward sustainable agriculture.

With this in mind, it was apparent that more research needed to be carried out in the field of photovoltaics and water pumping, both for practical and modelling purposes. The amount of water pumped is dependent on the amount of photovoltaic energy available, which is governed by the amount of solar radiation reaching the earth's surface at a given site. Therefore, the focus of this research was solar radiation and photovoltaic electrical output. Historical observed solar radiation data was used to validate the solar

radiation predicted by the modified Hargreaves-Samani inland model in the Montréal region. This, along with meteorological data, was used to predict the available photovoltaic energy. This prediction was compared to the observed PV energy from the field research carried out in 2005 and 2006. The field research involved monitoring electrical output and back-of-panel temperature of two 42 W solar panels, which were directly connected to a 12 V surface water pump. The pressure and flow of the water output was also monitored. The overall goal was to determine the accuracy of the models through the use of historical and monitored data, so that these models could then be applied to regions of similar latitude and climate for the design of future PV pumping systems.

3.0 MATERIALS AND METHODS

3.1 Site Selection and Description

The research was to be conducted from June to October 2005 at a field site located on Macdonald campus of McGill University. Due to unavoidable setbacks, such as delays in the arrival of equipment, the installation was not complete until August 2005. At the beginning of August 2005, system errors were revealed and corrected, such as leaks and clogging in the lines and calibration of the sensors was carried out. On account of this delay, it was decided that further studies would need to be performed throughout the winter and spring. Hereafter, summer installation will refer to the PV pumping system that was monitored from August 2005 to October 2005 and winter installation refers to the system that was monitored from November 2005 to May 2006. The summer and winter installations were kept as similar as possible and the actual data collection was consistent throughout.

The winter installation enabled an additional seven months of data collection, thus rendering the overall data set more valuable. Though the data collected in the winter was not considered practical in terms of irrigation requirements in the Montréal region, it was useful in the assessment of the selected models. And though not covered in this research, the winter experimental setup could prove to be helpful in diminishing costly greenhouse fees incurred by conventional irrigation and heating.

In the following sections, the summer and winter installations are explained in detail. To avoid repetition, from section 3.2 and on, they are discussed in the same sections as their similarities outnumber their differences. The SI system is used throughout, however, imperial units are included in brackets where standard sizing is usually measured in imperial units, such as pipe diameter and wire gauge.

3.1.1 Summer installation

The selection of this site was based on financial and time constraints. Several requirements also had to be fulfilled, including the proximity to a water source and an appropriate location to install a drip irrigation system as well as the need for an open, un-shaded space to promote optimum efficiency for the solar panels. The selected site was

located on Macdonald Campus of McGill University, on the north side of highway 40, near the Ste. Anne de Bellevue weather station and the Morgan Arboretum. This site was located at latitude 45.25 N, longitude -73.55 W and elevation 39 m (Environment Canada, 2006). Water for the small-scale drip irrigation system was provided from the pond on site. The drip irrigation system covered an area of approximately 400 m^2. An overall view of the summer installation and the water source are shown in Figure 3.1. The summer field setup is illustrated in Figure 3.2.

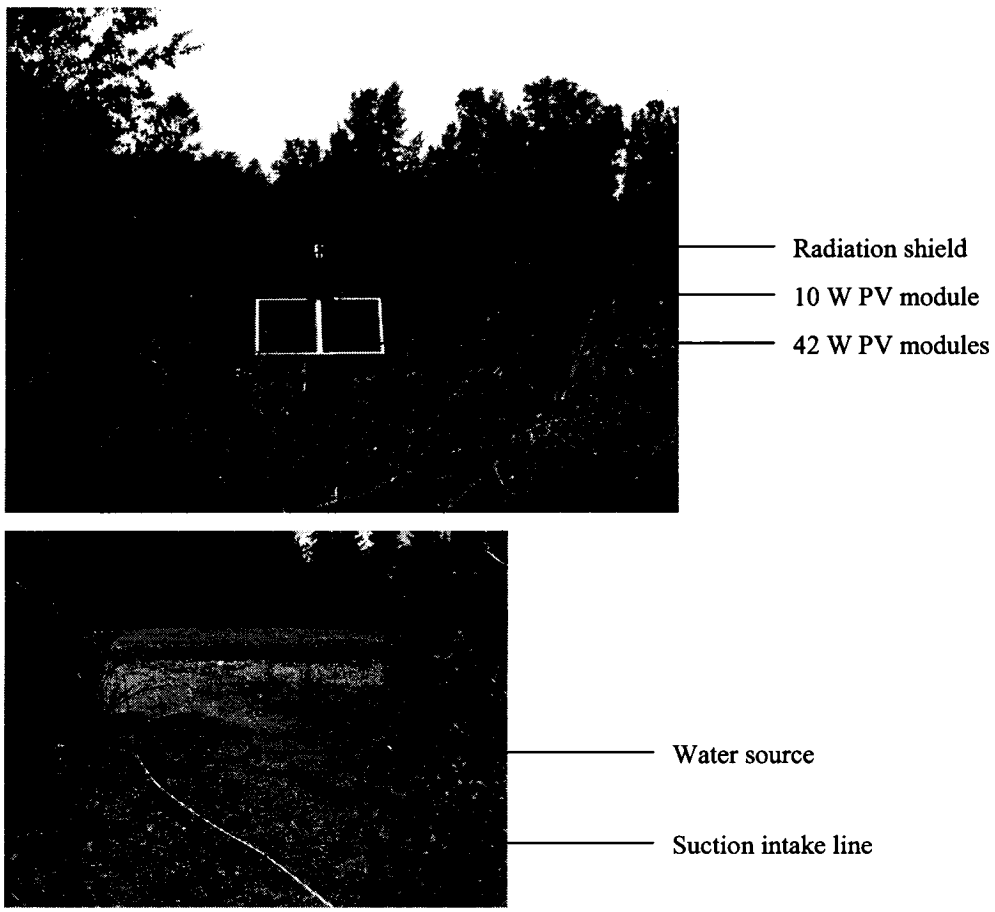

Figure 3.1: Summer installation and water source

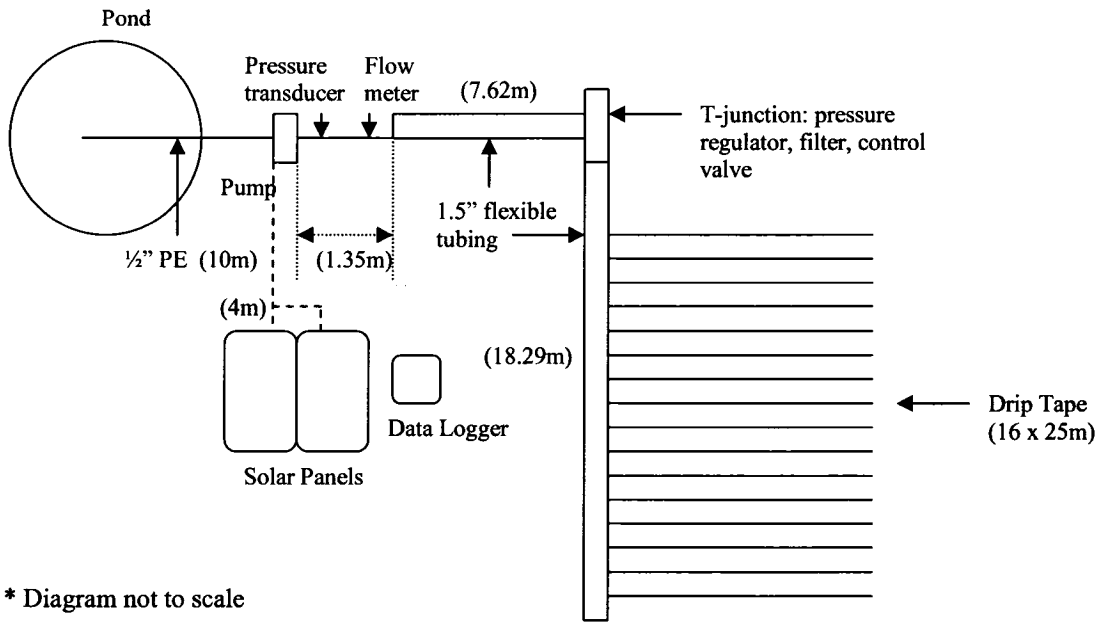

Figure 3.2: Summer field schematic

3.1.2 Winter installation

The selection of this site was based on the installation requirements. The solar panels and ambient temperature probe had to be installed outdoors in an open space. The water pump, piping, data logger, and sensors had to be installed indoors to prevent freezing. Distance between the two installations had to be minimal to ensure the lowest possible voltage drop due to resistance in the cables. It was decided to setup beside and within the new greenhouse on Macdonald campus, south of highway 20. This site was located at latitude 45.25 N, longitude -73.55 W and elevation 27 m (Environment Canada, 2006). On the south side of the greenhouse, the ambient temperature probe and the two solar panels were installed facing due south. The cables were run, 25 m, through a flexible conduit into the basement of the greenhouse. The water for the mock-up drip irrigation system was provided from a water reservoir 0.9 m in diameter and approximately 1.5 m in height. Water was pumped from the reservoir through a similar piping system and the same sensors as the summer experiment. Rather than continuing on to drip tape, the water was circulated back to the reservoir. The winter field setup is shown in Figure 3.3.

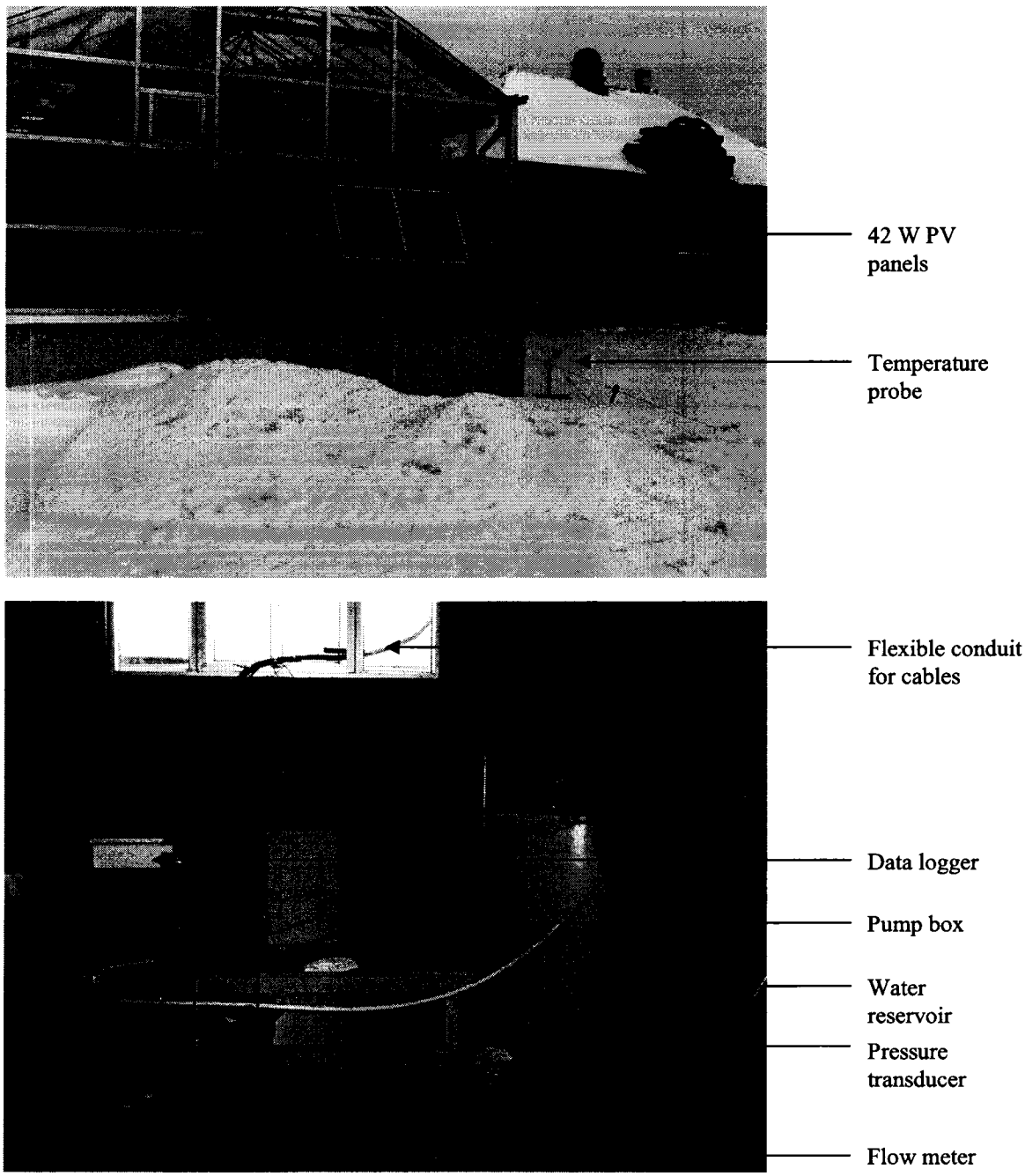

Figure 3.3: Winter installation – overall view

3.2 Equipment Selection and Description

3.2.1 Photovoltaic and water pump system

Equipment selection was carried out to provide all necessary equipment at minimal cost. Due to the nature of solar energy technology and research, the capital investment is inherently quite high. However, one goal of this research was to minimise

costs through appropriate compromise of such variables as pressure, condition of water source, and available power; therefore making this technology accessible to all interested. Initially, one 42 W solar panel (US42, Uni-Solar, Michigan) was to be purchased and used to power a 12 V submersible pump. The 42 W panel would have provided a nominal 12 V at 3 A to 3.5 A. However, a 12 V submersible pump, which required a maximum of 3 A for start-up and operation, proved to be quite costly, at approximately $900. A less expensive submersible pump would require larger current for start-up and operation, which would necessitate the use of a larger PV array. Therefore to keep the cost of the PV panels to a minimum, a 12 V positive displacement surface diaphragm pump (2088-443-144, Shurflo, California) was selected. It is important to note that a surface pump is intended to only pump clear water, unlike a submersible pump which is capable of handling brackish water. Therefore it was essential that a succession of appropriate filters be used to clean the pond water before it entered the pump. These filters were a minimal addition to the overall cost.

It was thus determined that the most cost effective system would be two US42 solar panels to provide sufficient current for the selected Shurflo 12 V surface water pump. To regulate the input voltage to the pump a linear current booster (PPT 12/24-7A, Solar Converters Inc., Ontario) was required between the solar panels and the pump. Also selected in this process was the least expensive drip irrigation system (PlastiTech, Québec), which consisted of drip tape and flexible hose for the main line. The total cost for the aforementioned components was approximately $1400. The cost for each component can be found in the Appendix.

3.2.2 Data logger and sensors

From prior experience and intended future use in the department, a Campbell Scientific data logger (CR23X-3, Campbell Scientific Canada Corp, Alberta) was selected along with all necessary components. The CR23X-3 was selected for the number of input channels, output power supply, rechargeable base, and ease of use. This data logger can operate on a small 10 W solar panel connected to the rechargeable battery and is therefore ideal for field installations where AC power is not an option.

The ambient temperature as well as the module cell temperature directly affects the electrical output of the solar panels. Ambient temperature was measured by one thermistor (107L, Campbell Scientific Canada Corp, Alberta) protected from direct sunlight by a radiation shield (41303, Campbell Scientific Canada Corp, Alberta). The back-of-panel temperature was measured using four T-type thermocouples, two fixed to the back of each panel, also shielded from direct sunlight. The four thermocouples were used to determine the average back-of-panel temperature. These parameters were recorded by the data logger and measured against the data logger reference temperature. It was possible to measure the voltage output of the solar panels directly by the data logger through a 10:1 voltage divider (VDIV10.1, Campbell Scientific Canada Corp, Alberta). The output current had to be measured by a through-hole DC current transducer (CR5210-5, HCS Heaters Controls and Sensors Ltd., Ontario). The CR Magnetics through-hole sensor, otherwise known as a Hall Effect sensor, was selected so as not to provide resistance and interfere with the true power measurements of the solar panels, which is the product of the current and voltage. The DC current transducer gave an output of 0-5 V, recorded directly by the data logger. The direct current voltage output was proportional to the DC current sensed.

The water flow pressure was measured by a non-submersible pressure transducer (PT 420, Druck via SRP Control Systems Ltd., Ontario), which gave a 4-20 mA output to be read by the data logger in voltage via a 100 ohm resistor (CURS100, Campbell Scientific Canada Corp, Alberta). The 4-20 mA output was proportional to the selected input range, in this case, 0-172.4 kPa (0-25 psi). A paddle wheel flow meter (F3.30.H.01, Chemline Plastics Ltd., Ontario) was selected for its relative low cost, ease of use, and 4-20 mA output, which is proportional to 0.15 m s^{-1} to 8 m s^{-1} of flow. Much like the pressure transducer, the 4-20 mA output of the flow meter was converted to a 0.4-2 V scale through a 100 ohm resistor to be read by the data logger.

3.3 Experimental Design and Instrumentation

3.3.1 Tilt angle

The main factors affecting the optimal tilt angle of the solar array include latitude, orientation with respect to the equator, season, and cloudiness (Lewis, 1987). In the

Northern Hemisphere, the panels must face south to maximise the incident solar radiation due to the position of the sun in the sky.

It is interesting to note that adjusting the tilt of non-fixed solar panels on a monthly basis has been observed to provide up to and over a 4% improvement in efficiency compared with fixed solar panels at the same latitude (Yakup and Malik, 2001; Kacira *et al.*, 2004), whereas tracking systems improved the daily PV power output on average by 20% - 25% (Nijegorodov and Jain, 1997; Kacira *et al.*, 2004; Vilela *et al.*, 2003; Al-Mohamad, 2004). When a photovoltaic pumping system is driven by a tracking array, the increase in volume of water pumped (37% - 41%) exceeds the gain in incident irradiance (19% - 24%) (Vilela *et al.*, 2003; Bione *et al.*, 2004). In this study, it was not practical to change the panel tilt on a monthly basis nor was it feasible to use a tracking device due to the associated cost. Therefore, a compromise was made to change the panel tilt angle on a seasonal basis.

The photovoltaic array was installed to face magnetic south. To determine the optimal angle in the summer and winter seasons, the declination or the angular position of the sun at solar noon, δ (in degrees), must be calculated (Cooper, 1969).

$$\delta = 23.45\sin(2\pi(284+n)/365) \qquad (3.1)$$

where n = number day of year (DOY)

and sin( ) is calculated in radians.

The tilt angle for the summer should be the latitude minus the average declination for the summer. Ste. Anne de Bellevue, Québec has latitude 45.25 N. The average declination is assumed to be 11.725° or one half of the maximum declination of $\pm$23.45° for June 21 (n=172) and December 21 (n=355), respectively. Therefore the optimal summer tilt angle for Ste. Anne de Bellevue is 33.525° and for winter is 56.975°, measured from the horizontal. Because the "summer" data was actually collected between August and October, the optimal tilt angle was taken to be 45°, approximately equal to the site latitude. The winter installation was fixed at 60°, slightly greater than the optimal tilt to avoid the collection of snow upon the panels.

3.3.2 Photovoltaic system and monitoring equipment

Two 42 W photovoltaic modules were mounted side-by-side on an aluminum frame that was fixed with U-bolts to a 51 mm (2") steel pipe and secured 1.2 m into the ground. In the summer, the panels were mounted 1.2 m above the ground surface for ease of installation and maintenance. In the winter, the panels were mounted 2 m above the ground surface to ensure they would remain free from shadow during the low sun of the winter months. The panels were positioned in a magnetic south facing direction at an angle of 45° from the horizontal in the summer and 60° in the winter.

The two 42 W solar panels were connected in parallel to increase the available current while keeping the voltage equal to that of one panel. In the summer, the panels were connected directly to the surface pump with wire of diameter 2.053 mm (12 AWG wire). The 2.053 mm diameter (12 AWG) wire traveled a distance of approximately 4 m to the pump, corresponding to a voltage drop of less than 3%. In the winter, the panels were connected directly to the surface pump with wire of diameter 2.588 mm (10 AWG wire). The 2.588 mm diameter (10 AWG) wire traveled a distance of approximately 25 m (through the flexible conduit) to the pump corresponding to a voltage drop of less than 5%. A linear current booster (located in the pump-box) was used to ensure that the voltage input to the motor was no greater than 14 V while at the same time maximising the available current, as the name suggests. The two DC current through-hole sensors were also located within the pump box to measure the current on either side of the linear current booster.

For the summer installation, the data logger battery was recharged by a small 10 W solar panel, which was secured with U-bolts to the steel pole directly above the two 42 W panels at a 90° angle from the horizontal to avoid any shading of the panels below. The data logger was also fixed to the steel pole with U-bolts beneath the mounting frame of the 42 W solar panels. During the winter installation, the data logger, located indoors, was charged by AC power in the greenhouse. The solar panel frames, negative output of the 42 W solar panels, and data logger were grounded to a copper rod fixed in the ground near the base of the steel pole.

In the summer installation, the temperature probe and radiation shield were positioned directly above the 10 W solar panel. For the winter installation, the temperature probe and radiation shield were fastened with a U-bolt to a 38 mm (1.5") pipe situated to the east of the panels, 1 m from the ground to ensure they would remain above the snow line.

Figure 3.4 shows the photovoltaic setup of the summer installation. The positioning of the panels, temperature probe, pump box, and data logger for the winter installation was seen in Figure 3.3. The thermocouples and copper grounding rod were positioned in the same way in both the winter and summer installations. The interior details of the pump box are shown in Figure 3.5.

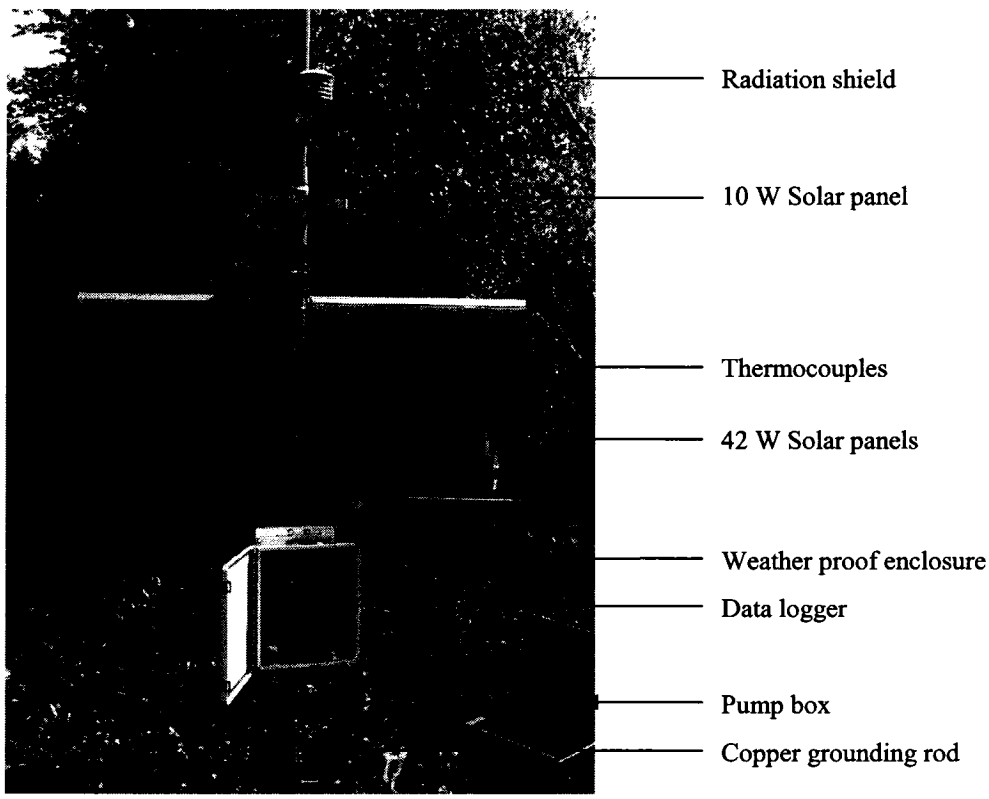

Figure 3.4: Photovoltaic system for summer installation

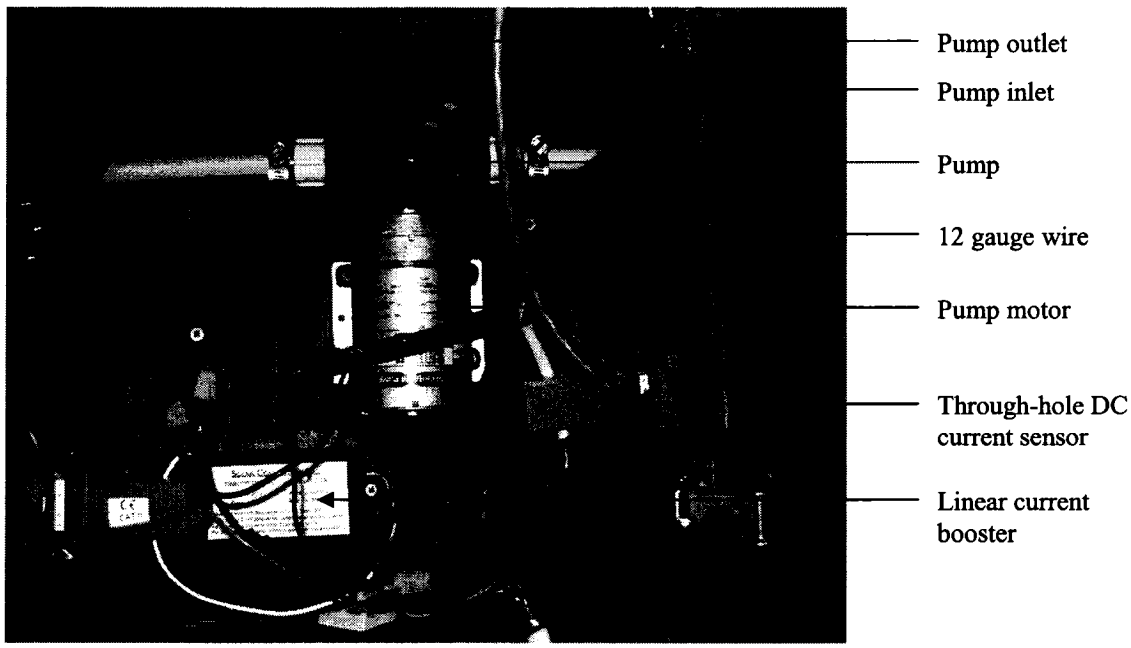

Figure 3.5: Pump box interior

Both the DC current sensors and paddle wheel flow meter required a power source. The paddle wheel flow meter required a supply voltage of 12 V, which was provided by the data logger itself. The DC current sensors, however, required a supply voltage of 24 V, which was not available directly from the data logger. Two rechargeable 12 V batteries connected in series were used to power the DC current sensors. The batteries were housed within the data logger weather proof enclosure (ENC12/14, Campbell Scientific Canada Corp, Alberta) and replaced approximately three to four times per month. Although this was practical for this particular study, in a remote location, it would be best to recharge these batteries with a 10 W solar panel. Two relays were also housed within the weather proof enclosure. Relays were used to toggle the solar panel and pump connection as well as the 24 V power source. The data logger was programmed to toggle "on" the relays at 9h00 and to toggle "off" the relays at 16h00 each day. This meant that the water pump was programmed to run for seven hours each day. Field observations and monitored parameters are discussed further in section 3.4. The data logger (CR23X-3) is shown in Figure 3.6. A schematic diagram of the data logger can be found in the Appendix.

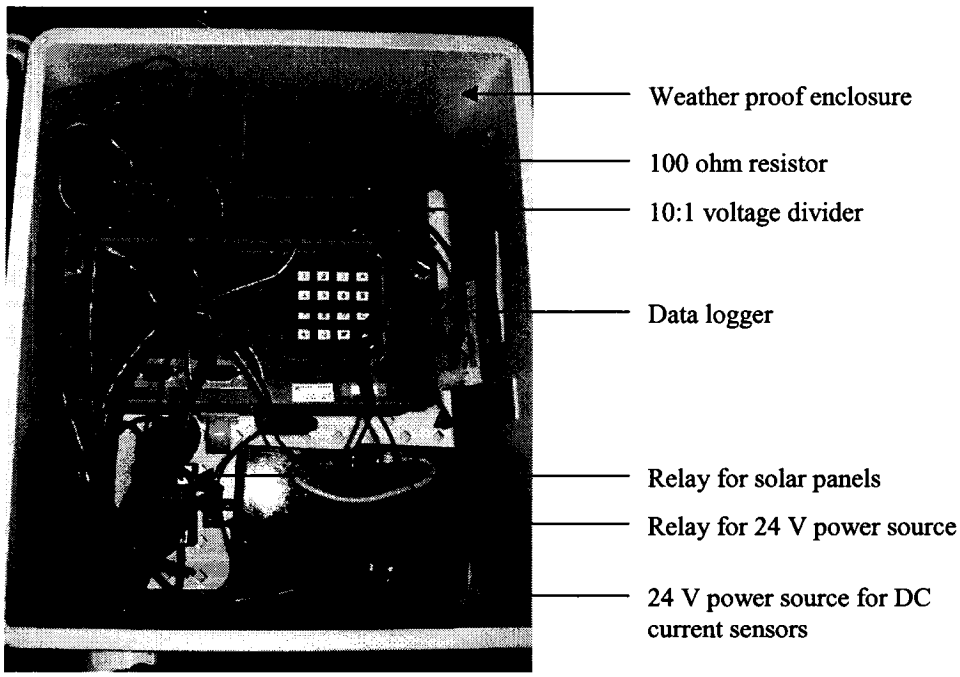

Figure 3.6: Data logger

3.3.3 Plumbing system and monitoring equipment

The surface pump was housed within a ventilated wooden box of 0.6 m x 0.4 m x 0.4 m. The main intent of the box was to protect the surface pump from rain and moisture, though it also provided security against theft and animals. The box was fixed to a 0.025 m x 0.10 m (1" x 4") plank of wood, approximately 1.5 m in length, which was used to stabilise the system. In the summer, two 0.025 m x 0.10 m (1" x 4") pieces of wood approximately 0.3 m in length were fastened perpendicular to the plank on either end, and secured approximately 0.2 m into the ground. This setup both stabilised and levelled the system. In the winter, the plank was secured to a large desk with four C-clamps to minimise vibration and to keep the system level.

For the summer installation, the pump drew water from the pond through 13 mm (½") polyethylene (PE) tubing of 10 m in length, and over an approximate rise of 2 m. It is important to note that the shorter the suction line, the more efficient the pump. Pump efficiency decreases when the intake line extends beyond approximately 5 m (Michael and Khepar, 1989). Due to the abundant algae growth in the pond (visible in Figure 3.1), a filter system was fixed to the intake end of the tubing, which consisted of three wire mesh layers of descending size from outer most to inner most, and finally a 50 mesh

intake filter (IRR S-84FV 3/8", PlastiTech, Québec) via a female adapter. This was designed to minimise the debris and algae that would inevitably enter the plumbing system, so as to prolong the life of the surface pump that necessitates the use of clear water. In the winter installation, the pump drew water from the reservoir through PE tubing, 5 m in length and over an approximate rise of 1 m.

The outlet of the pump was through the same 13 mm (½") PE tubing. The pressure transducer was located 0.72 m from the pump outlet to ensure a consistent flow. A male threaded T-junction was fit to the tubing as the attachment for the female threaded pressure transducer. The T-junction was secured to the plank of wood with two C-brackets. The paddle wheel flow meter was located 0.42 m from the pressure transducer and thus 1.14 m from the outlet, again to ensure a consistent, settled flow. An installation Tee fitting, designed specifically for the Chemline flow meter, was secured to the tubing. This Tee fitting was also secured to the plank with two C-brackets. In the event of air bubbles within the water flow, the flow meter was oriented on a 45° angle to increase the accuracy of measurement.

In the summer installation the total length of PE outlet tubing was 1.35 m, after which, it was coupled to 38 mm (1.5") flexible blue tubing (BOY LayFlat 1.5, PlastiTech, Québec). The flexible 38 mm (1.5") tubing extended 7.62 m to a T-junction, which consisted of a pressure regulator (IRR PR-075-L-12, PlastiTech, Québec), 155 mesh filter (1-0701-1151-1010, PlastiTech, Québec), and control valve. One side of the T-junction was open to a 38 mm (1.5") black oval hose (BOY ELD4040-060, PlastiTech, Québec) of 18.29 m in length. It was to this hose that the 16 lines of drip tape (203.2 μm - 0.3 m - 13.2 L min^{-1}, PlastiTech, Québec) were secured approximately 1 m apart. Each drip line was 25 m in length, thus forming an irrigation surface of approximately 400 m^2. For the winter installation, the total length of the PE outlet tubing was 7 m in which the water would circulate back to the reservoir.

Figures 3.7 and 3.8 show a detailed view of the plumbing system and associated sensors for the summer and winter installation, respectively.

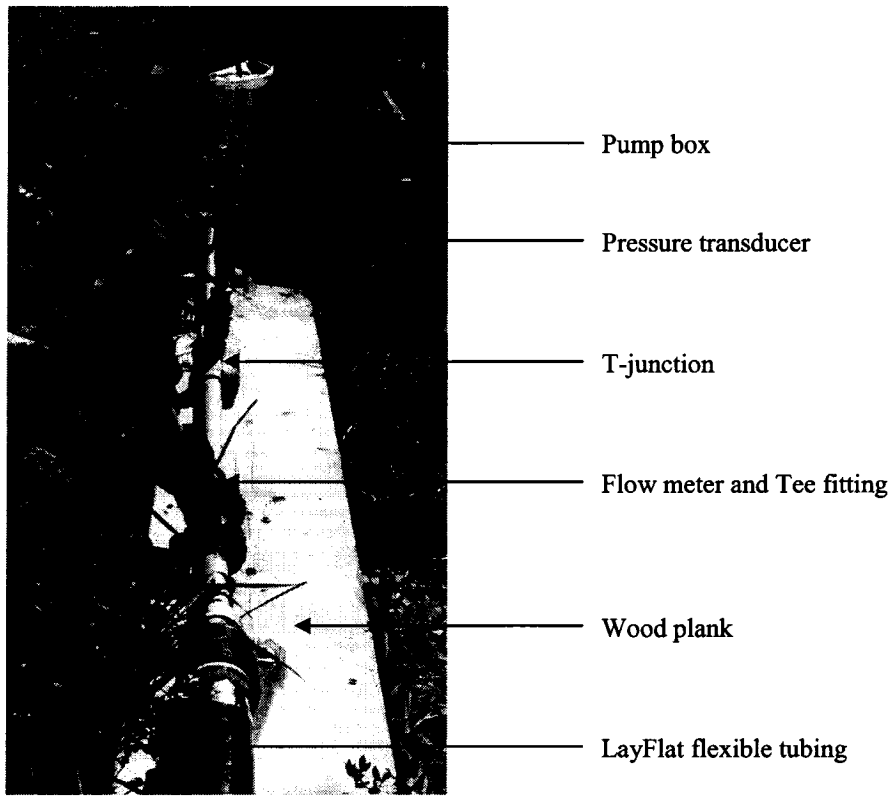

Figure 3.7: Summer plumbing

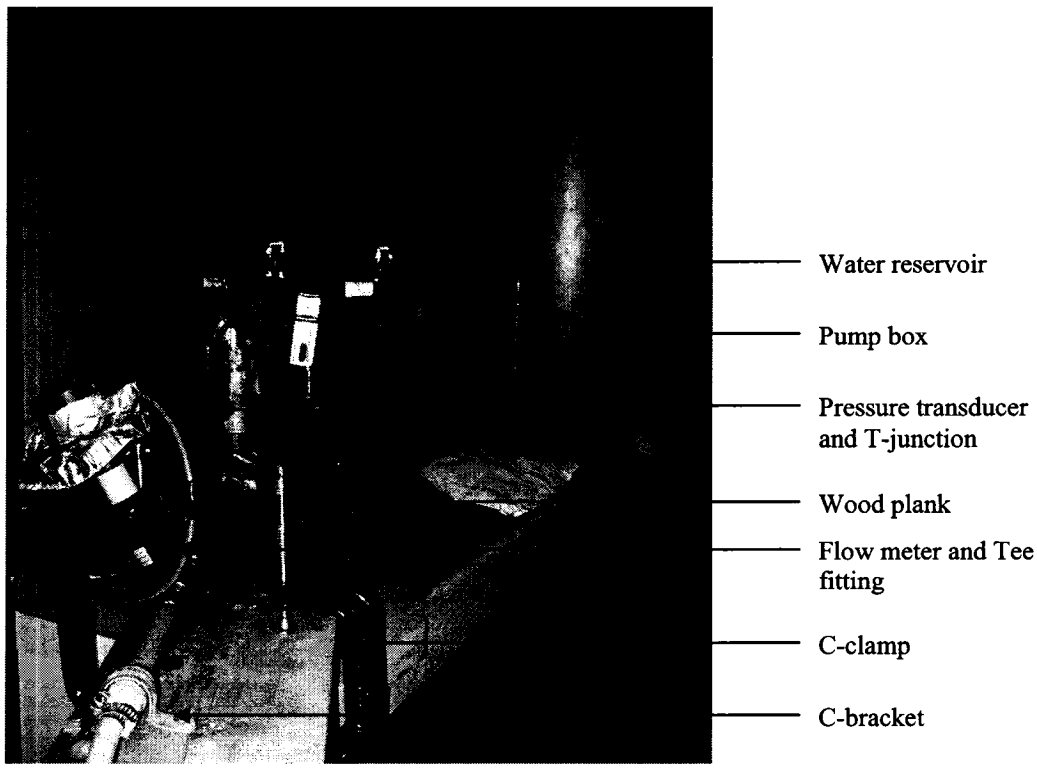

Figure 3.8: Winter plumbing

3.4 Field Observations and Measurements

3.4.1 Meteorological data acquisition

Important variables to consider for solar powered water pumping for irrigation are sunlight hours, solar radiation, precipitation, ambient temperature, relative humidity, as well as wind speed and direction. However, by using the modified Hargreaves-Samani inland model for the prediction of solar radiation, the meteorological inputs were minimised to the daily maximum and minimum temperatures. The Environment Canada weather station at Ste. Anne de Bellevue, located approximately 1 km and 3 km from the summer and winter field sites respectively, provided the daily average, maximum and minimum ambient temperature data as well as the daily precipitation. In the event of incomplete daily data, the Environment Canada weather station at Montréal Pierre Elliott Trudeau International Airport, located approximately 20 km from the field sites, provided the missing data.

The observed daily global horizontal solar radiation was required for comparison to the prediction model. Two sources of hourly solar radiation data were found for the Ste. Anne de Bellevue region, one from Mésonet (Mésonet, 2006) and the other from Ouranos (Ouranos, personal communications 2006). The Mésonet data, for Ste. Anne de Bellevue and Montréal Pierre Elliott Trudeau International Airport weather stations, did not exist prior to 2003, and the quality of the data had not been thoroughly checked before it was published. Alternatively, the hourly data collection available from Ouranos was instigated in 1988 with each hour checked and labelled for quality assurance.

3.4.2 Photovoltaic and water data acquisition

The voltage output of the two 42 W solar panels was measured directly by the data logger through a 10:1 voltage divider. It was measured continuously at 10 second sampling intervals, averaged and recorded every hour. As the solar panels were connected in parallel, the two voltages were expected to be the same. The ambient temperature was measured by one temperature probe shielded from direct sunlight. The temperature of the panels was measured using four T-type thermocouples, two fixed to the back of each panel, also shielded from direct sunlight. Both the ambient and module

temperatures were measured continuously at 10 second sampling intervals, averaged and recorded every hour.

The pump was programmed to run 7 hours per day from 9h00 to 16h00. Data was measured at 10 second sampling intervals and recorded every hour during this time for the current, pressure, and flow, all of which depend on an active pump. The measurements from the two Hall Effect DC current sensors (before and after the linear current booster) were periodically verified using a handheld multi-meter. The pressure transducer monitored the pressure of the flow 0.72 m beyond the outlet of the pump. The paddle wheel flow meter measured the rate of flow 1.14 m beyond the outlet of the pump. Pressure and flow at the pump outlet and at the drip lines were manually recorded several times throughout the course of the data collection to verify the accuracy of the sensors. The 10 second interval for sampling was selected for the abovementioned parameters due to the nature of the output, which was continually changing.

3.4.3 Field data analysis

3.4.3.1 Photovoltaic electrical output

The maximum difference observed between the hourly voltage measurements of the two solar panels was less than 0.1 V and the average observed difference was less than 0.01 V. As only one daily average voltage was required, the hourly averages of the individual panels were averaged to determine the overall hourly average voltage. This hourly average voltage was used to determine the daily average voltage by taking the average of the hours between 9h00 and 16h00 each day.

The hourly average current measurements were used to determine the daily average current by taking the average of the hours between 9h00 and 16h00. It was discovered through the DC current sensor verification, using a hand held multi-meter as well as the zero current data logger reading, that the DC current sensor observations were consistently recorded 0.32 A above the actual current. Because of this, the daily average current was calibrated by subtracting 0.32 A from the daily value. The daily average power was then determined as the product of the daily average voltage and the corrected daily average current, before the linear current booster.

The voltage at the output of the linear current booster was not continually measured. Because of this, the observed power determined for analysis was in fact the power directly available or the energy delivered from the photovoltaic modules. The results therefore do not account for the approximate 5% energy loss that occurs with the use of the linear current booster, which operates at 95% efficiency, as indicated by the manufacturer. However, due to the positioning of the data logger and DC current sensors (close to the load), the results do account for energy loss due to wire resistance. The percentage of voltage drop is a well-documented parameter that is governed by the amps drawn, voltage of the power source, gauge of the wire, and distance traveled. Each wire creates a resistance that is proportional to its cross-sectional area. Therefore the resistance increases as the gauge of the wire decreases. The voltage drop also increases with increasing distance that the current must travel. Because of this, the voltage drop expected in the summer was less than 3% and less than 5% for the winter installation (Windsun, 2006).

3.4.3.2 Water output

The water flow was monitored and recorded as an hourly average in L min^{-1}. Hourly averages were used to determine the daily average in L min^{-1} by taking the average between the hours of 9h00 and 16h00. The total daily flow was determined by multiplying the daily average in L min^{-1} by 60 minutes and 7 hours. The total monthly flow was determined by summing the appropriate DOY total daily flows.

3.5 Modelling

3.5.1 Solar radiation

The first step in determining the global horizontal solar radiation was to determine the extraterrestrial solar radiation. The daily extraterrestrial solar radiation was determined using equations (Equations 2.1 to 2.4) given in Allen *et al.* (1998). The input variables were DOY and site latitude, which was 45.25 N or 0.79 radians.

Daily global horizontal solar radiation was determined using the modified Hargreaves-Samani inland model. As seen in Equations 2.6 and 2.7, the input variables were DOY, site latitude, site elevation, and daily maximum and minimum ambient

temperatures. The site latitude was the same as that used to determine the extraterrestrial solar radiation, 45.25 N or 0.79 radians. Site elevation was determined to be 39 m, which is the same as that of the Ste. Anne de Bellevue weather station, located less than 1 km from the field site. As it was the inland model that was used, the empirical coefficient, κ_H, was taken as the nominal value of 0.16.

3.5.2 Photovoltaic electrical output

The predicted photovoltaic electrical output is governed by the module characteristics along with the available solar radiation in the plane of the PV array. Due to the fact that the observed power output takes into account the wire loss but not the power conditioning losses, Equation 2.8 was slightly modified to include only the miscellaneous PV array losses as seen in Equation 3.2.

$$E_{PV} = S\eta_p H_t (1-\lambda_p) \tag{3.2}$$

where $S = 1.38$ m^2 (area of the array)

η_p = average array efficiency

H_t = solar radiation in the plane of the PV array (MJ m^{-2} d^{-1})

λ_p = 5% summer, 7% winter (miscellaneous PV array losses).

Miscellaneous PV array losses include wire loss (3% summer, 5% winter) as well as dust and dirt collected on the panels, which account for an additional 2% power loss. To determine the average PV array efficiency, Equations 2.9 to 2.12 were applied. The module ratings for the Uni-Solar 42 W panels are as follows:

$T_r = 25$ °C (reference temperature)

$\eta_r = 6.1$ % (PV module efficiency at T_r)

$\beta_p = 0.11$ %/ °C (temperature coefficient for module efficiency)

$NOCT = 50$ °C (nominal operating cell temperature)

$T_{a,NOCT} = 30$ °C (ambient dry bulb temperature during NOCT test)

$G_{T,NOCT}$ = 2.88 MJ m^{-2} (instantaneous total solar irradiation on the array during NOCT test, taken at wind speed of 1 m s^{-1}).

The solar reflectance of optical components between the array and the sun, ρ, was assumed to be 1. To determine the correction factor for panel tilt (Equation 2.12), the optimal tilt angle was determined on a daily basis as the latitude, 45.25 N minus the daily declination. The actual tilt angle was taken as 45° from August 1, 2005 through to October 31, 2005 and 60° from November 1, 2005 through to May 31, 2006. The daily average array efficiency was then applied to Equation 3.2 to find the daily photovoltaic electrical output.

The HDKR model (Duffie and Beckman, 1991) was used to determine the daily solar radiation in the plane of the PV array, H_t, which is greatly affected by the beam, diffuse, and reflected components of the total global solar radiation. Because of this dependence on shifting skies, the daily total solar radiation in the plane of the PV array is in fact the sum of the hourly solar radiation in the plane of the PV array. The first step in this process was to determine the diffuse component of the daily total solar radiation by Equation 2.13. The input was the clearness index, which is determined in Equation 2.11, using the daily extraterrestrial and global solar radiation.

Further input parameters for this model, which is defined by Equation 2.13 through to Equation 2.35, included DOY, latitude, hour angle, panel tilt, and ground reflectance. The latitude remained consistent at 45.25 N as did the panel tilt which varied from 45° to 60° depending on the month. The hour angle varies by 15° per hour from solar noon. For hourly calculations, the value at the midpoint of the hour is used, as seen in Table 3.1.

Table 3.1: Hour angle, ω

Hour	ω (degrees)	ω (radians)
0.5	-172.5	-3.01
1.5	-157.5	-2.75
2.5	-142.5	-2.49
3.5	-127.5	-2.23
4.5	-112.5	-1.96
5.5	-97.5	-1.70
6.5	-82.5	-1.44
7.5	-67.5	-1.18
8.5	-52.5	-0.92
9.5	-37.5	-0.65
10.5	-22.5	-0.39
11.5	-7.5	-0.13
12.5	7.5	0.13
13.5	22.5	0.39
14.5	37.5	0.65
15.5	52.5	0.92
16.5	67.5	1.18
17.5	82.5	1.44
18.5	97.5	1.70
19.5	112.5	1.96
20.5	127.5	2.23
21.5	142.5	2.49
22.5	157.5	2.75
23.5	172.5	3.01

The ground reflectance, ρ_g, was determined on a monthly basis. The average monthly ambient temperature was calculated from the daily temperature averages. The ground reflectance was taken as 0.2 if the average monthly temperature was greater than 0 °C, 0.7 if less than -5 °C, and determined by linear interpolation between $0.2 < \rho_g < 0.7$ for temperatures between 0 °C and -5 °C, respectively. Table 3.2 shows the monthly average ambient temperature and associated ground reflectance coefficients (rounded to one decimal place) for August 2005 to May 2006 to be applied to the HDKR model.

Table 3.2: Ground reflectance, ρ_g

		Avg. Ambient Temp.	ρ_g
2005	Aug	21.15	0.2
	Sept	16.94	0.2
	Oct	9.76	0.2
	Nov	2.61	0.2
	Dec	-5.92	0.7
2006	Jan	-4.93	0.7
	Feb	-7.23	0.7
	Mar	-0.94	0.3
	Apr	7.24	0.2
	May	12.59	0.2

The hourly solar radiation in the plane of the PV array, determined by the HDKR model, was summed between the hours of 9h00 and 16h00 to establish the total daily solar radiation in the plane of the PV array, for the hours corresponding to the pump operation. This daily (9h00 to 16h00) total was then applied to Equation 3.2 to find predicted daily photovoltaic electrical output for direct comparison to observed PV electrical output. It is important to note that Equation 3.2 was used to determine the predicted PV electrical output for comparison to the observed PV electrical output. However, Equation 2.8 was used for the predicted PV electrical output for application to the water flow output model (Equation 3.5).

3.5.3 Water output

The wire to water efficiency is the product of the efficiency of the pump and the efficiency of the motor driving the pump. Pump efficiencies vary greatly depending on the technology and size. Typically, smaller capacity pumps are less efficient (< 50%) as compared with larger pumps. Combining a low pump efficiency with a typically low motor efficiency (approximately 50%), produces a very low overall wire to water efficiency (approximately 20 – 25%). Positive displacement diaphragm pumps tend to consume more power as the pressure increases. They can be hydraulically more efficient

(approximately 50%), though suffer from the same motor inefficiencies as other pump technologies (Evans, 2006).

With this in mind, there are several methods available to determine the expected volume of water given a certain input power. These methods differ in complexity as well as predictive accuracy and they depend on the available system information. The simplest method would be to use the pump specifications directly, which show the typical pump curve, and are provided by the manufacturer. However, this method would not fully take into account system pressure losses, such as pipe friction and changes in pipe diameter, which will vary from system to system. Thus, a more involved equation should be used when calculating the daily flow. Furthermore, a drip irrigation system requires the use of a pressure regulator between the drip lines and the pump. This causes a build-up of pressure at the pump outlet, as the pump is working to move the water and the regulator is restricting the flow. The resulting outlet pressure must also be taken into account when calculating the daily flow for a drip irrigation system. This is accomplished by converting the outlet pressure to equivalent head, combining the equivalent head with static head due to lift, thus determining a total head for the system.

The friction factor, *f*, is a function of the Reynolds number (Re) and the relative roughness of the pipe wall (*e/D*) which specifies the size of the bumps on the pipe wall relative to the diameter of the pipe. The Reynolds number indicates the type of flow (laminar, turbulent, or transitional) to be expected, and is determined from Equation (3.3) as seen in Munson *et al.* (1998).

$$\mathrm{Re} = \frac{\rho V D}{\mu} \tag{3.3}$$

where $\rho = 1000$ kg m^{-3} (density of water)

V = velocity of the fluid (m s^{-1})

D = diameter of the pipe (m)

$\mu = 1.12$ E -3 N s m^{-2} (dynamic viscosity of water at 15.6 °C).

Assuming an average flow velocity of 1 m s^{-1} and given the pipe diameter of 0.0127 m, the Reynolds number for the summer installation was 11340 kg m N^{-1} s^{-2}. This suggests turbulent flow, as Re > 3000. For turbulent flow, the friction factor may be determined by iteration using the Newton-Raphson method or by experimental curve fits, commonly the Moody chart, based on the Colebrook equation (Munson *et al.*, 1998).

$$\frac{1}{\sqrt{f}} = -2\log\left[\frac{e/D}{3.7} + \frac{2.51}{R\sqrt{f}}\right] \tag{3.4}$$

Equivalent roughness, *e*, for new drawn tubing is 0.0015 mm (Moody (1944) and Colebrook (1939), as referenced by Munson *et al.*, 1998). Thus, the relative roughness, *e/D*, is 0.000118. The relative roughness and Reynolds number were applied to the Moody chart (Munson *et al.*, 1998) to determine a friction factor, *f*, of 0.032.

The daily water delivered, *Q* (in L d^{-1}), was then determined using Equation (3.5) modified from RETScreen (2004) and Hrayshat and Al-Soud (2004).

$$Q = \frac{E_{PV}\eta_{sys}}{(\rho g(h_1 + h_2))(1+f)} \times 1000 \tag{3.5}$$

where E_{PV} = photovoltaic electrical output (J d^{-1})

η_{sys} = wire to water efficiency (%/100)

ρ = 1000 kg m^{-3} (density of water)

g = 9.81 m s^{-2} (acceleration due to gravity)

h_1 = 2 m (static head)

h_2 = 10.5 m, 14 m(equivalent head for 103.4 kPa, 137.9 kPa respectively), (Equation 3.6)

f = 0.032 (friction factor)

and 1000 is the conversion factor from m^3 to L.

The equivalent head due to outlet pressure is determined by Equation (3.6).

$$h_2 = \frac{p_{out}}{\rho g} \tag{3.6}$$

where h_2 = equivalent head (m)

p_{out} = outlet pressure (Pa)

and ρ, g remain as defined above.

The total head of a system can be determined in the same way, where outlet pressure is replaced with the total system pressure, the equivalent head then reflects the total head of the system. The wire to water efficiency was determined from the given pump specifications and applied to the water flow output prediction. The results are discussed in section 4.4.

4.0 RESULTS AND DISCUSSION

4.1 Meteorological Data and Analysis

Underlying all solar radiation prediction models, as well as photovoltaic electrical output models, are the meteorological inputs. These include the daily average, maximum, and minimum temperatures, daily precipitation, as well as the daily global horizontal solar radiation. Historically, these types of models have used long-term monthly daily averages, in both the development and application of the model, to predict the monthly totals. It is therefore imperative to understand how current meteorological data compares to the long-term averages.

The observed monthly temperature averages and total precipitation for August 2005 to July 2006 are shown in Table 4.1, along with the 30 year (1971-2000) temperature and precipitation data for Ste. Anne de Bellevue (Environment Canada, 2006). It can be seen that the observed monthly daily average temperatures are higher than the 30 year normal. Accordingly, the daily maximum and minimum temperatures also exceed the 30 year normal. The total monthly precipitation exceeds the 30 year normal except for December 2005, which falls 0.3 mm below the normal. In fact, the total precipitation for October 2005 is greater than the 30 year normal by more than 100 mm, and furthermore the monthly precipitation for February and March 2006 exceed the long term average by more than 200 mm.

Table 4.1: Ste. Anne de Bellevue - temperature and precipitation data

		Observed Data				*30 Year (1971-2000) Normal*			
		Temp. (°C)			**Precip.**	**Temp. (°C)**			**Precip.**
Year	**Month**	*Daily Avg*	*Max*	*Min*	*(mm)*	*Daily Avg.*	*Max*	*Min*	*(mm)*
2005	Aug	21	26.2	16.1	129.6	19.8	24.8	14.7	104.2
	Sept	16.7	21.8	12.1	99.6	14.6	19.5	9.7	96
	Oct	10.1	13.3	6.2	190.8	8.1	12.4	3.8	77.2
	Nov	2.6	6.9	-1.7	118.1	1.7	5.1	-1.8	86.4
	Dec	-5.8	-2.3	-9.5	77.9	-7	-2.7	-11.2	78.2
2006	Jan	-4.5	-1.1	-8.8	151.6	-10.4	-5.7	-15	67.8
	Feb	-7.2	-3.3	-11.2	261.2	-8.6	-4	-13.2	58.4
	Mar	-0.9	3.3	-5.2	271.9	-2.6	1.9	-7	71.4
	April	7.2	13.1	1.4	114	5.9	10.7	1	69.6
	May	14.2	19	9.4	167	13.2	18.6	7.7	71.4
	June	18.7	23.6	13.7	90.6	18.1	23.4	12.9	88.6
	July	22.2	27.1	17.2	135.2	21	26.2	15.7	93.6

(Source: Environment Canada, 2006)

These findings are an important indication of how the data for each month and year varies. As seen from Table 4.1, model predictions using long-term climate data may not fully represent the actual solar radiation and photovoltaic electrical output available from August 2005 to July 2006.

Observed global solar radiation data is much more difficult to obtain. It is not a commonly observed parameter and the quality of the data is often questionable. Long term hourly global horizontal solar radiation for Montréal Pierre Elliott Trudeau International Airport was available from Ouranos (Ouranos, personal communications 2006). Each hour was checked and labelled for quality assurance. Any missing or suspect hourly values, where the global solar radiation was greater than 0 MJ m^{-2} hr^{-1} (during sunlight hours), were taken as missing, thus rendering the entire day a missing value. The hourly values were totalled to determine the requisite daily global horizontal solar radiation.

4.2 Solar Radiation Prediction Results

Global horizontal solar radiation is a crucial variable to consider when designing a photovoltaic water pumping system. Not only does it directly affect the irrigation

scheduling due to crop evapotranspiration, it is also a direct input to PV electrical output prediction models. Therefore, for each locale, it is important to establish an accurate solar radiation prediction model in order to determine both the amount of water required and the amount of PV power available to deliver this water.

4.2.1 Total daily solar radiation

Six years (2000 to 2005) of observed global horizontal solar radiation data for the Montréal region were compared with the modified Hargreaves-Samani inland solar radiation prediction model. After eliminating days with suspect or missing hourly values from the observed data, this gave a data set of 2000 days. There were 21 days missing in year 2000, 110 days in 2001, 27 days in 2002, 12 days in 2003, 3 days in 2004, and 19 missing days in 2005. This gives a total of 192 days missing in the six year data set.

Figure 4.1 illustrates the distribution of solar radiation throughout the year. Logically, the maximum solar radiation occurs in the summer and the minimum occurs in the winter, with a smooth curve between the two extremes. It is apparent from Figure 4.1 that the modified Hargreaves-Samani inland prediction model for global solar radiation follows closely the observed global solar radiation. The maximum observed solar radiation, in 2004, was 32.14 MJ m^{-2} d^{-1}, which occurred on June 11, and the minimum observed solar radiation was 0.55 MJ m^{-2} d^{-1}, which occurred on November 29, 2004. The maximum predicted solar radiation occurred on June 14, 2004 at 28.94 MJ m^{-2} d^{-1}, and the minimum predicted solar radiation was 1.82 MJ m^{-2} d^{-1}, which occurred on December 12, 2004.

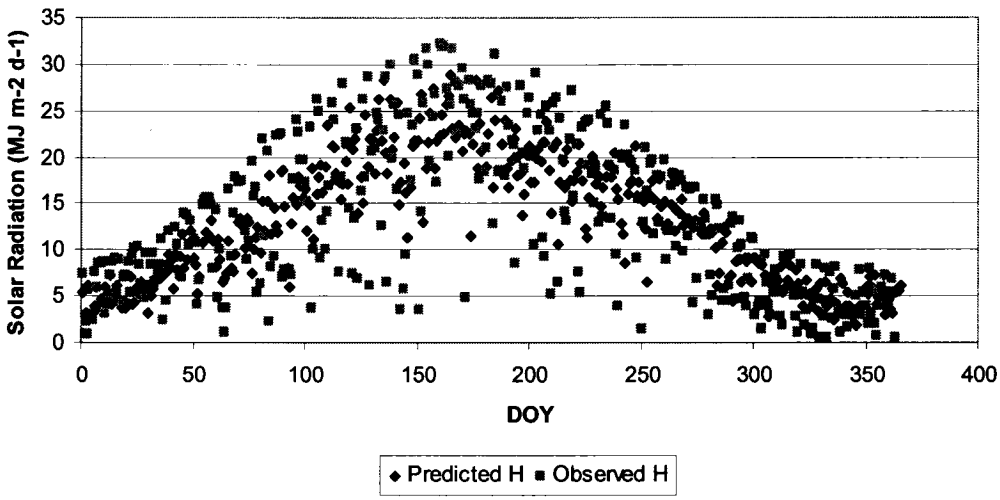

Figure 4.1: Daily global horizontal solar radiation (2004)

The observed solar radiation and predicted solar radiation values were assessed on a daily basis by linear regression. Performance of the modified Hargreaves-Samani inland model for global solar radiation was evaluated using the square of the correlation coefficient (r^2), bias, root mean square error (RMSE), and mean absolute error (MAE). Figure 4.2 illustrates the linear relationship between the predicted solar radiation at Ste. Anne de Bellevue, and the observed solar radiation from the Montréal Pierre Elliott Trudeau International Airport weather station as provided by Ouranos (2006). In Figures 4.2 and 4.8, the solid line represents the actual r^2 between the predicted and observed solar radiation and the dashed line represents the perfect fit, where $r^2 = 1$.

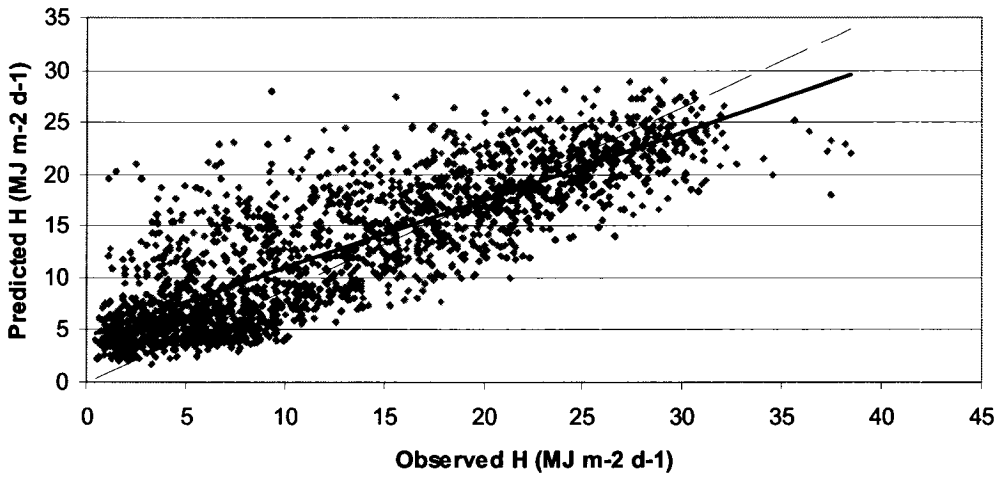

Figure 4.2: Daily global horizontal solar radiation (2000 – 2005)

On average, the modified Hargreaves-Samani inland model under predicted daily global horizontal solar radiation with a bias of -0.26 MJ m^{-2} d^{-1}. The overall r^2 value was 0.69 between the predicted and observed solar radiation data. A good correlation would give an r^2 value greater than 0.9, as suggested by Ball *et al.* (2004). RMSE and MAE were 4.82 MJ m^{-2} d^{-1} and 3.80 MJ m^{-2} d^{-1}, respectively.

There are several circumstances that could contribute to the discrepancies between the predicted and observed global solar radiation. The modified Hargreaves-Samani inland prediction model for global solar radiation was developed for general inland regions, meaning that the weather patterns should be governed by a large land mass rather than a large body of water. Although there are no exceptionally large bodies of water surrounding Montréal, it is an island nonetheless and therefore may not specifically fit the "inland" parameters. The development of a site specific model would likely improve the correlation; however this would initially require a significant amount of accurate solar radiation data, which is not easily attained. It has been recently shown by Ball *et al.* (2004), that use of a site specific κ_H coefficient with the modified Hargreaves-Samani model improves the predictive accuracy over the use of the nominal inland coefficient. However it was stated in the same paper, that where solar radiation data is not sufficient to develop a site specific coefficient, the nominal inland value is suitable.

Several factors related to the observed solar radiation data could also affect the correlation results with the predicted global solar radiation. For accurate solar radiation observations, the pyranometer requires meticulous maintenance, as it must remain dust, dirt, and snow free year round. However, given the quality assurance of the hourly solar radiation data from Ouranos (2006), this is not assumed to be a significant contributor to the r^2 value of 0.69. Another factor to consider, in terms of observed solar radiation, is the cloud cover. The modified Hargreaves-Samani inland model was used to predict the global solar radiation at the field site in Ste. Anne de Bellevue. However, due to a lack of observed solar radiation data at this site, the observed data was taken from Montréal Pierre Elliott Trudeau International Airport, located approximately 20 km from the field site. Though the temperature and precipitation data between these two sites does not significantly differ, it is possible that the continually shifting clouds would cause a difference in the observed daily solar radiation data at the two sites.

Finally, the modified Hargreaves-Samani inland model directly predicts the daily solar radiation, whereas the observed daily global solar radiation is in fact a sum of the hourly values for each day. Due to the changing cloud cover, in each day there will be many peaks and troughs that affect the overall daily observed value. It is thought that by taking monthly summations and using a 7 day moving average, these apparent differences will be reduced.

4.2.2 Monthly daily solar radiation

The overall performance of the modified Hargreaves-Samani inland model for daily global solar radiation, for the six year period for Ste. Anne de Bellevue, was better than the monthly performance. It can be seen that the performance of the model varies from month to month. Figures 4.3 to 4.6 illustrate a selection of the monthly differences in the linear regression, which are representative of the respective seasonal variations.

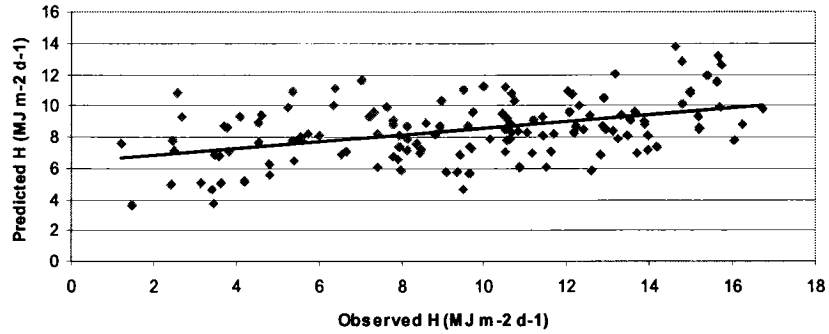

Figure 4.3: February - daily global horizontal solar radiation (2000 – 2005)

The number of data points for the February plot was 134 days. The square of the correlation coefficient was found to be 0.19 indicating a poor correlation between the predicted and observed solar radiation values. RMSE and MAE were less than the overall values at 3.67 MJ m^{-2} d^{-1} and 3.08 MJ m^{-2} d^{-1}, respectively. Much like the overall prediction, the February model under predicted the daily global horizontal solar radiation with a bias of -1.08 MJ m^{-2} d^{-1}.

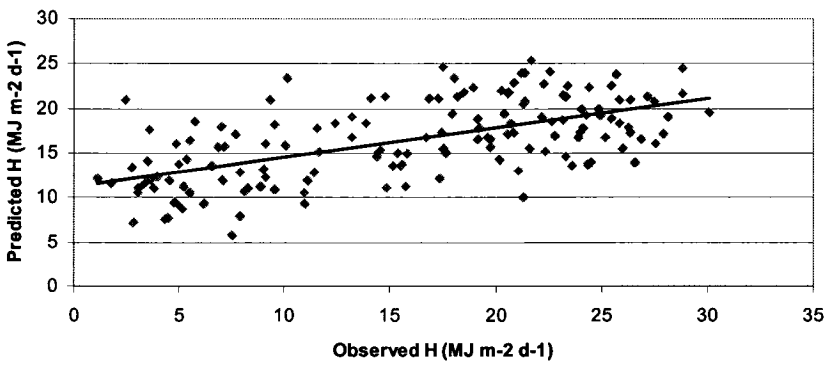

Figure 4.4: April - daily global horizontal solar radiation (2000 – 2005)

The number of data points for the April plot was 147 days. The square of the correlation coefficient was found to be 0.36 indicating a poor correlation between the predicted and observed solar radiation values. RMSE and MAE were greater than both the overall values and the other monthly values at 6.47 MJ m^{-2} d^{-1} and 5.36 MJ m^{-2} d^{-1}, respectively. The April model over predicted the daily global horizontal solar radiation with a bias of 0.59 MJ m^{-2} d^{-1}.

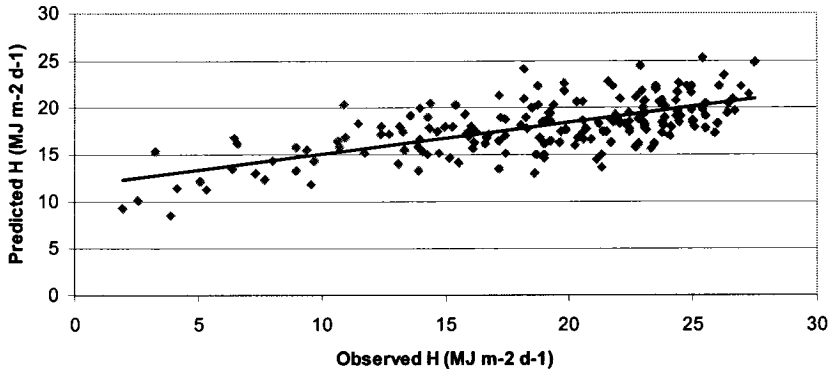

Figure 4.5: August - daily global horizontal solar radiation (2000 – 2005)

The number of data points for the August plot was 181 days. The r^2 value was 0.44. RMSE and MAE were 4.50 MJ m^{-2} d^{-1} and 3.83 MJ m^{-2} d^{-1}, respectively. The August bias was -0.73 MJ m^{-2} d^{-1}, thus under predicting the daily global horizontal solar radiation.

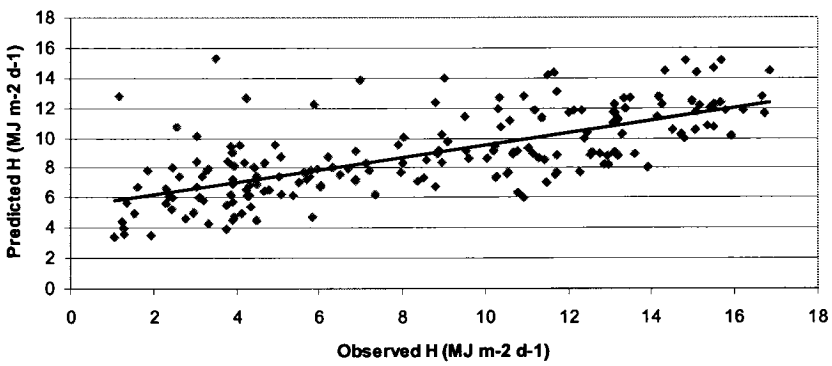

Figure 4.6: October - daily global horizontal solar radiation (2000 – 2005)

The number of data points for the October plot was 184 days. The r^2 value was similar to the August value at 0.46. RMSE and MAE were 3.35 MJ m^{-2} d^{-1} and 2.72 MJ m^{-2} d^{-1}, respectively. The October model, much like April, over predicted the daily global horizontal radiation with a bias of 0.46 MJ m^{-2} d^{-1}.

Monthly variations in the solar radiation prediction model performance can be grouped into seasonal variations due to the nature of the model. The modified Hargreaves-Samani inland model only takes the maximum and minimum daily temperatures directly into account. Although the assumption is that the daily temperature

range implicitly accounts for cloudiness, there are other factors that affect these maximum and minimum temperatures (Samani, 2004).

Actual cloud cover and precipitation contribute greatly to the amount of solar radiation reaching the earth's surface. This suggests that the modified Hargreaves-Samani inland model should under predict the available solar radiation in the months with less cloud cover; such as those in the winter, including January, February, and March, as well as those in the overall clear summer, which would include June through September. In those months with greater cloud coverage, the model would then likely over predict the available solar radiation. This would include the rainy spring period of April and May, as well as the typically overcast late fall and early winter, from October through to December. Another factor in the under prediction of global solar radiation is the effect of snow cover. Actual snow cover increases the amount of reflected radiation, therefore increasing the observed solar radiation. The monthly variations from 2000 to 2005 are summarised in Table 4.2.

Table 4.2: Modified Hargreaves-Samani inland model performance - daily

	Jan.	Feb.	Mar.	Apr.	May	June
N (days)	161	134	149	147	185	171
Mean Obs. H (MJ m^{-2} d^{-1})	5.91	9.51	13.43	15.89	18.88	22.04
Mean Pred. H (MJ m^{-2} d^{-1})	5.26	8.42	11.80	16.47	19.61	21.60
r^2	0.04	0.19	0.17	0.36	0.41	0.52
RMSE (MJ m^{-2} d^{-1})	2.79	3.67	5.72	6.47	6.47	6.13
Bias (MJ m^{-2} d^{-1})	-0.65	-1.08	-1.63	0.59	0.73	-0.44
MAE (MJ m^{-2} d^{-1})	2.31	3.08	4.97	5.36	5.31	5.21
	July	**Aug.**	**Sept.**	**Oct.**	**Nov.**	**Dec.**
N (days)	175	181	176	184	172	165
Mean Obs. H (MJ m^{-2} d^{-1})	21.54	18.73	14.86	8.46	4.67	4.22
Mean Pred. H (MJ m^{-2} d^{-1})	20.33	18.01	14.50	8.92	5.42	4.34
r^2	0.34	0.44	0.49	0.46	0.22	0.06
RMSE (MJ m^{-2} d^{-1})	6.45	4.50	4.31	3.35	2.65	2.17
Bias (MJ m^{-2} d^{-1})	-1.21	-0.73	-0.36	0.46	0.75	0.12
MAE (MJ m^{-2} d^{-1})	5.05	3.83	3.63	2.72	2.27	1.80

Assuming that the modified Hargreaves-Samani inland model is used to predict the global solar radiation available for a solar powered drip irrigation system, then the most important months to assess are those in the growing season, namely June through to September. As seen in Table 4.2 by the negative bias, the model under predicts the global solar radiation in these months. This suggests that for the design of a solar powered drip irrigation system, the modified Hargreaves-Samani inland model still proves to be useful on a monthly basis, despite the poor linear correlations and relatively large errors. This is due to the fact that a solar powered drip irrigation system designed on an under prediction of global solar radiation will function if more solar radiation is available. If the inverse were true, in that the solar radiation prediction model consistently over predicted during the growing season, this would in fact be a concern during the design phase of a solar powered drip irrigation system due to the potentially insufficient solar radiation actually available.

4.2.3 Seven day moving average solar radiation

To smooth the inevitable peaks and troughs of the observed and predicted daily solar radiation values, a 7 day moving average was used on the daily solar radiation data. The 7 day moving window was selected for the purpose of irrigation scheduling where the prediction of weekly average solar radiation would be useful. The effect of using a moving average, on both the predicted and observed solar radiation is demonstrated in Figure 4.7, which shows a comparison of 15 days in September, 2004. It can be seen that by smoothing the extremes of the solar radiation data through the use of the 7 day moving average, the model prediction is greatly improved. However, it continues to under predict, as was seen in the daily performance of the September model (Table 4.2).

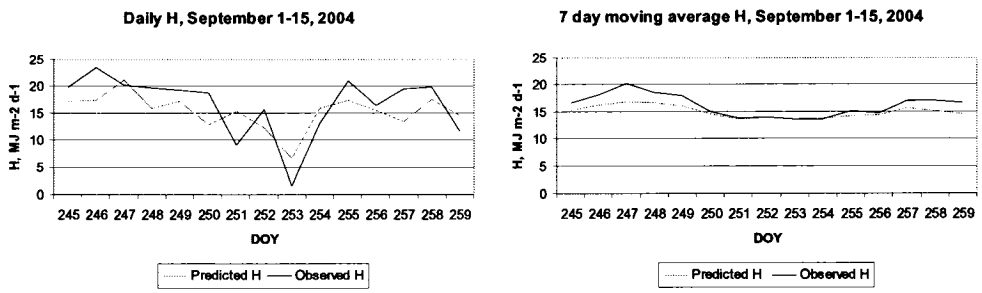

Figure 4.7: Comparison of daily to 7 day moving average solar radiation

The performance of the modified Hargreaves-Samani inland model for the prediction of global solar radiation with the 7 day moving average was then evaluated as before, for the total data set, as well as the monthly data sets. Figure 4.8 shows the improved linear relationship between the predicted and observed global horizontal solar radiation of the total data set, where N = 1994, as 3 days are lost on either end, due to the moving average.

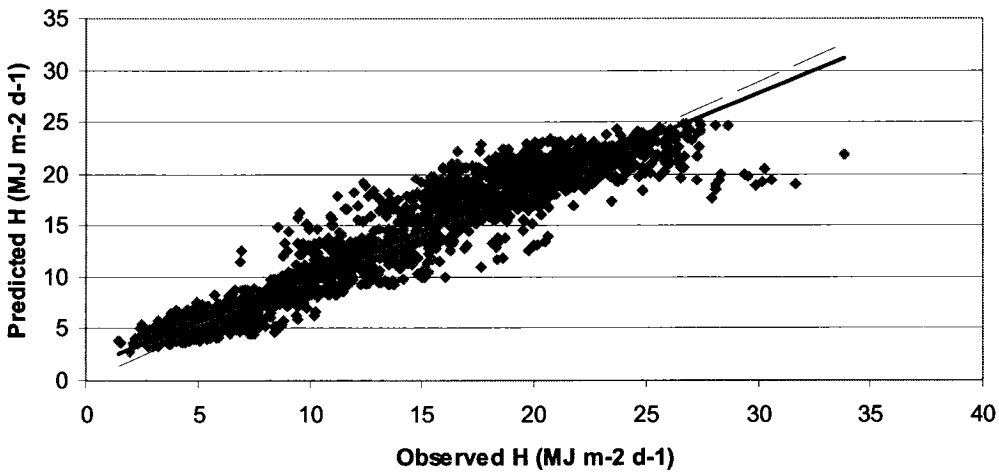

Figure 4.8: 7 day moving average global solar radiation (2000 – 2005)

The r^2 value was greatly improved to 0.91, representing a good correlation between the 7 day moving average of the predicted solar radiation and the 7 day moving average of the observed solar radiation. The bias was unaffected by the moving average,

however, both the RMSE and MAE were decreased to 2.10 MJ m^{-2} d^{-1} and 1.53 $MJm^{-2}d^{-1}$, respectively. This is a decrease of over 2 MJ m^{-2} d^{-1} for each error.

For the monthly data sets, Figure 4.9 is a representation of the improvement seen using the 7 day moving average on the observed and predicted solar radiation. Referring back to Figure 4.6, the reduced scatter is apparent in Figure 4.9.

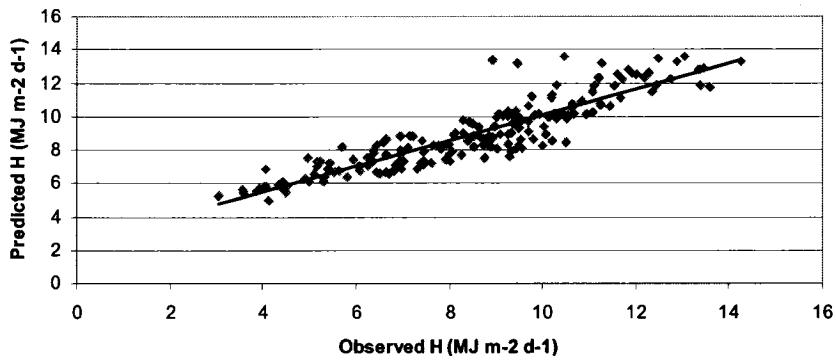

Figure 4.9: October - 7 day moving average global solar radiation (2000 – 2005)

Table 4.3 shows the improved r^2, RMSE, and MAE values from applying a 7 day moving average to the modified Hargreaves-Samani inland model. Correlation coefficients were greater for each month, excluding July, which saw a decrease in its r^2 value from 0.34 to 0.09. The greatest improvement in r^2 was seen in February with an increase of 0.41, followed by January and October, which both experienced an increase of 0.35. RMSE experienced the greatest reduction in spring with a decrease of 3.79 MJ m^{-2} d^{-1} in April and 3.99 MJ m^{-2} d^{-1} in May. This was followed by the summer months with reductions ranging from 2.87 MJ m^{-2} d^{-1} in July to 3.71 MJ m^{-2} d^{-1} in June. RMSE was least improved in January with a decrease of 1.16 MJ m^{-2} d^{-1}. MAE was also greatly decreased over the months, with spring having the greatest decrease of 3.14 MJ m^{-2} d^{-1} in April and 3.36 MJ m^{-2} d^{-1} in May. This was followed by the growing season with reductions ranging from 3.14 MJ m^{-2} d^{-1} in June to 2.52 MJ m^{-2} d^{-1} in September. MAE was least improved again in January with a decrease of 0.96 MJ m^{-2} d^{-1}. The bias remained relatively unaffected by the use of the 7 day moving average, on both the observed and predicted global solar radiation, for each month, with a range from a

decrease of 0.13 MJ m^{-2} d^{-1} in February to no change in April to an increase of 0.12 MJ m^{-2} d^{-1} in July. These changes are summarised in Table 4.3.

Table 4.3: Modified Hargreaves-Samani inland model performance – 7 day moving average

	Jan.	Feb.	Mar.	Apr.	May	June
N (days)	158	134	149	147	185	171
Mean Obs. H (MJ m^{-2} d^{-1})	6.04	9.36	13.33	15.84	19.02	21.98
Mean Pred. H (MJ m^{-2} d^{-1})	5.35	8.41	11.72	16.43	19.63	21.61
r^2	0.40	0.60	0.33	0.56	0.53	0.59
RMSE (MJ m^{-2} d^{-1})	1.63	1.53	2.84	2.68	2.48	2.42
Bias (MJ m^{-2} d^{-1})	-0.69	-0.95	-1.61	0.58	0.62	-0.36
MAE (MJ m^{-2} d^{-1})	1.35	1.16	2.25	2.22	1.95	2.08
	July	**Aug.**	**Sept.**	**Oct.**	**Nov.**	**Dec.**
N (days)	175	181	176	184	172	162
Mean Obs. H (MJ m^{-2} d^{-1})	21.60	18.81	14.80	8.43	4.75	4.20
Mean Pred. H (MJ m^{-2} d^{-1})	20.27	18.09	14.48	8.89	5.45	4.35
r^2	0.09	0.62	0.80	0.81	0.39	0.17
RMSE (MJ m^{-2} d^{-1})	3.58	1.59	1.37	1.15	1.26	0.78
Bias (MJ m^{-2} d^{-1})	-1.33	-0.72	-0.32	0.47	0.71	0.15
MAE (MJ m^{-2} d^{-1})	2.44	1.26	1.11	0.91	1.05	0.62

The modified Hargreaves-Samani inland model would be utilised to evaluate the available solar radiation during the growing season, in order to correlate with the irrigation scheduling. For the purpose of irrigation, a prediction of weekly average solar radiation may be more useful than the prediction of daily solar radiation values (Ball *et al.*, 2004). In this case, one can say that the modified Hargreaves-Samani inland model with a 7 day moving average of the predicted solar radiation gives a good overall result for Ste. Anne de Bellevue. Monthly, the 7 day moving average for the October data produces the most reasonable result with the highest r^2 value and second lowest RMSE and MAE. This does not coincide agreeably with crop water requirements. However, given the improvement of the solar radiation prediction model, with the use of the 7 day moving average for the spring and summer RMSE and MAE, it can be said that this would also be an adequate prediction for the purpose of irrigation scheduling and the design of a PV pumping system.

As the modified Hargreaves-Samani inland model uses temperature data to predict the global horizontal solar radiation for that specific DOY, it should be noted that the effectiveness of the model for future irrigation scheduling would be restricted to those years that are similar to the modelled year with respect to climate data and weather patterns (Ball *et al.*, 2004).

4.3 Photovoltaic Electrical Output Results

In the following sections (4.3 and 4.4), daily observations and daily predictions of PV electrical output and water flow output are considered. Observed PV electrical output was only monitored while the pump was operating as it was only then that a current was being drawn and thus generating power, as per the equation: P = VI. Given that both PV electrical output and water flow output observations were dependent on pump operation, the pump was programmed to operate for the same hours each day, from 9h00 to 16h00 for consistency. This meant that the "daily" total of observed PV power and observed volume of water pumped was in fact the total observed PV power used in 7 hours and the total volume of water pumped in 7 hours. For realistic comparison of observed PV electrical output and water flow to the corresponding predicted values, this same time frame must be considered in the predictions.

4.3.1 Photovoltaic electrical output and temperature

The performance of the photovoltaic array is dependent on the intensity of incident solar radiation, but also on the cell temperature. Temperature usually has a negative effect on solar module technologies, except for a-Si modules. Typically, an increase in cell temperature will cause a decrease in voltage and an increase in current. However, a-Si modules have shown less temperature dependence as well as a positive reaction, meaning that when the cell temperature increases, both the voltage and current increase, and therefore the overall output power increases. Figures 4.10 and 4.11 illustrate this trend. The voltage is the observed daily average voltage, between the hours of 9h00 and 16h00. The temperature in these plots is the observed daily average back-of-panel temperature (from 9h00 to 16h00). The back-of-panel temperature is as close an approximation as possible to the actual cell temperature. The back-of-panel temperature

is a suitable parameter to illustrate the relationship between temperature and photovoltaic output (Meike, 1998).

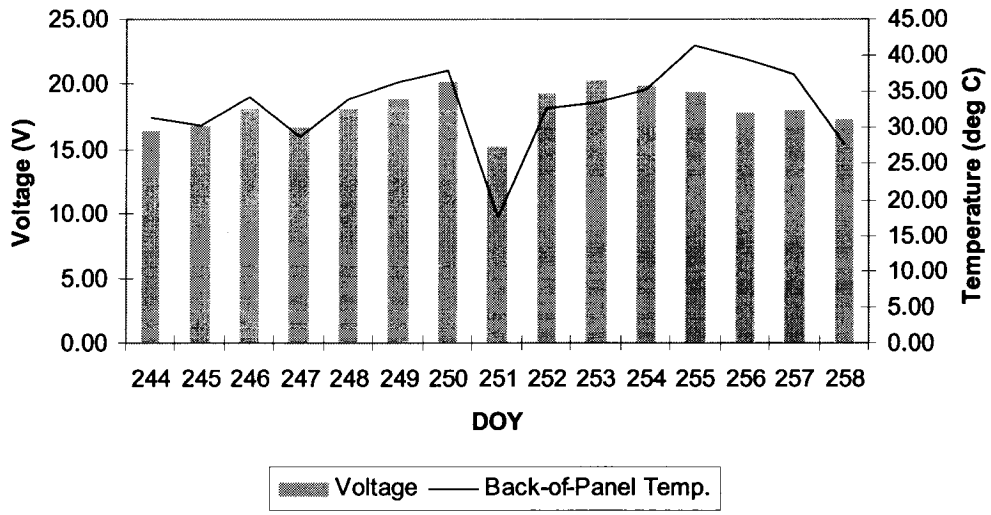

Figure 4.10: Back-of-panel temperature vs. voltage, September 1-15, 2005

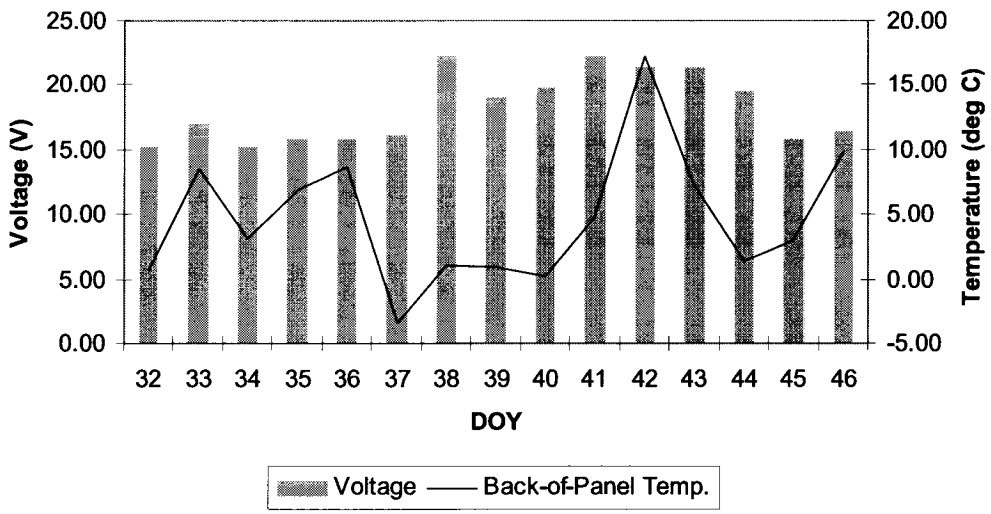

Figure 4.11: Back-of-panel temperature vs. voltage, February 1-15, 2006

del Cueto (2002) found the relationship where a rise in temperature results in an increased voltage to be true between the operating cell temperatures of 15 °C and 35 °C. Beyond this temperature range, the data was not consistent. This could explain why the relationship is most clearly demonstrated in Figure 4.10, where the daily average back-of-panel temperature exceeded 35 °C for only a few days. Though the trend is still apparent

in the winter months, it is not as clearly illustrated in Figure 4.11, where the daily average back-of-panel temperature remains below 15 °C for all but one day.

The operating cell temperature, and therefore back-of-panel temperature are governed by the type of panel mount, insolation, ambient temperature, as well as wind speed and direction. The panel mount was free standing, which allowed air to flow freely over the front and back surface of the panels. Because of this mounting design, seasonal variations in wind direction, and the effects of this wind on the panels may have accounted for the slight differences in the daily back-of-panel temperatures. As the panels were facing south, panel 1 was on the east side and panel 2 was on the west side. It is possible that long periods of rain, associated with the spring, resulted in more prevalent easterly winds, to which the eastern most panel would have been more exposed. Conversely, westerly summer winds would have exposed the western most panel to greater cooling. Table 4.4 shows the monthly average difference between daily average back-of-panel temperature and daily average ambient temperature (between the hours of 9h00 and 16h00) for each panel.

Table 4.4: Monthly average difference between back-of-panel and ambient temperatures

	Aug.	Sept.	Oct.	Nov.	Dec.	Jan	Feb.	Mar.	Apr.	May
Panel 1* (°C)	9.30	9.87	5.51	2.86	4.32	4.65	6.42	7.20	4.60	3.64
Panel 2** (°C)	8.99	9.53	5.41	2.45	4.93	5.27	7.49	8.61	7.26	5.68

*$Panel\ 1 = T_{panel\ 1} - T_{amb}$ **$Panel\ 2 = T_{panel\ 2} - T_{amb}$

There is also a direct relation between ambient temperature and back-of-panel temperature. Figure 4.12 illustrates that with a rise in ambient temperature, back-of-panel temperature also increases, but not always proportionally. Between August 2005 and May 2006, the maximum difference between daily average back-of-panel temperature and daily ambient temperature was 24.42 °C on February 11, 2006, when the ambient temperature was -7.12 °C and the panel temperature was 17.3 °C. The minimum difference between the two temperatures was 0.03 °C on November 24, 2005, when the ambient temperature was -3.16 °C and the panel temperature was -3.13 °C. The

differences between ambient temperature and back-of-panel temperature vary due to the intensity of solar radiation. On a cloudy day, the back-of-panel temperature will not greatly exceed the ambient temperature. However, on a sunny day, when the panels are absorbing a greater amount of photons, back-of-panel temperature can go well beyond ambient temperature, as was seen on February 11, 2006, where the temperature difference was 24.42 °C.

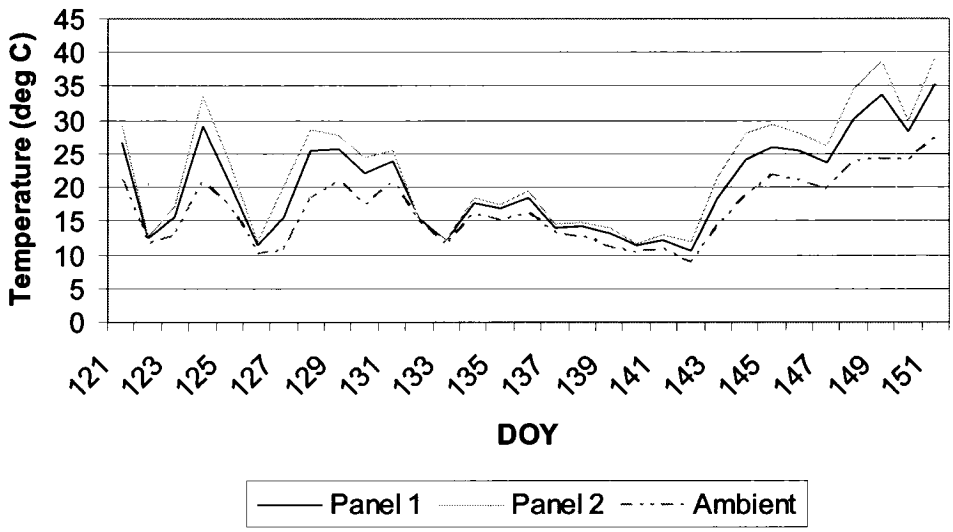

Figure 4.12: Back-of-panel and ambient temperatures, May 1 – 31, 2006

The relationship between back-of-panel temperature, ambient temperature, and the photovoltaic electrical output is illustrated in Figures 4.13 and 4.14. Similar to the trend previously discussed where an increase in back-of-panel temperature causes an increase in voltage, accordingly it can be seen in these two plots that an increase in daily average back-of-panel temperature results in an increase of daily total photovoltaic electrical output, calculated for a 7 hour period corresponding with the pump operation between 9h00 and 16h00. Throughout the data collection period, there were days that did not follow this trend. For example, in Figure 4.13 there is a daily average back-of-panel temperature increase from day 249 to day 250 of close to 2 °C, yet the daily power output decreases by just over half its value from 0.44 MJ d^{-1} to 0.20 MJ d^{-1}.

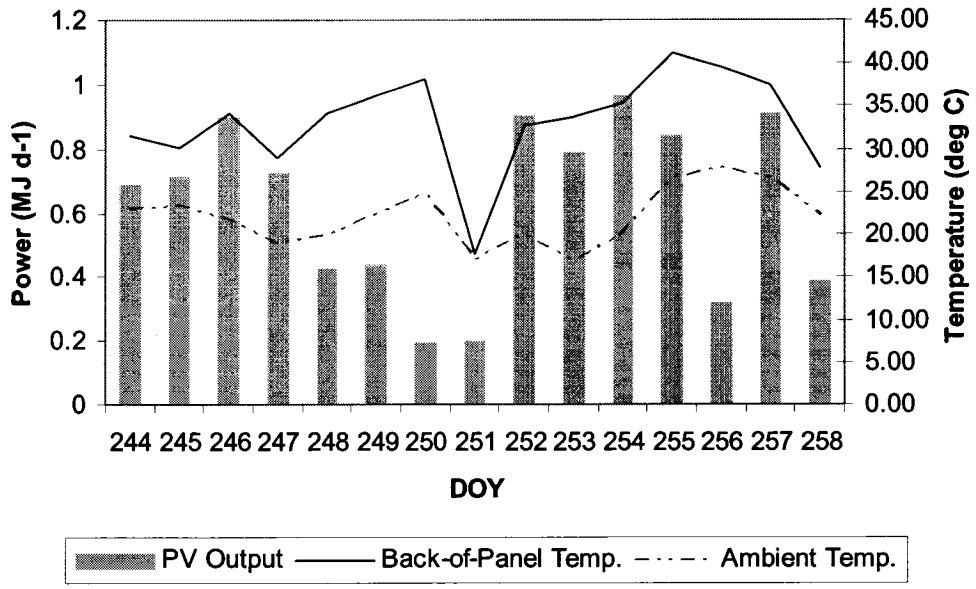

Figure 4.13: Photovoltaic electrical output vs. temperature, September 1-15, 2005

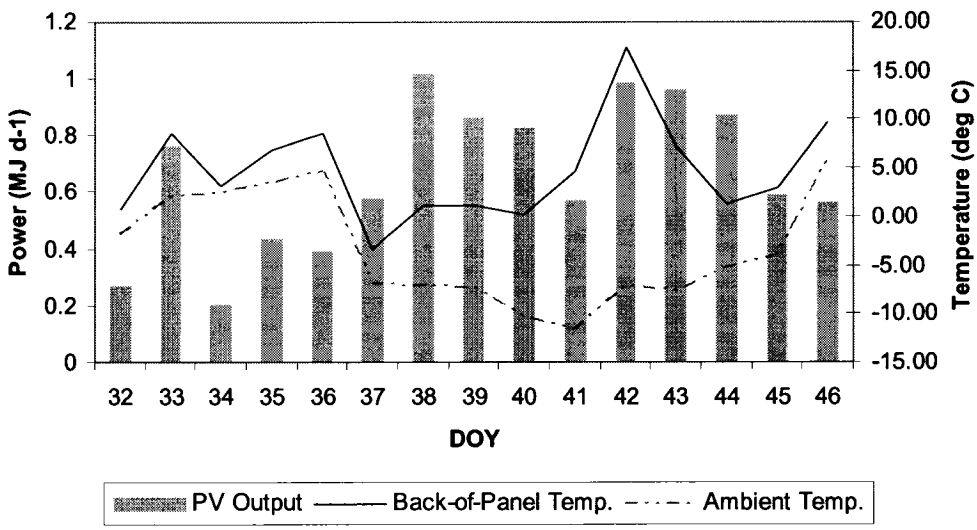

Figure 4.14: Photovoltaic electrical output vs. temperature, February 1-15, 2006

This is explained by the fact that the observed output power is determined by the product of the voltage and current, P = VI. It was seen in Figure 4.10, that from day 249 to 250, the daily average voltage increased. Because current also increases with a rise in temperature, the daily power output should increase from day 249 to 250, but it clearly does not (Figure 4.13). This is due to the load. In this case, the load was a 12 V surface water pump, which did not perform to its full capacity each day, meaning it was not

drawing the maximum amount of current required, thus affecting the overall power output. The pump was rated to draw a minimum of 5.3 A with open flow, and the current required would increase as the pressure increased. This was not the case. The pump drew on average between 1 A and 2.5 A, causing a significant decrease in the potential daily power output. The pump would have required a full servicing to locate the problem, and with time and financial constraints this was not possible. It is therefore only for general trends that the relationship between daily temperature and photovoltaic electrical output are considered, and not for specific values to be directly applied to other applications.

4.3.2 Daily photovoltaic electrical output

There are many factors involved in the prediction of daily photovoltaic electrical output. This means that there are many possibilities for error. As seen in Figure 4.15, there is not a good linear correlation between the observed daily PV power and the daily predicted PV power.

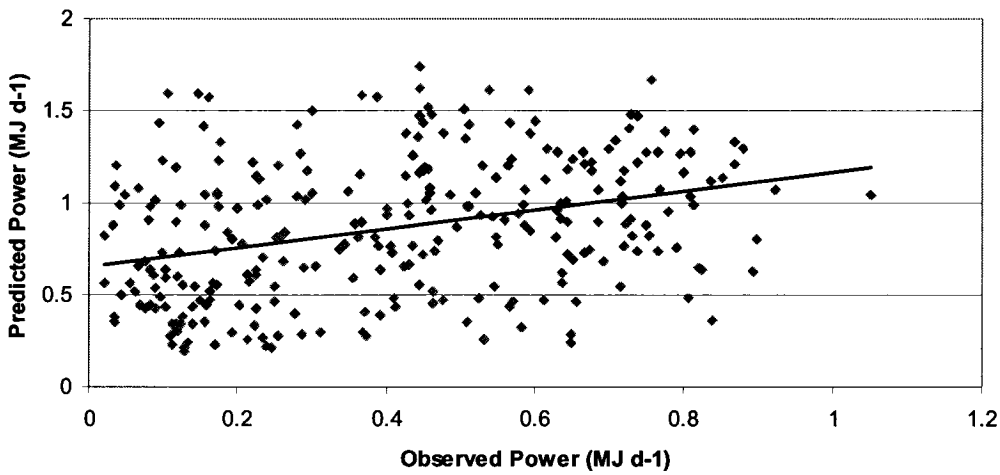

Figure 4.15: Daily photovoltaic electrical output, August 3, 2005 – May 31, 2006

The number of data points for this comparison was 276. The correlation coefficient, r^2, between the predicted and observed daily power, is poor at 0.11. This model over predicts the daily power output with a bias of 0.46 MJ d^{-1}. RMSE and MAE were 0.59 MJ d^{-1} and 0.47 MJ d^{-1}, respectively. These errors are very high, as they are

greater than the mean observed power, 0.41 MJ d^{-1}, and more than half the mean predicted power, 0.87 MJ d^{-1}.

For ease of observation and analysis, a selection of the daily prediction for output power and observed daily power, can be seen in Figure 4.16. It is apparent that the prediction is not accurate; however, it does follow the same general trend as the observed photovoltaic electrical output values. This is further emphasized by the use of a 7 day moving average for both the predicted and observed daily PV electrical outputs, which is discussed in detail in section 4.3.4.

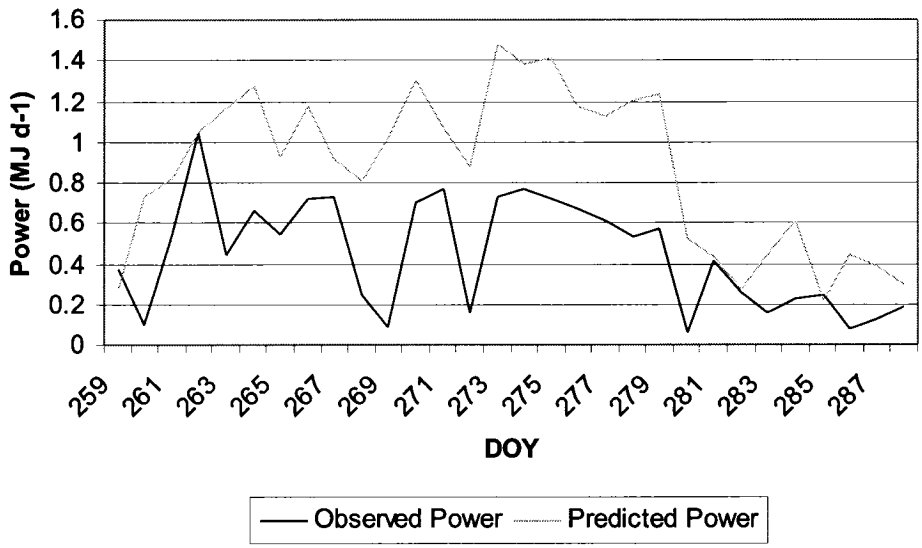

Figure 4.16: Daily photovoltaic electrical output, September 16 – October 15, 2005

The prediction of daily output power does not take a specific load into account, but rather is a prediction for the maximum possible output of a particular module technology with a specified surface area and assumed power losses (Equation 2.8). The losses are assumed to be 2% for dirt and dust on the surface of the solar panels, 3% to 5% for wire loss, and an additional 5% for power conditioning losses. Depending on the maintenance of the solar panels, the 2% loss for dust and dirt will vary. In this prediction, for comparison of predicted PV electrical output to the observed data, the 5% power conditioning loss was not taken into account due to the location of the DC current sensor, as seen in Equation 3.2. Furthermore, the observed output power is greatly affected by the load capacity. Due to the fact that the water pump was not fully operational, the

observed daily output power was much less than initially expected. This explains why the predicted daily power is grossly over estimated for this particular system. This renders a direct comparison to be of little value other than for recognising trends. Nonetheless, there are factors inherent in the model that could contribute to poor daily power output predictions. The predicted photovoltaic electrical output is based on two components: the average array efficiency and the solar radiation in the plane of the PV array.

Average array efficiency (Equation 2.9) is a function of the module ratings and the average module temperature. The module ratings, including PV module efficiency (η_r) and the temperature coefficient for module efficiency (β_p), are determined under standard test conditions (STC) in a controlled environment for an amorphous silicon (a-Si) 42 W Uni-Solar panel. It is possible that these standard ratings do not hold true for each and every a-Si 42 W panel manufactured that are exposed to varying environmental conditions. a-Si modules stabilise at different performance levels, depending on the environmental conditions and the temperature history of light exposure. The average module temperature (Equation 2.10) is dependent on further typical ratings developed under STC, including the nominal operating cell temperature (NOCT), the ambient dry bulb temperature ($T_{a,NOCT}$), the instantaneous total solar irradiation on the array during the NOCT test ($G_{T,NOCT}$), and an assumed solar reflectance of optical components between the array and the sun (ρ) of 1. Furthermore, the $G_{T,NOCT}$ value is measured at a wind speed of 1 m s^{-1}. In reality, the average module temperature will vary markedly under fluctuating environmental conditions from this laboratory design. This is partially addressed in Equation 2.10 in that the STC ratings are modified by the predicted clearness index, K_T. This would account for the varying incident solar radiation. However, it does not account for the varying wind conditions, which could influence the back-of-panel temperature and thus PV module temperature. It would also be important to locally assess the actual solar reflectance of optical components between the solar array and the sun, due to the increasing and varying amount of air borne pollutants.

Calculation of solar radiation in the plane of the PV array adds further discrepancies to the photovoltaic electrical output prediction on a daily basis. This is due to the continually changing beam, diffuse, and reflected components of the incident solar

radiation. Despite the transient nature of beam, diffuse, and reflected solar radiation, they are determined using only the daily total global solar radiation. Using the correlation developed by Collares-Pereira and Rabl (1979) (Equation 2.13), the diffuse component of solar radiation is determined on a daily basis. Conversion factors (Collares-Pereira and Rabl, 1979; Liu and Jordan, 1960) are then used to convert the daily total solar radiation and daily diffuse component of solar radiation to the corresponding hourly values, which in turn are used to calculate the hourly reflected component of global solar radiation. These conversion factors were developed using long-term averages, where the ratio, r_t (Equations 2.22), is equivalent to the monthly average hourly total solar radiation divided by the monthly average daily total solar radiation. Similarly, the ratio, r_d (Equation 2.25), is equivalent to the monthly average hourly diffuse solar radiation divided by the monthly average daily diffuse solar radiation. This provides the average intensity of total and diffuse radiation at different times of a typical day (Liu and Jordan, 1960). However, these ratios based on long term averages cannot fully represent true radiation intensities on a daily basis, as the distribution of diffuse solar radiation on a daily basis is very irregular depending on cloudiness, dust, and air borne pollutants (Tamura *et al.*, 2003). Despite daily irregularities, in this study these ratios are used to determine the hourly diffuse, beam, and reflected components of solar radiation on a daily basis, which in turn are applied to the HDKR model to determine the hourly solar radiation in the plane of the PV array, again on a daily basis.

Furthermore, the correction factor for cloudiness (Equation 2.35), used in the HDKR model for solar radiation in the plane of the PV array, is determined from these average or typical hourly predictions, thus not fully representing the variations of diffuse, beam, and reflected radiation on a daily basis. Studies are being done to determine a method using minutely data which would more accurately represent the movement of the sky, and thus the varying components of solar radiation, as stated in section 2.4.2. An additional concern is the effect of ground snow cover. The coefficient for ground reflectance, ρ_g, is based on temperature data alone, and not actual snow cover, or even a combination of temperature and precipitation. Ground snow cover would greatly increase the amount of reflected radiation reaching the solar panels, therefore increasing the available power. Concerns regarding the coefficients for cloudiness and ground

reflectance are more apparent in the monthly comparison discussed in the following section.

Figure 4.16 illustrates that the PV electrical output model is sufficient to predict no more than the trends of photovoltaic power output in the Montréal region for this particular system. It would be interesting to repeat this study with a fully operational system to determine a better understanding of the models' potential. However, in an attempt to improve the accuracy of the prediction results, PV electrical output model improvement could include: calibration to the specific solar modules in use; accurately accounting for cloud cover and ground snow cover on a daily basis; and using minutely data, when available, to predict the solar radiation in the plane of the PV array.

4.3.3 Monthly daily average photovoltaic electrical output

For this particular study, there are two methods of improving the results from section 4.3.2. One is to use a 7 day moving average of the predicted and observed daily PV electrical output, which will be discussed in section 4.3.4, and the other is to use monthly daily averages of the PV electrical output to compare the predicted and observed output power. It was thought that by taking the daily average PV electrical output for each month, the discrepancies between the observed and predicted power would be reduced. This was not the case, as seen in Figure 4.17, which illustrates the monthly daily averages of both observed and predicted PV power.

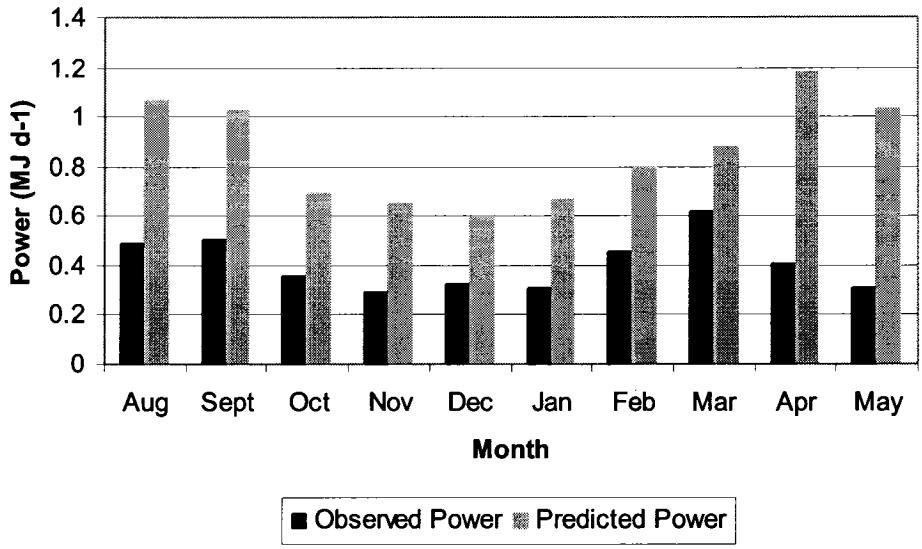

Figure 4.17: Monthly daily average power output, August 2005 – May 2006

These results are very interesting for several reasons. As previously mentioned, there was a positive bias of 0.46 MJ d^{-1} for the overall prediction, from August 2005 to May 2006, indicating an over prediction of the daily PV electrical output. However, as seen in Figure 4.17, the magnitude of this bias varies considerably from month to month. Table 4.5 shows the monthly bias between the predicted and observed PV power.

Table 4.5: Monthly daily average power bias

	Aug.	Sept.	Oct.	Nov.	Dec.	Jan	Feb.	Mar.	Apr.	May
Bias (MJ d^{-1})	0.58	0.53	0.33	0.36	0.27	0.35	0.35	0.26	0.77	0.72

To directly compare the values of predicted output power and observed output power in this study would be ineffective due to the pump inefficiencies. However, it is interesting to note that the smallest bias between observed and predicted monthly daily average power is seen in March, followed by December. Furthermore, the largest bias, 0.72 MJ d^{-1}, is seen in April, which is almost three times that of the preceding month. It would have been interesting to continue this study through June and July of 2006 to determine if the power bias continued to rise or if it had reached a plateau in April and declined through the summer. Reasons for these monthly variations could be similar to those described in section 4.2.2. The large over prediction in the spring could be due in

part to the inaccuracy of the coefficient for cloud cover in the PV electrical output model, thus over predicting on cloudy days. The smaller bias in the winter months could be due in part to an actual under prediction of the PV electrical output model in the winter months due to the fact that ground snow cover is not directly taken into account, but rather a ground reflectance coefficient, ρ_g, is used that is governed by temperature alone. These inefficiencies in the PV electrical output prediction model are shared with the solar radiation prediction model. It is therefore thought that when the solar radiation is under predicted, the photovoltaic electrical output would also be under predicted, and vice versa.

It is important to reiterate that this observed power output is not an accurate indication of the potential power output in the Montréal region, as the pump was not operating at full capacity, as well as functioning inconsistently. In this system, it would be a much higher quality assessment if it were possible to divide the predicted daily power output into its voltage and current components, and then to make a comparison of the observed and predicted daily average voltage. This is not possible though due to the nature of the PV electrical output prediction model.

4.3.4 Seven day moving average photovoltaic electrical output

As expected, the use of a 7 day moving average on the predicted and observed PV output power smoothed the daily variations, while allowing the trends to be more apparent. This is illustrated in Figure 4.18, showing a comparison of daily photovoltaic electrical output data.

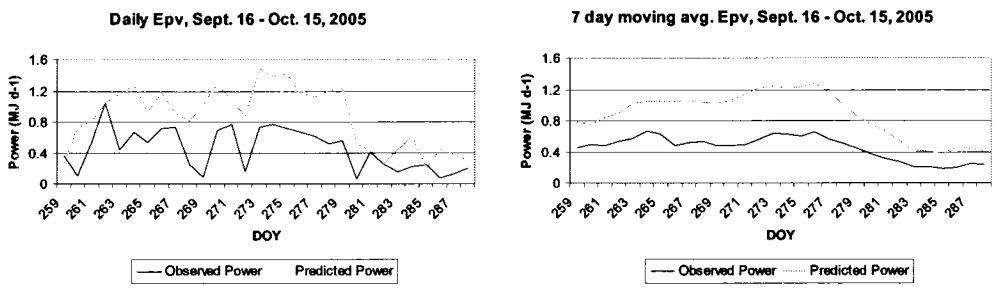

Figure 4.18: Comparison of daily to 7 day moving average photovoltaic electrical output, September 16 – October 15, 2005

The overall daily and monthly performance of the photovoltaic electrical output model was slightly improved through the use of a 7 day moving average of the predicted and observed PV electrical output. Table 4.6 shows the small changes seen in the linear relationship between the overall predicted and observed power output.

Table 4.6: Overall photovoltaic electrical output model performance

	Daily	*7 day moving avg.*
N (days)	276	270
Mean Observed Epv (MJ d^{-1})	0.41	0.41
Mean Predicted Epv (MJ d^{-1})	0.87	0.86
r^2	0.11	0.17
RMSE (MJ d^{-1})	0.59	0.51
Bias (MJ d^{-1})	0.46	0.45
MAE (MJ d^{-1})	0.47	0.45

For the total data set, RMSE and MAE did show slight improvement; as did the square of the correlation coefficient, which increased to 0.17, though this is still poor. As expected, the bias remained relatively unaffected by the use of a 7 day moving average on the observed and predicted PV electrical output. For the monthly data sets, the PV model performance greatly varied with the use of a 7 day moving average, as seen in Table 4.7. Figure 4.19 shows an improved prediction seen in October 2005, as the scatter is much less.

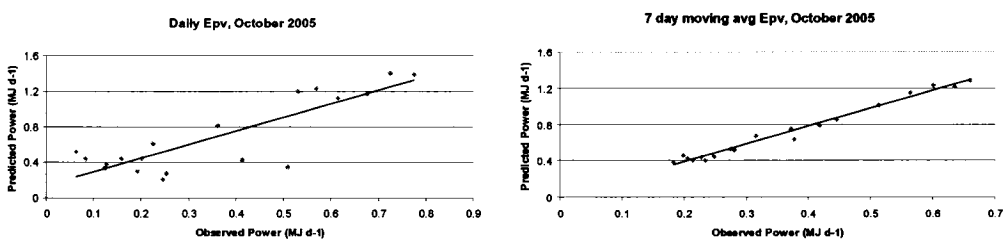

Figure 4.19: Comparison of daily to 7 day moving average photovoltaic electrical output, October 2005

There were only 19 data points used in this scatter plot. However, linear correlation improved from r^2 of 0.72 using daily observations, to 0.98 using the 7 day moving average on both the predicted and observed PV electrical output. RMSE only slightly improved, decreasing from 0.41 MJ d^{-1} to 0.38 MJ d^{-1}, whereas MAE remained the same at 0.35 MJ d^{-1}. The bias in fact increased from 0.33 MJ d^{-1} to 0.35 MJ d^{-1} with the use of the 7 day moving average for both the predicted and observed PV electrical output.

Improvement of the square of the correlation coefficient, seen in October, was not common for all months. Similarly, RMSE and MAE improved only slightly with the use of the 7 day moving average on the observed and predicted PV electrical output. A summary of the monthly data is provided in Table 4.7.

Table 4.7: Monthly photovoltaic electrical output model performance

Daily	*Aug*	*Sept*	*Oct*	*Nov*	*Dec*	*Jan*	*Feb*	*Mar*	*Apr*	*May*
N (days)	26	30	19	20	31	31	28	31	29	31
Mean Obs. Epv (MJ d^{-1})	0.49	0.50	0.36	0.30	0.33	0.31	0.45	0.62	0.41	0.31
Mean Pred. Epv (MJ d^{-1})	1.07	1.03	0.69	0.65	0.60	0.67	0.80	0.88	1.18	1.03
r^2	0.001	0.05	0.72	0.06	0.03	0.32	0.01	0.11	0.16	0.05
RMSE (MJ d^{-1})	0.65	0.62	0.41	0.50	0.48	0.47	0.52	0.39	0.82	0.80
Bias (MJ d^{-1})	0.58	0.53	0.33	0.36	0.27	0.35	0.35	0.26	0.77	0.72
MAE (MJ d^{-1})	0.58	0.53	0.35	0.42	0.34	0.37	0.42	0.30	0.77	0.72
7 day moving average	*Aug*	*Sept*	*Oct*	*Nov*	*Dec*	*Jan*	*Feb*	*Mar*	*Apr*	*May*
N (days)	23	30	19	20	31	31	28	31	29	28
Mean Obs. Epv (MJ d^{-1})	0.49	0.50	0.37	0.28	0.32	0.32	0.45	0.61	0.41	0.28
Mean Pred. Epv (MJ d^{-1})	1.06	1.03	0.72	0.63	0.58	0.68	0.80	0.86	1.18	1.03
r^2	0.14	0.001	0.98	0.65	0.22	0.66	0.07	0.14	0.004	0.01
RMSE (MJ d^{-1})	0.57	0.55	0.38	0.35	0.29	0.37	0.39	0.32	0.77	0.78
Bias (MJ d^{-1})	0.56	0.53	0.35	0.34	0.26	0.36	0.35	0.26	0.76	0.75
MAE (MJ d^{-1})	0.56	0.53	0.35	0.34	0.26	0.36	0.35	0.26	0.76	0.75

The square of the correlation coefficient increased in August, October, November, December, January, February, and March, indicating an improvement in the PV model performance on a monthly basis. October showed the best correlation followed by January. However, November showed the greatest improvement in r^2 with an increase of 0.59 with the use of the 7 day moving average on both the predicted and observed PV electrical output. In the months of September, April, and May, the linear correlation between the observed power and predicted power actually decreased with the use of the 7 day moving average. Despite the weakening of the linear correlation, the 7 day moving average did provide a decrease, however slight, in both RMSE and MAE for each month, except for May. The greatest improvement was seen in December with a decrease in RMSE of 0.18 MJ d^{-1} and a decrease of 0.079 MJ d^{-1} MAE. This was followed by November with reductions in RMSE and MAE of 0.15 MJ d^{-1} and 0.078 MJ d^{-1}, respectively. The least improved month was May with a RMSE decrease of 0.02 MJ d^{-1} and in fact an increase in MAE of 0.02 MJ d^{-1}.

It was expected that the linear correlation would be poor between the observed and predicted daily power due to the pump inefficiencies. With a fully operational pump and an improved PV model through calibration, site specific coefficients, and ratings specific to the individual solar modules, the use of a 7 day moving average on the predicted PV electrical output could prove useful in determining the power availability for the weekly irrigation requirements. For this particular system, the photovoltaic electrical output model can only be used to assess the general trends of power availability, and how this relates to temperature and global horizontal solar radiation.

4.4 Water Flow Output Results

4.4.1 Pump curve

The prediction of water flow output for a drip irrigation system is governed by the pump and motor specifications, input power, lift, outlet pressure, and type of pipe. A pump curve shows the typical relationship between pressure or head, and flow. The pump curve and specifications for the surface water pump (2088-443-144, Shurflo, California), used in this field study, are shown in Figure 4.20.

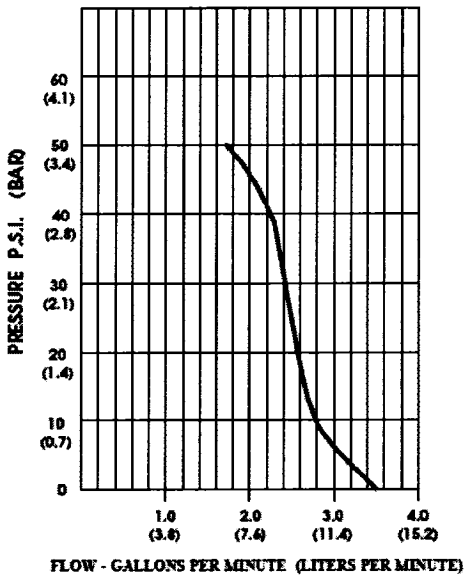

PRESSURE (PSI)	FLOW (GPM/LIT)	RPM MIN/MAX	CURRENT (AMPS)	VOLTAGE (VOLTS)
OPEN	3.50/13.2	2160/2210	5.3	12 VDC
10	2.83/10.7	2130/2180	5.8	"
20	2.56/9.7	2050/2110	7.0	"
30	2.31/8.7	2015/2030	8.0	"
40	2.02/7.6	1960/1975	9.1	"
50	1.75/6.6	1915/1930	9.9	"

(Source: Shurflo product data sheet)

Figure 4.20: Shurflo 2088-443-144 pump specifications

Throughout the field research, the pump was not operating at full capacity, which meant that it was not drawing the maximum available current. The photovoltaic modules provided between 4 A and 5 A on a sunny day, yet the pump only drew from 1 A to 2.5 A, thus greatly decreasing the expected flow. To ensure that it was not the solar panels operating below their maximum power point, a 12V/6A power source was used to test the pump with the AC power in the greenhouse. With this power source, the pump only drew 2.1A. Figure 4.21 illustrates the actual corresponding pump curves using the photovoltaic modules and the 12V/6A power source, respectively.

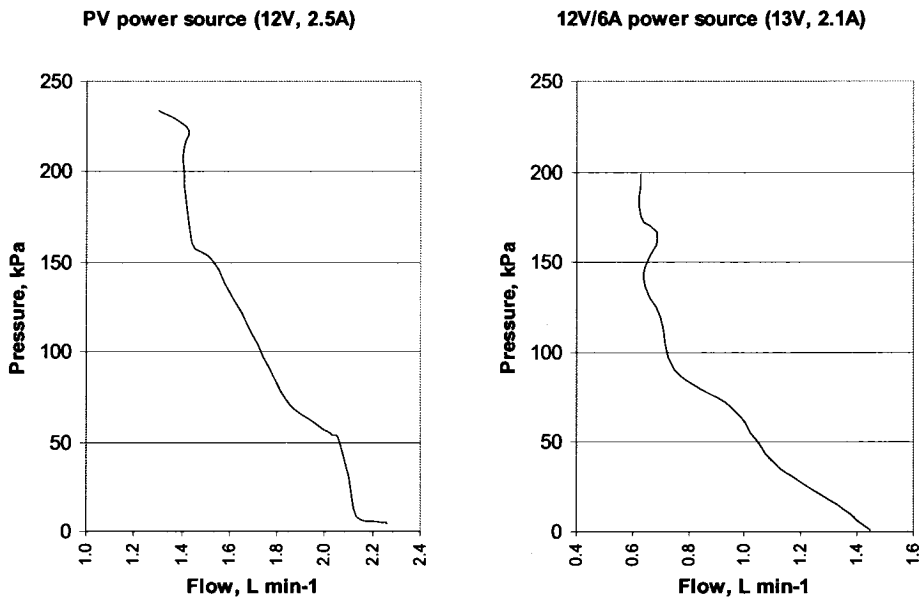

Figure 4.21: Observed Shurflo 2088-443-144 pump curves

It is clear in these two pump curves (by PV and 12V/6A power), that the observed flow is much lower than the typical specifications to the corresponding pressure. For example, in the given specifications, at 137.90 kPa (20 psi) the flow is 9.7 L min^{-1}. However, the observed pump curve shows a flow of approximately 1.7 L min^{-1} for the PV power source at 138 kPa (20 psi) and for the 12V/6A power source, at 138 kPa (20 psi), the flow is approximately 0.68 L min^{-1}. This is 8.0 L min^{-1} less flow for the PV power source and approximately 9.0 L min^{-1} less flow for the 12V/6A power source than the given pump specifications. The poor pump efficiency is further discussed in section 4.4.4.

In the following sections, the units for pressure are kPa. However, for consistency to the original specifications provided by the manufacturer, the corresponding psi is included in brackets.

4.4.2 Observed water output

4.4.2.1 Daily output

Of the 276 days of data employed in the photovoltaic electrical output section, 267 days were viable for water output analysis; with 5 missing days in August, 16 missing

days in October, 10 missing days in November, 5 missing days in March, and 1 missing day in April. The results discussed below are not to be read as accurate data, due to the pump inefficiencies, but are meant only to represent the potential trends seen between water flow output and photovoltaic electrical input. The expected trend is represented in Figure 4.22, which illustrates the observed water flow as it compares with the observed power output.

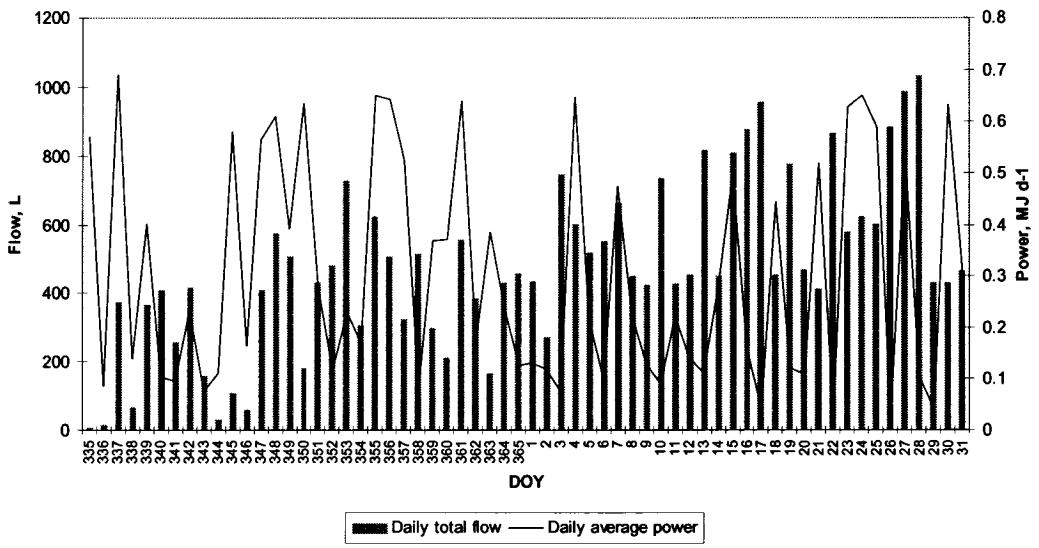

Figure 4.22: Daily power vs. flow, December 1, 2005 – January 31, 2006

It is seen in Figure 4.22 that as the available power increases from the PV modules, typically the volume of water pumped also increases until a maximum rpm is reached, and vice versa. The results that depend on the functioning of the pump, which include both the water flow output and the power output, are to be taken for general trends only and not as a representation of the power and associated water available in this region. However, the two observations are relatively comparable as they are affected in a similar manner by the inefficient pump. It is important to note that this was not always the case. The summer installation experienced obstruction of the suction intake. Due to the abundant algae growth, the smallest filter at the intake was prone to clogging. When the filter was clogged, the input power and speed of the pump did not vary, however, the flow was greatly reduced, if not completely stopped. In this situation, it was not possible to directly associate the PV power input with the water output. The filter was cleaned

every few days in an attempt to avoid this situation. Furthermore, observed water flow depends on the input power but also on the outlet pressure; the greater the pressure the lower the flow. This is why for the same amount of input power the flow can vary greatly, as seen in Figure 4.22. To illustrate this, the photovoltaic electrical output on January 18, 2006 and January 22, 2006 was similar at 0.035 MJ d^{-1} and 0.034 MJ d^{-1}, respectively. However, the corresponding pressure and flow for January 18 were 7.32 kPa and 454 L d^{-1}, respectively. Whereas, for January 22, the corresponding pressure and flow were 5.06 kPa and 867 L d^{-1}, respectively.

Variable pressure is a concern for the repeatability of water flow data. Drip irrigation systems operate under pressure, typically regulated at 82.7 kPa (12 psi), due to the structural limitations of the drip lines, as indicated by the manufacturer. During the summer installation, the drip lines were thus regulated, which meant that the pressure between the pump outlet and the drip line pressure regulator was monitored to be in the range from 1.4 kPa to 137.9 kPa (0.2 to 20 psi). The outlet pressure is governed by the flow. If the flow from the pump exceeds the regulated flow of the drip lines, then the pressure regulator will restrict the flow, thus increasing the pressure between the pump and the pressure regulator. During the winter, there was no pressure regulator as there were no drip lines, but a valve was included in the system to keep the pressure at 82.7 kPa (12 psi). This was only true for sunny conditions and when the pump was relatively operational. When the pump was functioning inefficiently or with a lower insolation during cloud cover, the speed of the pump would decrease, and accordingly, the pressure would drop.

This variable pressure makes observed water flow data difficult to assess, as well as unreliable. The data was erratic due also to the fact that the flow meter was calibrated for a fully operational pump, which would provide an accuracy of ± 1% and repeatability of ± 0.5%. However, with a reduced flow, the calibration becomes less effective, and the accuracy is greatly reduced to ± 10%, according to the manufacturer (Chemline Plastics Ltd., Ontario).

4.4.2.2 Monthly output

For the purpose of this study, Figure 4.23 illustrates the monthly daily average flow as it compares to the monthly daily average power available. It is important to remember that this is a gross under representation of the potential photovoltaic electrical output, and water flow output for this region, given the poor pump performance.

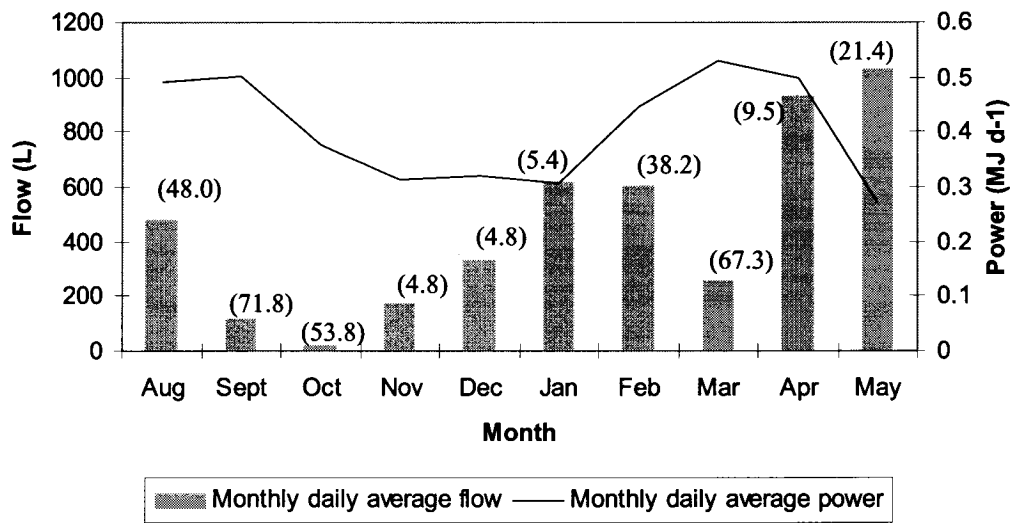

Figure 4.23: Monthly daily average flow vs. power with pressure inset (in kPa), August 2005 – May 2006

The monthly daily average pressure was included, as an inset, in Figure 4.23 to emphasise the variation and to stress that these results overall are not directly comparable to the predicted results in section 4.4.3, which depend on constant pressure or head.

Disregarding October and November as there were 16 and 10 missing observation days, respectively, the other months show unexpected results. The 5 missing days in March (March 26 – 30, 2006) correspond to days with no precipitation, according to Climate Data Online (Environment Canada, 2006). If these days were sunny or slightly overcast, it is possible that the total flow shown in Figure 4.23 is an underestimation of the potential flow in that month. This is also true for 3 of the 5 missing days in August (August 7, 9, 24, 2005). According to Climate Data Online (Environment Canada, 2006), there was precipitation on August 1 and 2, 2005. There was no precipitation recorded for

the missing day in April (April 27, 2006). With only 1 missing day in April, the total flow and power are assumed to be a good representation of the system for the month.

In the acceptable months, it is generally seen that lower pressures result in higher flows. However, the relationship between photovoltaic electrical input to the pump and output flow, is not apparent in the monthly daily average. In Figure 4.23, the unpredictability of this data is illustrated in April and May. At a monthly daily average pressure of 21.4 kPa and a power input of 0.27 MJ d^{-1}, May has a monthly daily average flow of 1034 L d^{-1}. April, on the other hand, has a lower pressure at 9.5 kPa and a slightly higher power input at 0.5 MJ d^{-1}, and is therefore expected to have a higher volume of flow. However, as seen in Figure 4.23, the April flow is approximately 100 L less than the May flow, at 935 L d^{-1}. If both the pressure and the power were to increase, than a decrease in flow would have been expected, however this was not the case.

4.4.3 Predicted water output

To simulate the potential pressures in an irrigation system, the water output predictions were carried out at a pressure of 103.4 kPa (15 psi) and 137.9 kPa (20 psi). The wire to water efficiency is the product of the efficiency of the pump and the efficiency of the motor driving the pump. The wire to water or overall system efficiency, to be used in the water output predictions, was determined using the given specifications (Figure 4.20) applied to the following Equation 4.1:

$$\eta_{sys} = \frac{\rho g Q h_{total}}{E_{in}} \tag{4.1}$$

where Q = flow ($m^3 s^{-1}$)

h_{total} = total system head (m)

E_{in} = rated energy input for a given pressure and flow (W)

and ρ, g remain as previously defined.

The overall system efficiency varies with pressure, as each pump has an optimal operating point, and the efficiency decreases on either side of this point. Therefore, using

the given specifications, the system efficiency was determined for the two selected pressures of 103.4 kPa (15 psi) and 137.9 kPa (20 psi). At an outlet pressure of 103.4 kPa (15 psi), the equivalent head is 10.5 m (by Equation 3.6). Given an initial lift of 2 m (approximate lift during field research), the total head is 12.5 m. A total head of 12.5 m corresponds to a total pressure of 122.6 kPa (17.8 psi) (Equation 3.6). Referring to Figure 4.20, the corresponding flow, Q, at this pressure is approximately 9.9 L min^{-1}, which is equal to 0.000165 m^3 s^{-1}. The energy input is approximately 78.2 W (Figure 4.20). Therefore, the system efficiency at 122.6 kPa (17.8 psi) is determined to be approximately 26% (Equation 4.1). At an outlet pressure of 137.9 kPa (20 psi), the equivalent head is 14 m (by Equation 3.6). Given a lift of 2 m, the total head is 16 m. A total head of 16 m corresponds to a total pressure of 157 kPa (22.8 psi) (Equation 3.6). Referring to Figure 4.20, the corresponding flow, Q, at this pressure is approximately 9.5 L min^{-1}, which is equal to 0.000158 m^3 s^{-1}. The energy input is approximately 87.6 W (Figure 4.20). Therefore, the system efficiency at 157 kPa (22.8 psi) is determined to be approximately 28% (Equation 4.1).

The predicted water output refers to the flow calculated using power input from the PV electrical output prediction model. The PV input power for the water flow predictions (unlike for direct comparison to observed PV electrical output) took into account the rated energy loss of 5%, across the linear current booster (Equation 2.8). Predicted monthly daily average PV electrical output was applied to Equation 3.5, to determine the predicted monthly daily average water output. Table 4.8 summarises the predicted output flow (by Equation 3.5) at a specified: constant pressure (P) with equivalent head (h_2); corresponding system efficiency (η_{sys}), as found above; and input power. For all calculations, ρ = 1000 kg m^{-2}, g = 9.81 m s^{-2}, h_1 = 2 m, and f = 0.032. It is important to remember that the predictions of daily PV electrical output and daily water flow output were calculated for a 7 hour day of pumping, between the hours of 9h00 and 16h00.

The expected water output refers to the flow calculated using the observed PV electrical output from the field data. To take into account the rated efficiency of the linear current booster, the observed PV electrical output was decreased by 5%. The observed monthly daily average PV electrical output, modified for the energy loss over

the linear current booster, was applied to Equation 3.5 to determine the expected monthly daily average water output. All other parameters remained as they were in the predicted water output calculations. Table 4.8 provides a summary of the inputs and outputs.

Table 4.8: Predicted and expected monthly daily average flow

	Inputs					*Output*	
	P (kPa)	**h2 (m)**	***ηsys (%)***	*Predicted* **Epv (MJ d^{-1})**	*Expected* **Epv (MJ d^{-1})**	*Predicted* **Q (L d^{-1})**	*Expected* **Q (L d^{-1})**
Aug	103.4	10.5	26	1.01	0.47	2083	957
	137.9	14	28	1.01	0.47	1753	805
Sept	103.4	10.5	26	0.98	0.48	2007	981
	137.9	14	28	0.98	0.48	1689	826
Oct	103.4	10.5	26	0.66	0.34	1347	702
	137.9	14	28	0.66	0.34	1133	591
Nov	103.4	10.5	26	0.63	0.28	1302	579
	137.9	14	28	0.63	0.28	1096	487
Dec	103.4	10.5	26	0.58	0.31	1187	638
	137.9	14	28	0.58	0.31	999	537
Jan	103.4	10.5	26	0.65	0.30	1330	611
	137.9	14	28	0.65	0.30	1119	514
Feb	103.4	10.5	26	0.78	0.43	1595	882
	137.9	14	28	0.78	0.43	1342	742
Mar	103.4	10.5	26	0.85	0.59	1749	1214
	137.9	14	28	0.85	0.59	1471	1021
Apr	103.4	10.5	26	1.14	0.39	2348	799
	137.9	14	28	1.14	0.39	1976	672
May	103.4	10.5	26	1.00	0.29	2056	599
	137.9	14	28	1.00	0.29	1730	504

These results, for the most part, are not directly comparable to the observed water flow due to the variation in pressure. It should be assumed that with fully operational equipment (pump and panels), the water flow should be similar to the predicted water output. This suggests that a system with a lift of 2 m, running under an outlet pressure of 103.4 kPa, with an input of 1 MJ d^{-1}, will pump approximately 2050 L d^{-1} of water. A power input of 0.5 MJ d^{-1}, at the same pressure and lift, will enable approximately 1030 L d^{-1} of water flow. This implies that when a system is kept under constant total head, a linear relationship exists between the input power and the water output. A system with a lift of 2 m, running under an outlet pressure of 137.9 kPa, with a power input of 1 MJ d^{-1},

will pump approximately 1730 L d^{-1} of water. A power input of 0.5 MJ d^{-1}, at the same pressure and lift, will enable approximately 860 L d^{-1} of water flow, again showing a linear relationship at a constant total head.

As stated previously, in this study predicted and observed water flow are not realistically comparable due to pressure variation and pump inefficiencies. It was found that despite the higher pressure, the water flow prediction greatly exceeded the observed water flow output, over a range of 700 L d^{-1} to 1900 L d^{-1}. However, the observed flow was greater than the expected flow in April and May by approximately 100 L d^{-1} and 400 L d^{-1}, respectively. This can be explained by the fact that the outlet pressure of observed flow in these months was considerably less (94 kPa less in April, 82 kPa less in May) than the pressure assumed for the prediction of water flow. From this, it was inferred that the expected water output calculated using the observed photovoltaic power, modified for energy loss over the linear current booster, was still an over prediction for this particular system, due to the pump inefficiencies.

For the purpose of irrigation, it is interesting to determine the area that could be irrigated with the observed, expected, and predicted daily water output. This is accomplished by dividing the daily volume of water pumped (m^3) by the desired depth of irrigation (m), to attain the daily possible irrigated area (m^2). Assuming a standard irrigation depth of 0.005 m per day, and using the monthly daily average water output for August, the potential area under irrigation, on a daily basis, for the observed output (483 L at 48 kPa outlet pressure, 2 m lift) is approximately 97 m^2. Assuming the same irrigation depth for the expected and predicted August water flow output (957 L and 2083 L respectively, at 103.4 kPa outlet pressure, 2 m lift), the expected area possible for irrigation is approximately 191 m^2 and the predicted area for irrigation is approximately 417 m^2, which consequently would be sufficient for the original design of the intended irrigation area of 400 m^2.

To realise flows similar to the predicted water flow, the pump must be fully operational, the pressure must be kept constant, and the power input to the pump must also be constant. To achieve this, it would be necessary to have intermediary power storage, as it is impossible to ensure that the photovoltaic electrical output will be constant due to its dependence on cloud cover, rain, temperature, and wind. Otherwise, a

variable speed motor that adjusts its speed with incoming power, to keep the pressure and flow constant would also suffice. Using a variable speed motor to control the flow rather than a valve is also more efficient in terms of energy use. In terms of future observations, the most efficient scenario and most repeatable study would be to pump the water to an elevated storage tank at open pressure. From the storage tank, the water could then be fed by gravity, or otherwise to the drip lines. This would reduce the number of variables to consider in the observed water flow, as the total head could be kept constant regardless of the PV electrical output, and thus pump speed.

4.4.4 Pump diagnosis

Diaphragm pumps are designed to operate over a wide range of voltage and current. This is appropriate for a PV pumping system, where the PV array is directly connected to the pump and the output power will fluctuate throughout the day. However, the trade-off for this wide operating range is a lower efficiency. The surface water pump used in this research (2088-443-144, Shurflo, California) had a rated operating efficiency of up to 32%, as given by the manufacturer, depending on the input power and operating pressure. Based on the observed monthly daily average flow, pressure, and input power, the operating efficiency of the pump during this study was on average 5%, with a range from 0.4% up to 15.5%, depending on the operating conditions. This is below the expected efficiency. Possible factors contributing to this low efficiency are as follows: pressure loss at the intake due to algae and filter; long intake suction line; energy loss through excessive heat and vibration of the pump during operation; faults in the working components of the pump; energy loss through the linear current booster; and low current draw.

Pressure loss at the intake is typically negligible in the design and operation of a pump (Enright, personal communications 2006). The addition of a filter, if clean, does not significantly add to this pressure loss. Though it appears, in Figure 4.23, that the overall flow improves from the summer installation (August to October) to the winter installation (November to May), at a similar pressure and input power there is no great difference in pump performance. Due to the fact that there was no great improvement in the efficiency (at a similar pressure and power) between the summer installation, when

algae were a concern and the winter installation, where the water source was clean, pressure loss at the intake is not considered to be a large contributing factor. The suction line in the winter installation was half the length of that in the summer installation, yet still long at 5 m. Change of length in the suction line from 10 m to 5 m did not have an effect on the efficiency of the pump in this particular study. It would have been interesting to test if the efficiency of the pump increased with a suction line of less than 5 m.

During operation, the pump was hot to touch and there was a greater amount of noise and vibration than alluded to in the manufacturers' literature, which implies that energy was being lost. The pump was taken apart to inspect the diaphragms and axis of rotation, there were no visible faults located. An oversight of this study was the absence of continual monitoring of the voltage between the linear current booster and the pump. The current was continually monitored in this location; however, only manual recordings of the voltage were taken periodically throughout the course of the study. The linear current booster was rated at 95% efficiency, as stated by the manufacturer. This 5% energy loss was taken into account in the application of both predicted and observed PV electrical output to the water flow prediction. Through the manual recordings using a hand-held voltmeter, the linear current booster was found to be approximately 90% efficient at those times, therefore the PV power input to the pump motor was approximately 5% greater than observation suggested.

Finally, the pump drew on average 1 A to 2.5 A, when rated to draw more than 5.3 A if operating under pressure. To ensure that the supply power from the PV modules was sufficient, the pump was tested using a 12 V/6 A power supply, which was connected to the AC power of the greenhouse. With this known power source, the pump only drew 2 A. The outlet pressure was adjusted in an attempt to find the optimal efficiency of the pump with the known power source, yet there was no affect on the current draw.

It is probable that a combination of the aforementioned factors contributed to the low efficiency of the pump. Nevertheless, due to the fact that when the pump was tested with varying pressures and a known constant power supply, there was no change in the current draw, leading to the probability that there was an inherent deficiency with the pump motor. This is considered to be the greatest contributor to the poor overall system

efficiency. Given the time and financial constraints of this research, it was not possible to investigate this further.

5.0 CONCLUSIONS

This research project was developed to both monitor and model the key parameters involved in a PV water pumping system for practical application. Parameters of interest were global horizontal solar radiation, photovoltaic electrical output, and water flow output. Field research was carried out on Macdonald campus of McGill University in Ste. Anne de Bellevue, Québec, from August 2005 to May 2006. The field work was divided into a summer and winter installation. The experimental setup was kept as similar as possible and the data collection was consistent throughout. The summer installation was operational from August 2005 to October 2005. The winter installation was operational from November 2005 to May 2006. Parameters monitored included: ambient temperature, back-of-panel temperature, voltage, current, pressure, and flow. Additional meteorological data obtained from Environment Canada weather stations, located at Ste. Anne de Bellevue and Montréal Pierre Elliott Trudeau International Airport, included temperature, precipitation, and global horizontal solar radiation. The global solar radiation for Ste. Anne de Bellevue was modelled using the modified Hargreaves-Samani inland model. This prediction was compared to the observed solar radiation. The photovoltaic electrical output was modelled using a combination of PV module and installation specifications (including PV module surface area and manufacturer ratings, tilt angle, site latitude, and elevation), meteorological input data, and solar geometry. The water flow output model was based on pump and installation specifications (including manufacturer pump ratings, type of piping, lift, and outlet pressure) along with the PV input power. Field data were used to determine the observed PV electrical output and water flow. This was compared to model predictions. The main conclusions drawn from this research are as follows:

i. The modified Hargreaves-Samani inland prediction model for global solar radiation performed well on a daily basis. The linear correlation coefficient for the observed and predicted solar radiation was 0.69. Use of a 7 day moving average, on both observed and predicted solar radiation, greatly improved the

square of the correlation coefficient to 0.91. This shows that weekly data may be more useful than daily predictions for the purpose of irrigation scheduling.

ii. Amorphous silicon solar modules are known to have a better performance in warmer climates, where daily average temperature is between 15 °C and 35 °C. This was verified by the fact that the voltage output increased with a rise in ambient and back-of-panel temperatures. Current also increases with rising temperature. Power is the product of voltage and current, thus the overall power output improves with temperature increases.

iii. The observed PV power output was less than expected. This was due to the fact that the pump was operating below full capacity, thus not drawing the maximum available current. Therefore, it was not possible to determine the accuracy of the PV electrical output prediction model. However, the observed PV electrical output generally followed the same daily trends as the predicted PV power. This suggests that the model is fundamentally correct, though it is not known from this research if the predicted magnitudes would coincide well with the output power of a fully operational system.

iv. The observed water flow output was less than expected. The flow meter was calibrated for the expected flow. Low flow decreased the accuracy of the flow meter causing erratic flow data. The low flow was due to the fact that the pump was operating below full capacity. Low amperage draw, long suction intake, and low lift may have contributed to the poor pump efficiency. Flow predictions are carried out under constant pressure and input power. It was not possible to keep the pressure or power constant with this system as the PV modules were connected directly to the pump. This along with the poor pump performance renders a comparison between the observed data and predicted flow impractical.

Overall this research justified the use of the modified Hargreaves-Samani inland model for the prediction of global solar radiation in the Montréal region for the purpose of irrigation scheduling and as an input for the modelling of PV electrical output. Conclusions on the accuracy of the PV power prediction model and calculation of water flow could not be drawn based solely on the comparisons with observed data. It is

assumed, based on the literature, that the PV electrical output and water flow predictions would give a good indication of the potential for solar powered irrigation systems in the Montréal region, despite the results of this study.

6.0 RECOMMENDATIONS

Based on this research, the following recommendations are made for future studies:

Field work:

i. A longer period of data collection, in a single location, would be recommended. At least two complete years would allow year to year and month to month comparison. This would also provide the time to identify and correct all potential defects in the system, from leaks to wiring to pump efficiency to sensor calibration.

ii. It would be important to measure the voltage after the linear current booster as well as before. In this way, the actual efficiency of the linear current booster could be determined as well as the power input directly to the pump motor. This would provide sufficient information to determine the true overall efficiency of the pump.

iii. To maximise the efficiency of the photovoltaic modules and thus greatly increase the volume of water pumped, use of a sun-tracking system should be considered. A tracking system allows the panels to follow the movement of the sun through out the day. An automated two dimensional tracking system is recommended. However, there are less expensive options. A tracking mechanism developed by Wolfgang Scheffler (1986) originally for solar cookers, works on a spring controlled with mechanical clockwork. For a simpler system, the panels could be mounted on a rotating pole. In this way, they could be manually rotated, three times a day, to face the sun. The mounting bracket could also be designed with a sliding and locking mechanism, so that the tilt angle could be easily changed on a weekly or monthly basis.

iv. A more efficient PV pumping system could be studied including the use of a variable speed motor and submersible pump. If a surface water pump must be used due to cost or maintenance concerns, then it would be important to shorten the length of the suction intake to a maximum of 5 m.

v. Battery storage would decrease the overall system efficiency, however if precise and continual power delivery was a concern due to the type of pump, this would be an important consideration.

vi. Pumping water directly to a storage tank would decrease the number of variables to consider in the design phase, as the outlet pressure would be kept constant.

vii. If possible, use of a clean water source would eliminate the possibility of obstruction in the suction intake, while at the same time prolonging the life of the pump.

Modelling:

viii. To improve performance of the modified Hargreaves-Samani inland model for global solar radiation, a site specific coefficient could be used if long term quality solar radiation data is available.

ix. To improve the PV electrical output model, further studies could be done in the development of a more accurate cloud cover coefficient as well as a ground reflectance coefficient that takes actual snow cover into consideration, perhaps based on a combination of average temperature, precipitation, and relative humidity.

x. The use of minutely or hourly (as opposed to daily) global solar radiation input data to determine the beam, diffuse, and reflected components of solar radiation could improve the prediction of hourly solar radiation in the plane of the PV array.

Finally, it would be recommended to take this technology to a rural or developing area, in order to research practical applications. Considerations for successful application would include many more parameters than a similar study in North America could incorporate, from identifying local interest and technicians for operation and maintenance, to finding appropriate and readily available materials and technologies.

7.0 REFERENCES

Al-Mohamad, A. 2004. Efficiency improvements of photo-voltaic panels using a Sun-tracking system. *Applied Energy*. 79: 345-354.

Allen, R. G. 1997. Self-calibrating method for estimating solar radiation from air temperature. *Journal of Hydrological Engineering*. 2(2): 56-67.

Allen R. G., L. S. Pereira, D. Raes, and M. Smith. 1998. Crop evapotranspiration: guidelines for computing crop water requirements. *FAO irrigation and drainage paper 56*. FAO, Rome.

Annandale, J. G., N. Z. Jovanovic, N. Benade, and R. G. Allen. 2002. Software for missing data error analysis of Penman-Monteith reference evapotranspiration. *Irrigation Science*. 21(2): 57-67.

Ball, R. A., L. C. Purcell, and S. K. Carey. 2004. Evaluation of solar radiation prediction models in North America. *Agronomy Journal*. 96(2): 391-397.

Bione, J., O. C. Vilela, and N. Fraidenraich. 2004. Comparison of the performance of PV water pumping systems driven by fixed, tracking and V-trough generators. *Solar energy*. 76: 703-711.

Braun J. E., and J. C. Mitchell.1983. Solar geometry for fixed and tracking surfaces. *Solar Energy*. 31(5): 439-444.

Bristow, K. L. and G. S. Campbell.1984. On the relationship between incoming solar radiation and daily maximum and minimum temperature. *Agricultural and Forest Meteorology*. 31: 159-166.

Burt, C. M., A. J. Clemmens, R. Bliesner, J.L. Merriam, and L. Hardy. 2000. *Selection of irrigation methods for agriculture*. On-farm irrigation committee of the environment and water resources institute. ASCE.

Census of Agriculture. 2001. Statistics Canada. Available at: http://www40.statcan.ca/l01/cst01/agrc05a.htm

Collares-Pereira M., and A. Rabl. 1979. The average distribution of solar radiation-correlations between diffuse and hemispherical and between daily and hourly insolation values. *Solar Energy*. 22: 155-164.

Cooper, P. I. 1969. The absorption of radiation in solar stills. *Solar Energy*. 12: 333–346.

Daud, A-K., and M. M. Mahmoud. 2005. Solar powered induction motor-driven water pump operating on a desert well, simulation and field tests. *Renewable Energy*. 30: 701-714.

del Cueto, J. A. 2002. Comparison of energy production and performance from flat-plate photovoltaic module technologies deployed at fixed tilt. *Photovoltaic Specialist Conference, 2002*. Conference Record of the Twenty-ninth IEEE. New Orleans, Louisiana. 1523-1526. Available at: http://ieeexplore.ieee.org/iel5/8468/26685/01190901.pdf?tp=&arnumber=1190901&isnumber=26685

Duffie, J. A., and W. A. Beckman. 1991. *Solar engineering of thermal processes*, 2nd Edition. New York, USA: John Wiley & Sons, Inc.

Ellis, A. W, and D. J. Leathers. 1999. Analysis of cold airmass temperature modification across the US Great Plains as a consequence of snow depth and albedo. *Journal of Applied Meteorology*. 38(6): 696-711.

Enright, P. 2006. Personal communications.

Environment Canada. 2006. Climate Data Online. Available at: http://www.climate.weatheroffice.ec.gc.ca/climateData/canada_e.html.

Erbs, D. G., S. A. Klein, and J. A. Duffie.1982. Estimation of the diffuse radiation fraction for hourly, daily, and monthly-average global radiation. *Solar Energy*. 28(4): 293-302.

Evans, D.L. 1981. Simplified method for predicting photovoltaic array output. *Solar Energy*. 27(6): 555-560.

Evans, J. 2006. Energy conscious AC domestic booster systems. Available at: www.pacificliquid.com

FAO Statistics Division. 2004. FAO Country Profiles. Available at: http://www.fao.org/ES/ess/yearbook/vol_1_2/pdf/Canada.pdf

Galdabini, S., G. Giuliani, and N. Robotti. 1992. Photoelectricity within classical physics: from the photocurrents of Edmund Becquerel to the first measure of the electron charge. *Proceedings of the Conference on 'History of Physics in Europe in the 19th and 20th Centuries'*. Como, Italy. 149 - 156. Available at: http://fisicavolta.unipv.it/percorsi/pdf/napesi.pdf#search=%22Edmond%20Becquerel%20in%201839%20%22

Gottschalg, R., J. A. del Cueto, T. R. Betts, and D. G. Infield. 2005. Seasonal performance of a-Si single and multijunction modules in two locations. *Photovoltaic Specialist Conference, 2005*. Conference Record of the Thirty-first IEEE. 1484-1487. Available at: http://ieeexplore.ieee.org/iel5/9889/31426/01488423.pdf?isnumber=31426&arnumber=1488423

Gxasheka, A. R., E. E. van Dyk, and E. L. Meyer. 2005. Evaluation of performance parameters of PV modules deployed outdoors. *Renewable Energy*. 30: 611-620.

Hamidat, A., B. Benyoucef, and T. Hartani. 2003. Small-scale irrigation with photovoltaic water pumping system in Sahara regions. *Renewable Energy*. 28: 1081-1096.

Hamza, A. A., and A. Z. Taha. 1995. Performance of submersible PV solar pumping systems under conditions in the Sudan. *Renewable Energy*. 6(5-6): 491-495.

Hargreaves, G. H., and Z. A. Samani. 1982. Estimating potential evapotranspiration. *Journal of Irrigation and Drainage Engineering*, Div. ASCE. 108: 225-230.

Hay, J. E. 1976. A revised method for determining the direct and diffuse components of the total short wave radiation. *Atmosphere*. 14: 278-287.

Hishikawa, Y., and S. Okamoto. 1994. Dependence of the I-V characteristics of amorphous silicon solar cells on illumination intensity and temperature. *Solar Energy Materials and Solar Cells*. 33: 157-168.

Hrayshat, E. S., and M. S. Al-Soud. 2004. Potential of solar energy development for water pumping in Jordan. *Renewable Energy*. 29: 1393-1399.

Hsiao Y. R., and B. A. Blevins.1984. Direct coupling of photovoltaic power source to water pumping system. *Solar Energy*. 32: 489-498.

International Energy Agency. 2003. IEA Energy Statistics. Available at: http://www.iea.org/Textbase/stats/oecdbalancetable.asp?oecd=Canada&SubmitB=Submit&COUNTRY_LONG_NAME=Canada

Iqbal M. 1979. A study of Canadian diffuse and total solar radiation data—I: monthly average daily horizontal radiation. *Solar Energy*. 22: 81-86.

Kacira, M., M. Simsek, Y. Babur, and S. Demirkol. 2004. Determining optimum tilt angles and orientations of photovoltaic panels in Sanliurfa, Turkey. *Renewable Energy*. 29: 1265-1275.

Kimball, J. S., S. W. Running, and R. Nemani. 1997. An improved method for estimating surface humidity from daily minimum temperature. *Agricultural and Forest Meteorology*. 85: 87-98.

King, D. L., W. E. Boyson, and J. A. Kratochvil. 2002. Analysis of factors influencing the annual energy production of photovoltaic systems. *Photovoltaic Specialist Conference, 2002*. Conference Record of the Twenty-ninth IEEE. New Orleans, Louisiana. 1356-1361. Available at: http://ieeexplore.ieee.org/iel5/8468/26685/01190861.pdf?tp=&arnumber=1190861&isnumber=26685

Lewis, G. 1987. Optimum tilt of a solar collector. *Solar and Wind Technology*. 4(3): 407-410.

Li, D. H. W., and J. C. Lam. 2004. Predicting solar irradiance on inclined surfaces using sky radiance data. *Energy Conversion and Management*. 45: 1771-1783.

Liu, B. Y. H. and R. C. Jordan. 1960. The interrelationship and characteristic distribution of direct, diffuse and total solar radiation. *Solar Energy*. 4(3): 1-19.

Madramootoo, C. A., N. Visvanatha, S. Kulshreshtha, G. Pearson, B. Hobin, and H. Fyles. 2006. Analysis of issues constraining sustainable irrigation in Canada and the role of Agriculture and Agri-Food Canada. A report prepared for Agriculture and Agri-Food Canada, Prairie Farm Rehabilitation Administration. Available from Brace Centre for

Water Resources Management, Macdonald campus of McGill University, 21111 Lakeshore Road, Ste. Anne de Bellevue, QC, H9X 3V9.

Meek, D. W. 1997. Estimation of maximum possible daily global solar radiation. *Agricultural and Forest Meteorology*. 87(2-3): 223-241.

Meike, W. 1998. Hot climate performance comparison between poly-crystalline and amorphous silicon cells connected to an utility mini-grid. Paper presented at *Solar '98*, Christchurch, NZ.

Meneses-Rodriguez, D., P. P. Horley, J. Gonzalez-Hernandez, Y. V. Vorobiev, and P. N. Gorley. 2005. Photovoltaic solar cells performance at elevated temperatures. *Solar Energy*. 78: 243-250.

Mesonet – Montreal. 2006. Available at: http://www.mesonet-montreal.ca/

Meyers, D. R. 2005. Solar radiation modeling and measurements for renewable energy applications: data and model quality. *Energy*. 30(9): 1517-1531.

Michael, A. M., and S. D. Khepar. 1989. *Water well and pump engineering*. New Delhi: Tata McGraw-Hill Publishing Company Limited.

Munson, B. R., D. F. Young, and T. H. Okiishi. 1998. *Fundamentals of fluid mechanics*, Third Edition. New York, USA.: John Wiley & Sons, Inc.

Nijegorodov, N., and P. K. Jain. 1997. Optimum slope of a north-south aligned absorber plate from the north to the south poles. *Renewable Energy*. 11(1): 107-118.

Orgill J. F. and K.G. T. Hollands. 1977. Correlation equation for hourly diffuse radiation on a horizontal surface. *Solar Energy*. 19: 357-359.

Ouranos. 2006. Personal communications.

Pulfrey, D. L., P. R. B. Ward, and W. G. Dunford. 1987. A photovoltaic-powered system for medium-head pumping. *Solar Energy.* 38(4): 255-265.

RETScreen International. 2004. Photovoltaic project analysis chapter. In *Clean energy project analysis: RETScreen engineering & cases textbook.* CANMET Energy Technology Centre – Varennes. Natural Resources Canada. Available at: www.retscreen.net

Rivington M., K. B. Matthews, and K. Buchan. 2002. A comparison of methods for providing solar radiation data to crop models and decision support systems. *1st biennial meeting of the International Environmental Modelling and Software Society.* Lugano, Switzerland. 193-198. Available at: http://www.sipeaa.it/tools/RadEst/RivingtonSRLADSS.doc

Ruth. D. W., and R. E. Chant. 1976. The relationship of diffuse radiation to total radiation in Canada. *Solar Energy.* 18: 153-154.

Ruther, G., G. Tamizh-Mani, J. del Cueto, J. Adelstein, A. A. Montenegro, and B. von Roedern. 2003. *Proceedings of 3rd World Conference on Photovoltaic Energy Conversion.* Osaka, Japan. 2011-2014.

Samani, Z. A. 2004. Discussion of "History and evaluation of Hargreaves evapotranspiration equation" by George H. Hargreaves and Richard G. Allen. *Journal of Irrigation and Drainage Engineering,* Div. ASCE. 130(5): 447.

Scheffler, W. 1986. Introduction to the revolutionary design of Scheffler reflectors. Available at: http://www.solare-bruecke.org/infoartikel/Papers_%20from_SCI_Conference_2006/21_wolfgang_scheffler.pdf#search=%22solar%20cooker%20barefoot%20college%22

Stanhill, G. 1966. Diffuse sky and cloud radiation in Israel. *Solar Energy*. 10(2): 96-101.

Tamura J., K. Kurokawa, and K. Otani. 2003. Estimation of hourly in-plane irradiation by using minutely horizontal data. *Solar Energy Materials & Solar Cells*. 75: 585-595.

Thornton, P. E., and S. W. Running. 1999. An improved algorithm for estimating incident daily solar radiation from measurements of temperature, humidity, and precipitation. *Agricultural and Forest Meteorology*. 93: 211-228.

Thornton, P. E., H. Hasenauer, and M. A. White. 2000. Simultaneous estimation of daily solar radiation and humidity from observed temperature and precipitation: an application over complex terrain in Austria. *Agricultural and Forest Meteorology*. 104: 255-271.

Tuller, S. E. 1976. The relationship between diffuse, total and extra terrestrial solar radiation. *Solar Energy*. 18: 259-263.

van Dyk, E. E., and E. L. Meyer. 2000. Long-term monitoring of photovoltaic modules in South Africa. *Photovoltaic Specialist Conference, 2000*. Conference Record of the Twenty-eighth IEEE. 1525-1528. Available at: http://ieeexplore.ieee.org/iel5/7320/19792/00916185.pdf?tp=&arnumber=916185&isnumber=19792

van Dyk, E. E., A. R. Gxasheka, and E. L. Meyer. 2005. Monitoring current-voltage characteristics and energy output of silicon photovoltaic modules. *Renewable Energy*. 30: 399-411.

van Dyk, E. E., E. L. Meyer, F. J. Vorster, and A. W. R. Leitch. 2002. Long-term monitoring of photovoltaic devices. *Renewable Energy*. 25:183-197.

Vilela, O. C., N. Fraidenraich, and C. Tiba. 2003. Photovoltaic pumping systems driven by tracking collectors: experiments and simulation. *Solar Energy*. 74: 45-52.

Windsun. 2006. Wire loss table. Available at: http://windsun.com/Hardware/Wire_Table.htm

Yakup, M. A. b. H. M., and A. Q. Malik. 2001. Optimum tilt angle and orientation for solar collector in Brunei Darussalam. *Renewable Energy*. 24(2): 223-234.

Younes, S., R. Claywell, and T. Muneer. 2005. Quality control of solar radiation data: present status and proposed new approaches. *Energy*. 30: 1533-1549.

8.0 APPENDIX

Cost of solar powered irrigation system

Equipment	Supplier	Purpose	Qty	Price/Unit*
US42	Glenergy – Pembroke, ON	Uni-Solar 42Watt solar panel (with 15' lead)	2	$380
Shurflo 2088-443-144 and filters	Glenergy – Pembroke, ON	Water pump and filters	1	$180
PPT 12/24-7A	Matrix Energy – Montreal, PQ	Linear current booster	1	$125
Drip Tape and Irrigation Equipment	PlastiTech – St. Remi, PQ	Drip irrigation system		$325

* Prices in Canadian dollars. **TOTAL: $1390 + tax**

Wiring Schematic for Data Logger CR23X

Analog inputs to measure data:

1. Thermocouple 1
2. Thermocouple 2
3. Ambient Temperature Probe
4. Pressure Transducer (through 100 ohm resistor)
5. Paddle Wheel Flow Meter (through 100 ohm resistor)
6. Panel 1 Voltage (through 10:1 voltage divider)
7. Panel 2 Voltage (through 10:1 voltage divider)
8. Combined Current Before Linear Current Booster
9. Combined Current After Linear Current Booster
10. Thermocouple 3
11. Thermocouple 4

Excitation, power, and control:

A. Switched excitation output (for temperature probe)
B. 12 V power supply (to power flow meter)
C. Control I/O (to toggle relay between panels and pump)
D. Control I/O (to toggle relay between 24 V power source and current sensors)